Quantum Coherence for Light Harvesting

David Paleček

LUND
UNIVERSITY

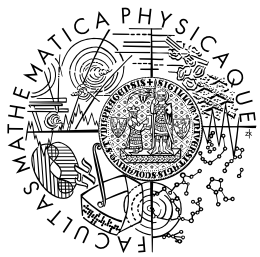

DOCTORAL DISSERTATION
by due permission of the Faculty of Science, Lund University, Sweden and Faculty of Mathematics and Physics, Charles University in Prague, Czech Republic

To be defended at lecture hall C, Kemicentrum, Getingevägen 60, Lund, Thursday 28 January 2016, 13:15.

Faculty opponents
David M. Jonas
Tomáš Polívka

Organization

LUND UNIVERSITY

Chemical Physics
P.O.Box 124
SE-221 00 LUND, Sweden

CHARLES UNIVERSITY

Chemical Physics and Optics
Ke Karlovu 3, Praha 2
121 00, Prague, Czech Republic

Author(s): **David Paleček**

Document name

Doctoral dissertation

Date of issue

2016-01-04

Sponsoring organization

Title and subtitle: **Quantum Coherence for Light Harvesting**

Abstract:

Almost all life on Earth depends on the products of photosynthesis ─ the biochemical process whereby solar energy is stored as chemical-rich compounds. The energy of captured photons is transferred through a network of pigment-protein complexes towards the reaction center. The reaction center is responsible for trans-membrane charge separation, which generates a proton motive force which drives all subsequent biochemical reactions. The ultrafast (femtosecond) nature of the primary processes in photosynthesis is the main reason for its astonishing efficiency. On this timescale, quantum effects start to play a role and can appear in measured spectra as oscillations. It has been hypothesized that these are evidence of wave-like energy transfer.

To unveil the fundamental principals of ultrafast excitation energy transfer in both natural and artificial light-harvesting systems, advanced spectroscopy techniques have been utilized. Coherent two-dimensional electronic spectroscopy is a state of the art technique which allows the most complete spectroscopic and temporal information to be extracted from the system under study. This technique has allowed us to identify a new photophysical process where the coherence of the initially excited state is shifted to the ground state upon an energy transfer step. Coherence dynamics caused by this process bear most of the signatures of pure electronic coherences, and can therefore be easily mistaken for coherent energy transfer. Our results imply that the wave-like energy transfer hypothesis should be reconsidered and tested against coherence shift mechanisms. Furthermore, we have demonstrated that the mixing between vibrational and electronic motions seem to be a general phenomenon in light-harvesting systems.

Key words: Coherent two-dimensional spectroscopy, Quantum coherence, Light harvesting, Photosynthetic reaction center, Energy transfer

Classification system and/or index terms (if any)

Supplementary bibliographical information

Language English

ISSN and key title

ISBN:978-91-7422-425-2 (print)
ISBN:978-91-7422-426-9 (PDF)

Recipient's notes

Number of pages: 185

Price

Security classification

Signature:  Date: **2015-12-08**

Název práce: Quantum Coherence for Light Harvesting
Autor: David Paleček
Katedra: Katedra Chemické Fyziky a Optiky (Univerzita Karlova v Praze) a Department of Chemical Physics (Lund University)
Vedoucí disertační práce: Roman Dědic a Donatas Zigmantas
Abstrakt: Téměř veškerý život na Zemi závisí na fotosyntéze — biochemickém procesu který ukládá energii ze světla do chemických vazeb. Energie zachycených fotonů je přenášena do reakčního centra sítí tvořenou pigment-proteinovými komplexy. Reakční centrum je zodpovědné za mezi-membránový přenos náboje generující proton-motivní sílu, která pohání všechny navazující biochemické reakce. Femtosekundová podstata primárních procesů fotosyntézy je hlavním důvodem jejich vysoké účinnosti. Na časové škále femtosekund se začínají projevovat kvantové efekty, které jsou detekovány v měřených spektrech jako oscilace signálu v čase. Jedna z hypotéz uvádí, že pozorované oscilace jsou důkazem vlnového přenosu energie.

Ke studiu fundamentální podstaty přenosu energie ve světlosběrných systémech (přírodních i umělých) jsou využívány vysoce sofistikované spektroskopické metody. Nejvyspělejší metodou, která umožňuje získat nejkompletnější spektroskopickou informaci v závislosti na čase a energii, je koherentní dvourozměrná elektronická spektroskopie. Tato metoda nám umožnila rozeznat nový fotofyzikální proces, při kterém se během přenosu excitační energie vyexcitovaná koherence přesouvá z excitovaného stavu do stavu základního. Tento proces má většinu charakteristik totožných s čistě elektronovou koherencí. A proto může být snadno zaměněn za důkaz vlnového přenosu energie. Naše výsledky ukazují, že hypotéza vlnového přenosu energie by měla být přehodnocena a testována vzhledem k mechanismu koherentního přesunu. Měření také naznačují, že mísení vibračních a elektronických přechodů je obecným jevem ve světlo-sběrných anténách.

Klíčová slova: Koherentní dvourozměrná elektronická spektroskopie, Kvantová koherence, Sběr světelné energie, Fotosyntetické reakční centrum, Přenos Energie

Prohlašuji, že jsem tuto disertační práci vypracoval(a) samostatně a výhradně s použitím citovaných pramenů, literatury a dalších odborných zdrojů.

Beru na vědomí, že se na moji práci vztahují práva a povinnosti vyplývající ze zákona č. 121/2000 Sb., autorského zákona v platném znění, zejména skutečnost, že Univerzita Karlova v Praze má právo na uzavření licenční smlouvy o užití této práce jako školního díla podle §60 odst. 1 autorského zákona.

V Lundu dne 8.12.2015. Podpis autora 

Faculty of Science, Department of Chemical Physics, Lund University, Sweden
&
Faculty of Mathematics and Physics, Department of Chemical Physics and Optics,
Charles University in Prague, Czech Republic
ISBN: 978-91-7422-425-9

Printed in Sweden by Media-Tryck, Lund University
Lund, 2015


A photon walks into a hotel. The desk clerk says, "Welcome to our hotel. Can we help you with your luggage?" The photon replies, "No thanks, I'm traveling light."

Contents

Acknowledgments

First of all are you, Donatas. Thank you for scientific parenting me, which eventually led to the birth of this “baby”. You cared and I enjoyed it so much. I will never forget you. Another big thanks goes to my second supervisor, Roman Dědic. Your guidance and advice were always useful, surprising, inspiring and funny. I would also like to thank all the other PIs from the Chemical Physics departments in Prague and Lund; Arkady, Ebbe, Ivan, Jakub Pšenčík, Jan Hála, Jan Valenta, Juraj Dian, Per, Tõnu Villy; You are making science the field worth staying in. Not much could have been done in my project without our collaborators from Gothenburg. Sebastian, Petra and Emil, your excitement and driving force is impressive.

To all the 2D guys I have met throughout my stays in Lund, Jakub, Jan, Sunny, Erling, Marcelo, Kil and Lukas. I enjoyed a lot the funny and business matters we went through together. My dear reviewers, Donatas, Marcelo, Erling, Karel, Joana and Maminka. Thank you for your comments, which made my thesis readable (except for Acknowledgments :).

To all the members of Chemphys in Prague and Lund. I wish I would be wiser not to work too much sometimes and rather enjoy more discussions with all of you. To my superheros: Máro, if there is a pure genuine love to a comrade, I feel it to you. Kájo, your easygoing brilliance in all parts of your life was great pleasure to watch and be part of.

Dear TriSydare, you trained me well. Without the endurance I gained with you, I would hardly made it to the finish line today. To all my friends and relatives in my homeland across the seas, my life would suck without you.

My lovely Joaninha, thanks for making me feel home here in Lund and for making me a better man. I love you too. My dearest parents, Maminko, Dušane and Zdendo; without you I would not be where I am and how I am. Thank you for supporting me in pursuing my dreams and in being myself, which you always did with love and patience.

Abstract

Almost all life on Earth depends on the products of photosynthesis — the biochemical process whereby solar energy is stored as chemical-rich compounds. The energy of captured photons is transferred through a network of pigment-protein complexes towards the reaction center. The reaction center is responsible for trans-membrane charge separation, which generates a proton motive force which drives all subsequent biochemical reactions. The ultrafast (femtosecond) nature of the primary processes in photosynthesis is the main reason for its astonishing efficiency. On this timescale, quantum effects start to play a role and can appear in measured spectra as oscillations. It has been hypothesized that these are evidence of wave-like energy transfer.

To unveil the fundamental principals of ultrafast excitation energy transfer in both natural and artificial light-harvesting systems, advanced spectroscopy techniques have been utilized. Coherent two-dimensional electronic spectroscopy is a state of the art technique which allows the most complete spectroscopic and temporal information to be extracted from the system under study. This technique has allowed us to identify a new photophysical process where the coherence of the initially excited state is shifted to the ground state upon an energy transfer step. Coherence dynamics caused by this process bear most of the signatures of pure electronic coherences, and can therefore be easily mistaken for coherent energy transfer. Our results imply that the wave-like energy transfer hypothesis should be reconsidered and tested against coherence shift mechanisms. Furthermore, we have demonstrated that the mixing between vibrational and electronic motions seem to be a general phenomenon in light-harvesting systems.

Popular Scientific Summary

The main reason that we humans exist at all is because of photosynthesis. The food we eat, the oxygen we breath, most of the energy that warms our homes and powers our electronics are all products of photosynthesis. Over millions of years, plants, algae and some bacteria have developed biomachinery to harness solar energy and thrive. They do this by fixing carbon into chemical compounds, which can turn into either nutrition or fossil fuels. Photosynthetic organisms use pigment molecules embedded in proteins to absorb photons. These absorb only part of the visible spectrum, with the remaining transmitted/reflected light giving photosynthetic organisms their color — often a multitude of shades of green. If the pigments were completely isolated from one another, the absorbed energy would be lost within a few nanoseconds (10^{-9} s) in the form of heat, which can not be further utilized. Hence, for efficient operation, the absorbed energy must be transformed into a more stable form — e.g. electrons and protons — within this time-frame. To this extent, the pigments interact to form a network which directs the energy through the various proteins within the photosynthetic membrane towards a special place called reaction center. In this pigment-protein complex, the absorbed energy is transformed into charges. To prevent charge recombination, the protons and the electrons are spatially separated and transferred to opposite sides of the photosynthetic membrane. The resulting proton-motive force is then used to drive the enzymatic reactions which fix carbon and power the cells.

The first steps of the light-harvesting processes described above are close to 100 % efficient. One of the main reasons for this high efficiency is the ultrafast timescale in which energy is transferred between the pigments. This can range from femtoseconds to picoseconds ($10^{-15} - 10^{-12}$ s). In order to study light harvesting processes, we therefore need to resolve the excitation energy flow both in energy and time. Coherent two-dimensional electronic spectroscopy (2DES) is a recently developed technique capable of extracting the most complete information on light-matter interactions within complex multi-pigment systems such as light-harvesting complexes. Using 2DES, we can resolve processes down to 10 fs time scale and follow their evolution on the energy map. On such timescales, the purely quantum-mechanical properties of matter — similar to Schrödinger's cat being simultaneously dead and alive — can be observed. It was suggested that these so called quantum coherences were facilitating ultrafast energy transfer and charge separation in photosynthesis, thereby enhancing light-harvesting efficiency.

These hypotheses were tested using advanced spectroscopic techniques, namely 2DES. Several light-harvesting systems were investigated. Coherent dynamics in the reaction centers of the naturally occurring *Rhodobacter sphaeroides* — purple photosynthetic bacterium — were studied. We explored the power and limitations of 2DES, and demonstrated for the first time a novel coherence shift process. Inspired by natural photosynthetic light-harvesting antennas, artificially formed bacteriochlorophyll aggregates were subsequently investigated at temperatures close to absolute zero. The basic spectroscopic parameters which define the function of the aggregate were extracted. Finally, a purely

artificial light-harvesting system was studied, comprised of well defined tubular aggregates of cyanine dyes. We identified complex interplay between excitation and vibrational motions which seems to be involved in energy transfer.

The introductory part of the thesis reviews the investigated systems, introduces 2DES as implemented in this work and describes the working principles of the new photophysical process; "Energy Transfer Induced Coherence Shift". The second part contains the author's original work of published papers and manuscripts relevant to light-harvesting processes.

List of Papers

Paper I. Coherent Picosecond Exciton Dynamics in a Photosynthetic Reaction Center. *Sebastian Westenhoff, *David Paleček, Petra Edlund, Philip Smith and Donatas Zigmantas.
J. Am. Chem. Soc, 134(40), 16484–7 (2012).

Paper II. Low Temperature Spectroscopy of Bacteriochlorophyll c Aggregates. David Paleček, Roman Dědic, Jan Alster and Jan Hála.
Photosynth. Res., 119(3), 331–338 (2014).

Paper III. Vibronic origin of long-lived coherence in an artificial molecular light harvester. *James Lim, *David Paleček, Felipe Caycedo-Soler, Craig N. Lincoln, Javier Prior, Hans von Berlepsch, Susana. F. Huelga, Martin B. Plenio, Donatas Zigmantas and Jürgen Hauer.
Nat. Commun., 6(7755) (2015).

Paper IV. Quantum Coherence as a Witness of Vibronically Hot Energy Transfer in Bacterial Reaction Centre. David Paleček, Petra Edlund, Sebastian Westenhoff and Donatas Zigmantas.
Manuscript

Paper V. Cross-polarized Transient Grating to Identify Electronic and/or Mixed Vibronic Coherence Beatings. David Paleček and Donatas Zigmantas.
Manuscript

Paper VI. Pitfalls of the Early Dynamics in the Cross-polarized Two-dimensional Electronic Spectroscopy. David Paleček, Petra Edlund, Emil Gustavsson, Sebastian Westenhoff and Donatas Zigmantas.
Manuscript

Paper VII. Quantitative Evaluation of the Vibronic Mixing in Relation to Excitation Energy Transfer in the Photosynthetic Reaction Center. David Paleček, Petra Edlund, Emil Gustavsson, Sebastian Westenhoff and Donatas Zigmantas.
Manuscript

Paper VIII. Mutational analysis reveals that long-lived quantum oscillations in a bacterial reaction center are intrinsic to the chromophore aggregate. Petra Edlund, David Paleček, Emil Gustavsson, Donatas Zigmantas and Sebastian Westenhoff.
Manuscript

*contributed equally

Publications Related to This Work

Paper IX. High-order Harmonic Generation Using a High-repetition-rate Turnkey Laser. Eleonora Lorek, Esben W. Larsen, Cristoph M. Heyl, Stefanos Carlström, S; David Paleček, Donatas Zigmantas and Johan Mauritsson.
Rev. Sci. Instrum., 85(123106) (2014).

Paper X. Trajectory Resolved High-order Harmonic Generation in Elliptically Polarized Fields in the Presence of Window Resonances
Esben W. Larsen, Stefanos Carlström, Eleonora Lorek, Cristoph M. Heyl, David Paleček, Anne L'Huillier, Donatas Zigmantas and Johan Mauritsson.
Submitted

Contributions to Publications

Papers II,IV,V,VI,VII: Performed the experiments, data analysis and interpretation. Wrote a major part of the manuscript.

Papers I,VIII: Performed the experiments, data analysis and interpretation. Commented on the manuscript.

Paper III: Performed the experiments, discussed interpretation and commented on the manuscript.

Papers IX,X: Assisted during the experiments and commented on the manuscript.

Abbreviations

2DES Coherent two-dimensional electronic spectroscopy

AP All-parallel

B Accessory bacteriochlorophyll *a* band in *Rhodobacter sphaeroides* reaction center

BChl Bacteriochlorophyll

BPheo Bacteriopheophytin

C8O3 Cyanine dye functionalized by hydrophobic and hydrophylic sidechains.

CCD Charged coupled device

CP Cross-polarized

DOS Density of states

EET Excitation energy transfer

ET Electron transfer

ES Excited state

ESA Excited state absorption

ETICS Energy transfer induced coherence shift

FT Fourier transform

GS Ground state

GSB Ground state bleach

H Bacteriopheophytin *a* band in *Rhodobacter sphaeroides* reaction center

HR Huang-Rhys

LH1 Light-harvesting antenna complex I

LH2 Light-harvesting antenna complex II

LO Local oscillator

NOPA Non-colinear optical parametric amplifier

P Special pair

PP Pump-probe

RC_{sph} Reaction center from *Rhodobacter sphaeroides*

SE Stimulated emission

TG Transient grating

Chapter 1

Introduction

Photosynthesis is the fundamental biochemical process which provides energy to almost all living organisms on Earth. The oxygenic form of photosynthesis uses sunlight to split water and fix carbon into sugars (glucose). It can be summarized as the infamous chemical equation:

$$6H_2O + 6CO_2 \xrightarrow{\text{light}} C_6H_{12}O_6 + 6O_2$$

Even though the overall energy conversion efficiency of photosynthesis is often much lower than 1 % [1], the primary steps — namely the light-harvesting processes — exhibit efficiencies close to 100 % [2]. These involve the capture of photons and the funneling of their energy towards a reaction center where charges can be separated and transferred across the membrane. In this way, an electrochemical potential is built up and used to drive all the subsequent biochemical reactions. Such impressive performance constantly draws scientific curiosity to understand the mechanisms of photosynthetic light harvesting. Moreover, it inspires new technological designs and solutions for artificial light-harvesting systems such as those utilized in photovoltaic cells and solar fuel devices. An ever increasing global energy consumption and the associated environmental threats call for new and sustainable energy sources to be found. Fortunately, even solar energy alone has the potential to sustain the energetic needs of mankind [3].

One of the main reasons for the high photosynthetic light-harvesting efficiency is its ultrafast nature; all the processes before charge separation are completed within a few picoseconds (10^{-12} s). In contrast, all the competing relaxation and reverse processes are typically about 2 orders of magnitude slower, thereby ensuring both unidirectionality and high efficiency. Throughout the course of evolution, light-harvesting systems have optimized the structural arrangement of the various pigments contained in the protein scaffolds, tuning the inter-pigment couplings and environmental interactions through the organization of the intra-membrane proteins. The extent of this fine-tuning of the light-harvesting machinery has been extensively discussed following spectroscopic observations of superposition state dynamics — a purely quantum mechanical phenomenon without classical analog. These so called coherent effects have been suggested to

facilitate energy transfer and increase the overall efficiency of light-harvesting. This thesis aspires to contribute to the fundamental understanding of quantum coherence in photosynthetic and artificial light harvesting systems, with a view to enabling its exploitation.

All initial photosynthetic processes involve the absorption of a visible or infrared light quantum, resulting in molecular excitation and its subsequent ultrafast energy equilibration. Time resolved optical spectroscopy is therefore a natural tool for studying light-harvesting systems. At the same time, the high degree of spectral congestion in light-harvesting systems (a result of the multiplicity of absorbing pigments) calls for high spectral (energy) resolution — something which is typically inaccessible in conventional ultrafast time-resolved experiments. The recently developed technique of coherent two-dimensional electronic spectroscopy (2DES) overcomes this limitation, and permits the maximum information available in both energy and time domains to be extracted. 2DES is considered a state of the art technique in optical spectroscopy, which has provided superior insight into light-harvesting processes.

The thesis is organized as follows. Chapter I introduces the light-harvesting systems that were investigated. Chapter II briefly describes coherence two-dimensional electronic spectroscopy and its polarization-control implementation. In Chapter III, the working principles of a newly identified photophysical process, denoted ETICS, are discussed. Part II contains reprints of the relevant publications and manuscripts.

Chapter 2

Investigated Light-harvesting Systems

Understanding the fundamental processes which underlie biological light-harvesting can help to inspire new designs of functional materials for photovoltaic and photochemical applications. Several natural and artificial light-harvesting systems which were studied in this thesis are introduced in this chapter. In the class of natural photosynthetic systems, we studied the reaction center of purple photosynthetic bacteria — introduced in Sections 2.1–2.3 — which is prototypical of the type II reaction centers found in higher plants. Such as reaction center is a pigment-protein complex responsible for trans-membrane charge separation which is a crucial part of the natural photochemical machinery. When tailoring artificial light-harvesting antennae, researchers often seek to imitate natural design schemes. One such cross-over system inspired by nature is the bacteriochlorophyll (BChl) *c* aggregate introduced in Section 2.4, which mimics chlorosomes — the light-harvesting antenna of green sulfur bacteria. Finally, a purely artificial light-harvesting system in the form of well-defined supramolecular tubular aggregates of cyanine based dyes is described in Section 2.5.

2.1 Purple Photosynthetic Bacteria

According to recent estimates, the bacterial biomass on earth exceeds that of all other lifeforms together, including that of animals and plants [4]. Purple bacteria represent a major group of photosynthetic bacteria inhabiting aquatic and terrestrial environments [5]. Their wide range of habitats and adaptability makes purple bacteria a species at the frontier of evolution, pushing the boundaries of functional photosynthesis. They can thrive at temperatures between $0 - 57\,^{\circ}\mathrm{C}$ (and can indeed survive freezing to well below $0\,^{\circ}\mathrm{C}$), salinities of up to 32% and pH ranges from 3 to 11 [5]. Purple bacteria can be categorized as anoxygenic phototrophs, i.e. they capture and store solar energy without oxygen production, instead using hydrogen sulfide in place of water as an electron source. Non-

sulfur purple bacteria do not store oxidized sulfide intracellularly as purple sulfur bacteria, but rather deposit it outside the cells [6].

This thesis focuses on the purple non-sulfur bacterium *Rhodobacter (Rba.) sphaeroides*, a research workhorse amongst photosynthetic bacteria. It can be found in ponds, lakes, waste lagoons and streams under layers of oxygenic species which absorb most of the blue and red parts of the visible spectrum [7]. The light available to *Rba. sphaeroides* therefore mostly consists of green and near infrared light above 750 nm, which is the reason why they mostly utilize bacteriochlorophyll *a* (BChl *a*) and carotenoids as their light-harvesting pigments [8].

2.2 Light-Harvesting Antennas

Following light absorption in the photosynthetic units of living organisms, the excitation energy migrates through the light-harvesting antennas until it reaches a reaction center (RC_{sph}), where trans-membrane charge separation takes place. Most of the light-harvesting pigments are located in the antennas, which serve as concentrators of the absorbed photons. They funnel the excitation energy along an energy gradient of progressively lower energy electronic states towards the RC_{sph} complex, which otherwise would be inactive most of the time [9, 10]. A model of the general organization of the complexes within the photosynthetic membrane of purple bacteria is currently available and is based on atomic force microscopy studies [11, 12]. Light-harvesting antenna complex I (LH1) almost completely encircles RC_{sph}, predominantly forming dimers, with a clear opening in the LH1 structure proposed to be an outlet for the reduced quinone to enter the quinone pool. LH1 antennas receive excitations from the network of light-harvesting complexes II (LH2) which capture most of the sunlight.

To create an effective energy gradient, several effects are utilized by the protein in order to tune the energy of the lowest singlet state of BChl *a*, which in solution typically peaks around 770 nm [13]. The redshift of the absorption band towards the near-infra-red region is achieved by the dielectric effect of the protein medium, by H-bonds between the protein and the pigments and by inter-pigment interactions [14].

A typical LH2 consists of two rings of BChls *a* which form spectroscopic bands absorbing around 800 nm (B800) and 850 nm (B850). In *Rba. sphaeroides* the B800 band is formed by 9 weakly coupled BChls *a* which exchange excitation energy on a time-scale of several hundreds of femtoseconds [15]. Within $0.8 - 0.9$ ps, the excitation energy is transferred to the B850 ring, which is comprised of 18 strongly coupled BChls *a* molecules [16]. The energy is delocalized among 3–4 pigments and moves along the ring with time constant of ~ 100 fs [17, 18]. This ensures efficient excitation transfer to the other LH2 or the LH1 complexes, independent of the geometrical arrangement of the antennae in the membrane. LH2 to LH1 excitation energy transfer (B850 to B875) is largely temperature independent and proceeds in $2 - 5$ ps [16, 19]. The rate limiting step of overall energy transfer is the excitation transfer from LH1 to the RC_{sph}, which

takes $20 - 50$ ps. This process is relatively slow, because of the large distance of ~ 40 Å between the complexes [16]. Such a big distance prevents oxidation of the LH1 by the RC_{sph}, which would result in a complete deactivation of the LH1 light-harvesting ability.

Carotenoids present in both LH2 and LH1 contribute to light-harvesting by moving energy transfer away from both S_1,S_2 singlet states to the BChl *a* molecules with $\sim 50\%$ efficiency. This energy transfer takes only $\sim 100 - 200$ fs due to the close proximity of the carotenoids to the BChls *a* [20]. The main role of carotenoids however is to quench the long-lived triplet states of the BChls, which can sensitize singlet oxygen — a strong and dangerous oxidizing agent, which is damaging to the cells [21].

2.3 Bacterial Reaction Centers

Rba. sphaeroides is a prototypical purple bacterium, which represents an important evolutionary step preceding oxygenic photosynthesis. It contains a simplified light-harvesting apparatus with only a type II reaction center — an ancestor of the photosystem II reactions centers found in higher plants and algae [22]. RC_{sph} is responsible for efficient trans-membrane charge separation and building up the proton gradient across the membrane. The proton flow across the membrane is then used by the trans-membrane enzyme adenosine triphosphate synthase to generate energy-rich compounds [23].

The protein scaffold of RC_{sph} embeds two quinones, two strongly coupled BChls *a* forming a special pair (P), two accessory BChl *a* monomers (B) and two bacteriopheophytins *a* (BPheo *a*) (H), all arranged in two branches of almost perfect C_2 symmetry (see Fig. 2.1). Although under physiological conditions, most of the excitation energy is transferred directly to P from LH1, all the accessory pigments of RC_{sph} can absorb light and serve as an energy funnel towards P, where the charge separation takes place. The known high-resolution crystallographic structure [24, 25], relative simplicity and range of possible modifications of the RC_{sph} make it an ideal model system for studying excitation energy transfer (EET) and electron transfer (ET).

The absorption spectrum of RC_{sph} clearly indicates how downhill EET proceeds (Fig. 2.1). After excitation of the H molecules absorbing around 760 nm, the excitation energy is transferred in approximately 100 fs to accessory B and in another 120 fs to the P, irrespective of its oxidation state [26–28]. The special pair is formed by two strongly coupled BChl *a* molecules with their monomeric transition dipole moments aligned roughly parallel to one another[29]. The strong coupling and charge transfer character of this excitonic transition explains the broad red-shifted absorption [30], where the lower excitonic state possesses most of the oscillator strength and peaks around 850 nm at RT. The weakly absorbing higher excitonic level of P is located under the B band, and it is discernible as a shoulder around 810 nm at 10 K [31].

Even though the two branches are almost symmetric and both participate in EET, only one of the branches is active in ET [32]. Electron transfer from P

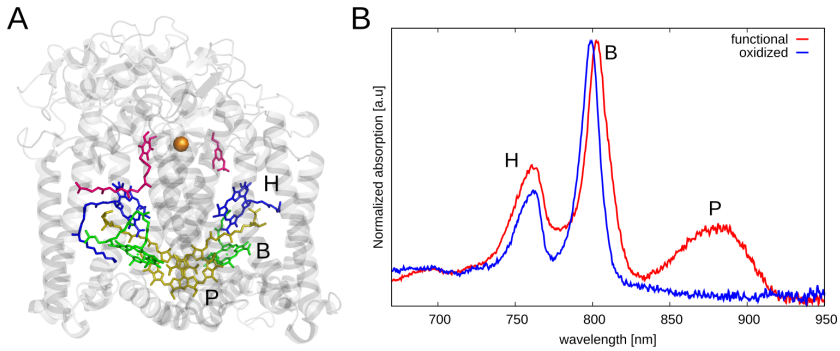

Figure 2.1: Bacterial reaction center. (A) Protein structure (gray) with the pigment cofactors arranged in C_2 symmetric branches. Strongly coupled BChl *a* dimer (P, yellow), two accessory BChl *a* (green) and two BPheo *a* (blue) form a spectroscopic aggregate with well separated absorption bands P, B and H, respectively (panel B, red). Oxidation of P leads to removal of the absorption upon formation of the P^+ state at 77 K temperature (blue).

to H occurs in ~ 3.5 ps, forming the P^+BH^- state which can be monitored via stimulated emission from P^- at 930 nm, H^- absorption around 680 nm and the blue shift of the B band [33] due to the Stark effect [34]. Two mechanisms for this ultrafast ET are discussed in the literature; a "two-step" model where B^- is a short lived (0.9 ps) but real intermediate [35, 36] and a "superexchange" mechanism where the B states are off-resonant and play the role of bridge intermediates for direct ET from P to H [37, 38]. Which of these processes dominates depends on the energetics between all three states involved [39, 40]: P^*BH, P^+B^-H and P^+BH^- with a potential role of vibrational relaxation in the excited state [41]. It is generally agreed that both mechanisms are present in wild-type RC_{sph}, with the two-step model dominating at room temperature and the superexchange mechanism being 100% responsible for ET at low temperatures, where it proceeds with a time constant of 1.2 ps [42, 43]. After the P^+BH^- is formed, the electron is transferred first to quinone Q_A and then to the final two-electron acceptor quinone Q_B with time constants of ~ 200 ps [36] and $\sim 140\,\mu$s [44], respectively.

There are numerous ways to alter the structural and environmental properties of BRC in order to study the BRC functions. Point mutations of the peptide chain can be used to study the role of proteins (H-bonding, electrostatics, slight structural asymmetry) in efficient charge separation and ET. It has for example been found that the protein pocket hosting the special pair is quite rigid during charge separation as compared to the rest of the structure [45]. Furthermore, the tyrosine residual m210 was identified as being crucial for ultrafast ET [46]. In Papers VII,VIII, we studied the effects of such mutations on the EET, coherent dynamics and vibronic coupling in oxidized RC_{sph}.

The application of time-resolved spectroscopy to RC_{sph} was pioneered by Kaufmann and coworkers [47]. Further development of femtosecond pump-

probe (PP) techniques led to superior time resolution for studying EET and ET dynamics. The femtosecond time duration of the pulses implies significant spectral breadth, which allows for excitation of superpositions of the energy eigenstates of the system. These can be either vibrational or excitonic depending on the character of the states involved in the particular superposition.

Vibrational coherence in the excited state of RC_{sph} has been observed in the stimulated emission band of P, leading to the conclusion that low-frequency modes drive the ultrafast ET along the reaction coordinate [48, 49]. Low-frequency beating signals in pump-probe anisotropy were interpreted as electronic coherence [27]. Higher frequency oscillations were reported by the Fleming group using two-color photon echo experiments, and were interpreted as proof of electronic coherence in RC_{sph} [50]. The more complex situation involving the mixing of electronic and vibrational degrees of freedom due to vibronic coupling, has recently been used to explain a range of coherent oscillations observed in experiments [51, 52].

Recent developments in the 2DES technique and the proposed role of quantum coherences in efficient EET and ET [53] call for a re-examination of the RC_{sph} complex to test current hypotheses and gain general insights into the fundamental principles of coherence effects in pigment-protein complexes. In early experiments, we identified a strong excitonic character to the quantum coherences (Paper I), however their lifetime exceeded the lifetime of the excited states by an order of magnitude. This was in strong disagreement with the well developed theory of dephasing of coherent superpositions of states [54]. Extended experiments and new analytic approaches allowed us to identify a new photophysical process, which we denoted as ETICS (Energy Transfer Induced Coherence Shift, Paper IV and Chapter 4). In the ETICS mechanism, the initial excited state coherence is shifted to the ground state (GS) of the donor upon an energy transfer step without the loss of its vibronically mixed character and phase information. It does however acquire the picosecond lifetime of the GS vibrational coherence. ETICS is independent of the particular geometry or pigment constitution and is general under the condition that the EET proceeds on a comparable timescale to the vibrational dephasing. Thus with ETICS we provide an alternative explanation for the readily observed long-lived coherences in the photosynthetic light-harvesting proteins.

2.4 BChl *c* aggregates

Chlorosomes, the light-harvesting antennae of the green sulfur bacteria, posses many unique properties. This is thought to be mainly due to the extremely hostile environments the bacteria have been found in, such as next to hydrothermal vents at the bottom of the oceans or at 100 meter depths of the Black sea [55]. Such extremely low-light conditions impose extra requirements on photon capture and light-harvesting efficiencies. Hence chlorosomes encapsulate over 10^5 BChl c molecules in large oval aggregate bodies ($200 \times 100 \times 30$ nm [56]) without any protein scaffold. This high pigment concentration ensures that every incoming

photon is absorbed. The lack of a protein scaffold lowers protein synthesis requirements, but also makes chlorosomes highly disordered aggregate whose exact structure remains unclear. Two competing models of tubular [57] and lamellar [58] organizations have been proposed. Another unique property of the chlorosomes is the self-organization of BChls *c*, which can be easily imitated when preparing artificial aggregates in non-polar solvents [59, 60] or aqueous solutions by addition of non-polar molecules such as quinones [61]. These act as aggregation inducing agents, not only in solution but also in the *in vivo* chlorosomes. Apart from their structural role, the quinones also have a functional role, quenching excessive excitation energy under aerobic conditions which can be harmful to the bacteria [62]. This property serves as inspiration in attempts to mimic the chlorosome light-harvesting functionality with self-aggregating artificial BChl *c* aggregate antennas.

In Paper II, the aggregation properties and effect on redox-dependent quenching by quinones were studied in artificial BChl *c* aggregates. We employed high-resolution spectroscopy techniques, namely hole-burning [63] and low-temperature fluorescence spectroscopy to obtain fundamental spectroscopic parameters for the aggregates. Recently, successful 2DES experiments in our group on the highly scattering whole bacterial cells provide hope that 2DES experiments are feasible also on BChl *c* aggregates. The information on BChl *c* aggregates presented in Paper II can be used to gain further insights into the organization of the aggregates and to test the theoretical concepts of the quantum coherence, when compared to 2DES experiments.

2.5 Cyanine dyes

Almost 80 years ago, Scheibe and Jelly observed peculiar spectroscopic properties of cyanine dyes in aqueous solution and assigned them to the formation of aggregates [64, 65]. Head-to-tail orientation of the monomeric transition dipoles constituting the aggregates leads to a red-shift of the main absorption band (J-aggregate), whereas a parallel arrangement leads to a blue-shift of the absorption (H-aggregate) [66].

A wide range of methods were employed to determine the structure of the aggregated form ranging from X-ray crystallography [67], low-temperature fluorescence spectroscopy [68], cryo-transmission electron microscopy [69] to atomic force microscopy [70]. A spectral shift and narrowing of the main absorption band is a manifestation of the excitonic interaction and results in a delocalization of the excitation energy among the number of monomers. The excitation energy can thus move freely among the coupled monomers which is a very desirable property for artificial light-harvesting systems and solar-cell applications [71]. Early studies of fluorescence quenching suggested that energy can be transferred over thousands of cyanine monomers [72], which was supported by exciton annihilation studies [73, 74]. More conservative estimates of the delocalization length between 30–100 monomers were obtained by excitonic models [75, 76] and scanning near-field optical microscopy [77].

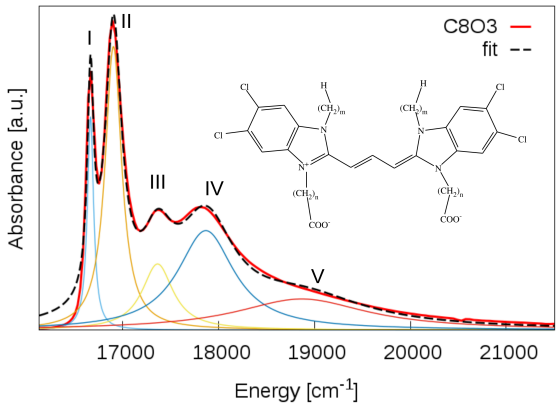

Figure 2.2: 5,5',6,6'-tetrachlorobenzimidacarbocyanine dyes (see inset) form a double-walled tubular aggregates in polyvinyl alcohol solution. The structural motif of the CmOn depends on the length of the alkane chains. Absorption spectrum of C8O3 is shown in red, together with the 5-lorentzian function fit (black). First two bands (I and II) are associated with transitions along the tubular axes, in contrast to band III, which is oriented perpendicular to the aggregate axis. Origin of the bands IV and V is not well established yet.

One recent advancement in the cyanine aggregate field is the functionalization of 5,5',6,6'-tetrachlorobenzimidacarbocyanine with hydrophobic and hydrophilic chains on the two sides of the chromophore [78, 79] (see Fig. 2.2). Control of the length of the side-chains determines the resulting highly ordered aggregate structure in aqueous solution. The ionic character, solubility and fluorescent quenching properties of the amphiphilic cyanine dyes are advantageous for biosensing of DNA [80] and polypeptides [81]. On the other hand, their modest photo-stability and ionic character limit their potential use in organic photovoltaic applications.

One of the most studied amphiphilic cyanine aggregates has the acronym C8O3 which forms double-walled tubular structures and rope-like bundles [79]. The diameter of the tubes is $\sim 10\,\text{nm}$ with the length of the bundles exceeding $100\,\mu\text{m}$. The walls are separated by 4 nm. Surprisingly complicated absorption and linear dichroism spectra are observed for C8O3 (see Fig. 2.2). The linear absorption consists of five bands (I-V) where the two lowest bands (I,II) are polarized along the tube axis and the band III is polarized perpendicular to the tube [82]. The origin of the weakly absorbing bands IV and V is still not fully understood. A delocalization length of 95 monomers has been determined by the two-color PP spectroscopy at 1.5 K [83]. Both vibrational and vibronically mixed coherence have been identified in the 2D spectra of C8O3 [84]. In Paper III, we extended the previous work by employing polarization-resolved 2DES and taking advantage of a macroscopically orientated sample in the liquid jet. In this way we were able to separate the excited state vibronically mixed coherences from the ground state contributions. The results also suggest that the coherences located

on the inner wall of the aggregate are shielded from the environment by the outer tube, which results in the extension of the dephasing time.

Chapter 3

Two-dimensional Electronic Spectroscopy

All conventional time-resolved spectroscopy techniques suffer from the fact that increasing temporal resolution through the use of shorter and shorter excitation pulses necessitates a broader spectral bandwidth, which results in the loss of spectral selectivity and resolution [85]. This drawback can be overcome by sophisticated approaches using Fourier transform techniques; e.g. coherent two-dimensional spectroscopy. In our laboratory we employ two-dimensional electronic spectroscopy (2DES), which is based on heterodyne detection via spectral interferometry [86, 87]. In the visible range, 2DES was introduced by Jonas and co-workers [88, 89], and later applied to photosynthetic pigment-protein complexes [90]. In a 2DES experiment a sequence of femtosecond laser pulses is employed to extract maximum possible information about induced polarization in the sample both in energy and time. An excellent introduction to the 2DES principles using Fourier optics approach was given by Jakub Dostál in his doctoral thesis [91]. Therefore, the working principle of 2DES is only briefly summarized in Sections 3.1 and 3.2. Section 3.3 introduces the concept of Feynman diagrams, an invaluable representation of system interaction with the electric fields and evolution, described by the nonlinear response function formalism. In Section 3.5 polarization resolved 2DES is described in connection with the additional information it provides for quantum coherent phenomena.

3.1 2DES in a Nutshell

In pump probe (PP) spectroscopy, the system is brought out of equilibrium by the first optical excitation pulse (pump) and is subsequently allowed to evolve freely in time. The second pulse (probe) then monitors the absorption changes induced by the pump pulse. Typically, the probe light is spectrally resolved and the ratio between the pump on and pump off probe intensities (transient absorption) is plotted as a function of the probe delay [92]. The uncertainty principle between

energy and time implies that the shorter the pulse (higher temporal resolution) the broader the pulse spectrum. For example, a Fourier-transform-limited 10 fs pulse centered at 800 nm has a bandwidth of 94 nm. All the states and their superpositions within the pulse bandwidth will be excited by such a pump pulse. Consequently the evolution of all the states, including superpositions will be intertwined and monitored together by the probe pulse.

To extend PP towards 2DES, the pump pulse is split into two identical replicas. The first two pulses create a spectral interference pattern when delayed in respect to each other. This time delay (t_1) — called the coherence time — is scanned in 2DES with interferometric precision (better than $\lambda/50$) to controllably alter the spectral interference patterns, which act as the pump pulse. In combination with the first two, the third pulse generates a third order polarization, which is emitted in a specific phase-matched direction and heterodyned with a fourth pulse, called local oscillator (LO, see Fig. 3.1). This type of 2DES is often denoted as "photon echo type". Several other implementations exist, but they will not be considered in this thesis [93, 94]. In the measurements, the interferometric signal is spectrally resolved on a CCD, thus providing spectral resolution along emission axis ω_3, in analogy to the spectrally resolved probe in PP. Fourier transform (FT) over the delay t_1 gives the spectral resolution within the spectrum of the pump pulse, i.e. excitation axis ω_1. In this way the 2D correlation map between excitation and emission energies (ω_1, ω_3) is constructed. The population delay t_2 has the same meaning as in PP; 2D spectra are measured at various time points after the pump excitation and the evolution of the spectral features is recorded. Whereas in PP the signal is "integrated" along excitation axis ω_1, in 2DES it is spectrally resolved. Both techniques however measure the same third order non-linear response and therefore monitor the same processes, so that direct correspondence between the two exists [95].

In our laboratory 2DES measurements are carried out using femtosecond, tunable, spectrally broad pulses from a non-colinear parametric amplifier (NOPA). The output of the NOPA is split into two replicas by a beamsplitter (for the alternative collinear setup see [96]). The second beam (which will be split into pulses 3 and 4) is delayed by a conventional optical delay stage. Both beams are focused by a spherical mirror onto a diffraction grating optimized for the ± 1 order of diffraction, producing four identical pulse replicas arranged in the four corners of a rectangle (so-called boxcar geometry, Fig. 3.2) [97, 98]. One of the crucial steps is to delay pulses 1 and 2 (first pair) with the necessary interferometric precision (Fig. 3.1). Two pairs of wedges, one in each beam, are inserted in the beams 1 and 2 and one wedge in the pair is moved in and out, thus producing either more or less dispersion delay to precisely scan t_1. Another spherical mirror focuses and overlaps all the beams in the sample plane. Beams 1, 2 and 3 are excitation pulses that induce the third order polarization that is emitted in the phase-matched direction collinear with the LO (Fig. 3.2). In the heterodyned detection scheme, the signal electric field interferes with the LO, resulting in a spectral interferogram which is detected by the CCD camera. A unique feature of our setup is the double lock-in detection system, implemented by opto-mechanical modulation of beams 1 and 2. Typically 1500 spectral interferograms are used

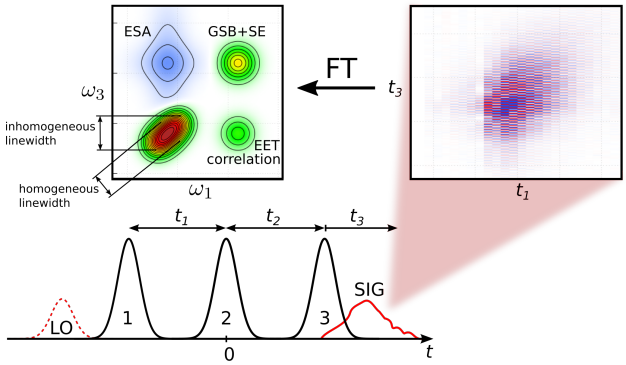

Figure 3.1: Pulse sequence used in 2DES experiment. Three excitation pulses generate the third order non-linear response signal, which is heterodyned with the LO. The spectral interferogram is Fourier transformed to produce 2D maps correlating excitation and emission energies (ω_1, ω_3). Diagonal peaks approximately correspond to the linear absorption and provide information about homogeneous/inhomogeneous broadening, whereas their dynamics inform about the population decays. Cross-peaks report spectral correlations that indicate couplings and energy transfer.

for lock-in filtering. In this way we substantially suppress any scatter from the sample [98]. For polarization control, a quarter waveplate is used to generate circularly polarized light. Four wire grid polarizers (aspect ratio ~ 800) in each of the beams then select the desired linear polarizations.

Accurate knowledge of the delay between the third pulse and LO allows to both the real and imaginary parts of the signal to be recovered. The real (imaginary) part of the signal corresponds to the imaginary (real) part of the refractive index and is related to absorption (refraction). For each population time t_2, the spectral interferogram is detected as (t_1, ω_3) and Fourier transformation and filtering leads to the resultant (ω_1, ω_3) 2D spectrum, as illustrated in Fig. 3.1. The real part of the signal integrated along ω_1 and normalized to the LO electric field corresponds to the PP spectrum. This feature is crucial for phasing, which determines the above mentioned delay between the third pulse and LO. Proper phasing allows the correct separation of the real and imaginary parts of the response [97].

3.2 Theoretical Basics

The theoretical description of the measured 3$^{\text{rd}}$ order nonlinear polarization in 2DES is usually based on a semi-classical approach, where the system is treated quantum mechanically and the excitation light is described classically

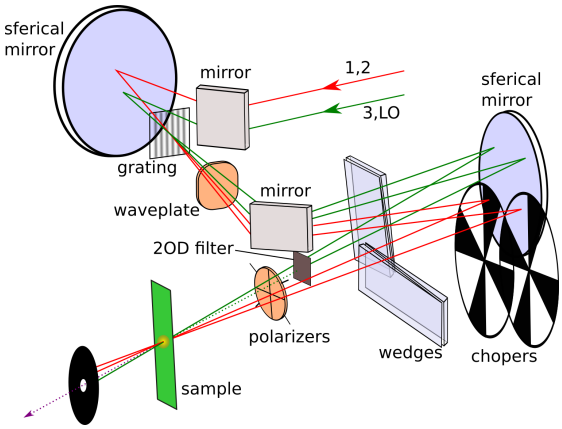

Figure 3.2: Scheme of the experimental setup. See text for details.

as an oscillating electric field. The following summary uses a bare minimum of equations, to provide basics of the theoretical background for the signals detected in the 2DES experiment. More thorough theory is discussed in detail elsewhere [99, 100].

In quantum mechanics the expectation value of the physical property described by the operator $\hat{O}$ for a pure state given by the wavefunction $|\psi\rangle = \sum_n c_n |n\rangle$, which in the eigenstate basis of Hamiltonian $\hat{H}$ can be expressed as:

$$\langle\psi(t)|\,\hat{O}\,|\psi(t)\rangle = \sum_{nm} \rho_{nm}(t) O_{mn} = \mathrm{Tr}(\hat{\rho}(t)\,\hat{O}) = \langle\hat{\rho}(t)\,\hat{O}\rangle\,. \tag{3.1}$$

Here $\rho = |\psi\rangle\langle\psi|$ is the density matrix of the system and Tr is a trace over the matrix. The time evolution density matrix determines the outcome of the observation. From the time dependent Schrödinger equation

$$\frac{\mathrm{d}}{\mathrm{d}t}|\psi(t)\rangle = -\frac{\mathrm{i}}{\hbar}\hat{H}(t)\,|\psi(t)\rangle\,, \tag{3.2}$$

we arrive at "Liouville von Neumann" equation:

$$\frac{\mathrm{d}}{\mathrm{d}t}\rho = -\frac{i}{\hbar}(\hat{H}\rho - \rho\hat{H}) = -\frac{\mathrm{i}}{\hbar}[\hat{H},\rho], \tag{3.3}$$

where [,] is a commutator. For the pure states, the equations 3.2 and 3.3 are identical.

The 2DES experiment is however conducted on an ensemble i.e. statistical average, and so 3.1 is instead written as as

$$\rho(t) = \sum_i p_i\,|\psi_i\rangle\langle\psi_i|\,, \tag{3.4}$$

where p_i is the probability of the system being in state $|\psi_i\rangle$. Note that the density matrix in eq. 3.4 represents a statistical mixture of states and can not be

in general represented by a wavefunction. The ensemble measurement leads to an additional term in the Liouville von Neumann equation describing relaxation and dephasing which is far from trivial to tackle [99]. Perturbation theory is applied to Eq. 3.3 for the time-dependent perturbation $W(t) = -\hat{\mu}E(t)$ instead of the full Hamiltonian $\hat{H}$. $W(t)$ describes interaction of the electric field

$$E(t) = 2E_0(t)\cos(\omega t + \vec{k}\cdot\vec{r}) = E_0(t)\left(\mathrm{e}^{-\mathrm{i}\omega t + i\vec{k}\cdot\vec{r}} + \mathrm{e}^{+\mathrm{i}\omega t - i\vec{k}\cdot\vec{r}}\right), \tag{3.5}$$

where $\hat{\mu}$ is the transition dipole moment of the quantum system, ω – the optical frequency of the laser field, $\vec{k}$ – a wave vector and $\vec{r}$ is a space vector.

The Liouville von Neumann equation can be solved iteratively by integration and the result is expressed as a series of $\rho^{(n)}$, where (n) is the order in powers of $W(t)$. The signal detected in 2DES experiments is proportional to the 3$^{\mathrm{rd}}$ order nonlinear polarization of the sample:

$$\begin{aligned} P^{(3)}(t) &= \int_0^\infty \mathrm{d}t_3 \int_0^\infty \mathrm{d}t_2 \int_0^\infty \mathrm{d}t_1 E_3(t-t_3)E_2(t-t_3-t_2)\cdot \\ &\quad \cdot E_1(t-t_3-t_2-t_1)R^{(3)}(t_3,t_2,t_1) \end{aligned} \tag{3.6}$$

where $R^{(3)}(t_3,t_2,t_1)$ is 3$^{\mathrm{rd}}$ order nonlinear response function

$$R^{(3)}(t_3,t_2,t_1) = -\left(-\frac{\mathrm{i}}{\hbar}\right)^3 \langle \hat{\mu}(t_3+t_2+t_1)\,[\hat{\mu}(t_2+t_1),[\hat{\mu}(t_1),[\hat{\mu}(0),\rho(-\infty)]]]\rangle \tag{3.7}$$

where $\rho(-\infty)$ is the equilibrium density matrix before interaction with the light fields. The $P^{(3)}(t)$ can be interpreted as a convolution of the system's response $R^{(3)}(t_3,t_2,t_1)$ with the three excitation pulses E_1, E_2, E_3, interacting with the system at times 0, t_1, t_1+t_2, respectively. After three interactions with the field the system ends up in the optical coherence state (off-diagonal element of the density matrix), which emits an electric field at time $t_3+t_2+t_1$. Each of the electric fields $E_i(t)$ contains a sum of the 6 fields from the 3 excitation pulses. Each interaction causes a perturbation of the density matrix through the transition dipole moment operator. The three commutators in eq. 3.7 give pairs of terms with mutually reverse order so that the dipole moment operator can act on both sides of the density matrix. Out of 8 combinations, only four are independent. Together with the laser fields, $6\times6\times6\times4 = 864$ combinations exist. Each of the possible interaction sequences (pathways) given by eq. 3.6 can be represented by so called double-sided Feynman diagram, described in the next section.

3.3 Feynman Diagrams

Fortunately, most of the 864 interaction pathways are either not physical or they can be eliminated by experimental design. If we take advantage of the known

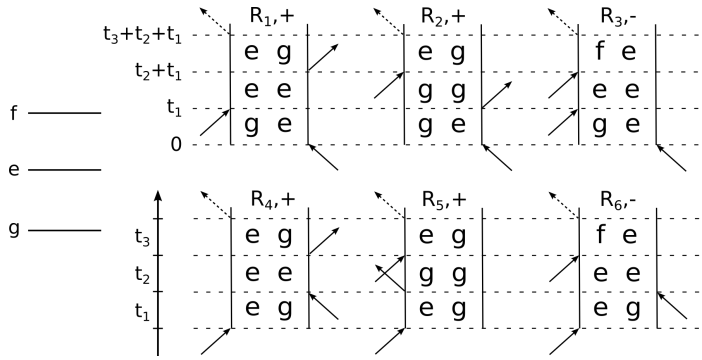

Figure 3.3: All Feynman diagrams excluding double quantum coherences for the three-level system. Excitation pulses interact (indicated by the arrows) with the density matrix (central part of the diagram) at delay times $0, t_1, t_2+t_1, t_3+t_2+t_1$. Pathways R_1, R_4 correspond to the stimulated emission, R_2, R_5 – to the ground state bleach and R_3, R_6 – to the excited state absorption. Pathways $R_1 - R_3$ describe the rephasing part of the response (first interaction from the right) compared to pathways $R_4 - R_6$, which are non-rephasing (first interaction from the left). An even number of interactions leads to a positive overall sign of the signal, whereas odd number of interactions leads to a negative sign.

pulse-ordering and rotating wave approximation [100], only four pathways will contribute to each phase-matching directions $-\vec{k}_1 + \vec{k}_2 + \vec{k}_3$ and $+\vec{k}_1 - \vec{k}_2 + \vec{k}_3$.

Each pathway can be viewed as a particular realization of the interactions from the subset of the 3$^{\text{rd}}$ order response. The six Feynman diagrams shown in Fig. 3.3 correspond to the following response functions:

$$\begin{aligned} R_1 &= i\langle\mu_3\mu_1\rho(-\infty)\mu_0\mu_2\rangle \\ R_2 &= i\langle\mu_3\mu_2\rho(-\infty)\mu_0\mu_1\rangle \\ R_3 &= -i\langle\mu_3\mu_2\mu_1\rho(-\infty)\mu_0\rangle \\ R_4 &= i\langle\mu_3\mu_0\rho(-\infty)\mu_1\mu_2\rangle \\ R_5 &= i\langle\mu_3\mu_2\mu_1\mu_0\rho(-\infty)\rangle \\ R_6 &= -i\langle\mu_3\mu_2\mu_0\rho(-\infty)\mu_1\rangle \end{aligned} \tag{3.8}$$

where $\mu_3 = \mu(t_3 + t_2 + t_1)$, $\mu_2 = \mu(t_2 + t_1)$, $\mu_1 = \mu(t_1)$, $\mu_0 = \mu(0)$. We note that we omit from the discussion double quantum coherence pathways [95]. The principle features of Feynman diagrams are listed below [100].

- The central part of a diagram contains the density matrix operator as it evolves in time, which flows vertically from bottom to top.
- The initial and final states are population states. Throughout the following discussion, the initial state will be always the ground state $|g\rangle\langle g|$, which is not displayed.

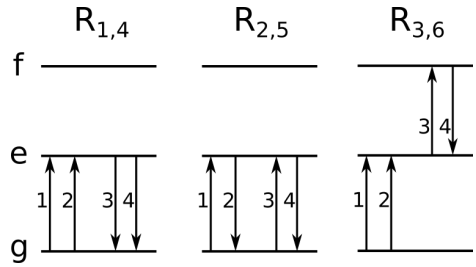

Figure 3.4: Analogous representation to the Feynman diagrams (or Liouville pathways) as in Fig. 3.3, shown on the system's energy levels.

- The interactions with the laser pulses are denoted by the arrows where their direction determines whether the field is $e^{-i\omega t+i\vec{k}\cdot\vec{r}}$ (pointing left) or $e^{+i\omega t-i\vec{k}\cdot\vec{r}}$ (pointing right).
- Interactions pointing towards the density matrix promote the *bra* or *ket* to higher levels, whilst interactions pointing outwards denote deexcitation of the relevant *bra* or *ket*.
- The frequency of the first and the last interactions determines the position of the signal in the 2D spectrum along ω_1, ω_3, respectively. The last interaction is the emission of the signal field (dashed line) and always points to the left.
- The overall sign of the diagram is determined by the number of the interactions with the *bra* side of the density matrix, i.e. from the right side of the $\rho(-\infty)$ in eq. 3.8.

In the following section we discuss how Feynman diagrams relate to the spectroscopic signals.

3.4 Contributing Signals

Fig. 3.3 shows all the possible pathways for a three-level system. They correspond to the same pathways as in Fig. 3.4, where they are represented as transitions between the energy levels of the system. Pathways $R_1 - R_3$ differs from $R_4 - R_6$ just by the time-ordering of the first two interactions. For example pathways R_1, R_2 evolve during t_1 and t_3 with switched *bra* and *ket* $|g\rangle\langle e|$ and $|e\rangle\langle g|$, respectively. This evolution corresponds to counter-propagating phase factors $e^{+i\omega_{01}t_1}$, $e^{-i\omega_{01}t_3}$ during t_1 and t_3, respectively. The ensemble dephasing, caused by the distribution of transition frequencies, and acquired during t_1 is reversed during t_3 which results in rephasing of the individual systems phase factors. In this way a photon echo is observed as a recurrence of the polarization signal when $t_3 = t_1$ [101]. The $R_1 - R_3$ pathways are therefore called "rephasing" and we can separate them by pulse ordering from $R_4 - R_6$. The latter are called

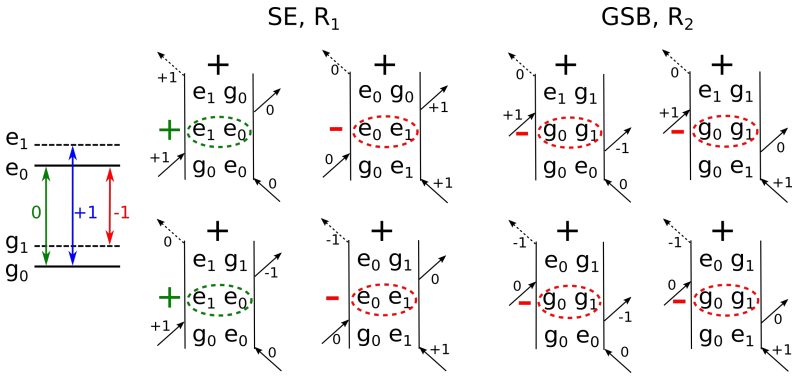

Figure 3.5: Coherence pathways for the four level scheme, which corresponds to the displaced oscillator model or alternatively to the excitonic dimer with a vibration included. The pathways are classified as SE or GSB and distinguished according to the $\pm\omega_2$ evolution (red and green). Overall sign of the pathway is denoted by a black sign above the diagram. The interactions including vibrational quanta are indicated by the numbers next to the interaction arrows.

"non-rephasing" pathways, which evolve with the same phase $e^{-i\omega_{01}t_1}$ and $e^{-i\omega_{01}t_3}$ during t_1 and t_3 (for the R_4, R_5) and represent a free induction decay [102].

In the 2DES experiment, the first two interactions prepare the density matrix, which then evolves freely during the population time t_2, in analogy to the delay between pump and probe pulses in PP experiment. Pathways R_1, R_4 evolve during t_2 in the excited state $|e\rangle\langle e|$, which is then probed and the final state becomes ground state $|g\rangle\langle g|$. Therefore these pathways correspond to stimulated emission (SE), which is typically plotted as a positive signal. On the other hand, diagrams R_2, R_5 evolve in the ground state $|g\rangle\langle g|$ during t_2. They represent ground state bleach pathways (GSB) and have positive sign, like SE. Pathways R_3, R_6 evolve in the excited state $|e\rangle\langle e|$ during t_2, but the last two interaction probe the absorption to the higher excited states. Therefore they correspond to the excited state absorption (ESA) and have opposite overall sign – negative in the 2DES convention.

All of the above mentioned pathways feature simple population-related dynamics due to relaxation, usually well described by multi-exponential models. Besides exciting populations, the broadband femtosecond excitation creates superpositions of the energy eigenstates of the sample, called coherences. These evolve in t_2 with the phase factor $e^{\pm i\omega_2 t_2}$ where the frequency ω_2 corresponds to the energy difference between the states in superposition. The evolution of the superposition can be observed experimentally as an amplitude oscillation along t_2 and is called coherence [103].

To illustrate the coherence pathways, we consider two electronic states with a single vibration level in both ground and excited states (see Fig. 3.5), used also as a model system in Chapter 4. Due to an increased number of pathways, only rephasing diagrams are shown. Four SE and four GSB pathways are identified

with R_1 and R_2 diagrams, respectively. Apart from signals that appear at different location in the 2D spectra (see Chapter 4 for details), the diagrams can be classified according to the phase factor, which is acquired during the t_2-evolution. In the case of the first two SE pathways, coherence $|e_1\rangle\langle e_0|$ evolves with phase $\mathrm{e}^{-\mathrm{i}\omega_2 t_2}$, which we denote as $+\omega_2$ evolution following the notation of [104]. Accordingly, for the other two SE pathways, the coherence $|e_0\rangle\langle e_1|$ evolves as $\mathrm{e}^{+\mathrm{i}\omega_2 t_2}$ and is denoted by $-\omega_2$. The analogous separation applies to the GSB pathways as well.

Full complex data have to be evaluated in order to separate the pathways according to the sign of ω_2. This is a unique feature of heterodyne detection schemes. Compared to PP, 2DES provides high spectral resolution along the excitation frequency ω_1, separates rephasing and non-rephasing pathways by the pulse ordering and for the coherence dynamics separates pathways according to the $\pm\omega_2$ evolution. These are the three most important ways in which 2DES disentangles highly congested signals. They were used in the analysis of the coherence oscillations in Paper IV. It is thus clear that for coherent phenomena, where the oscillation can substantially cancel out in PP measurements, 2DES is significantly superior and allows for more disentangled information and deeper understanding if analyzed carefully.

3.5 Polarization Resolved 2DES

Polarization Control

Polarization control in both steady state and time-resolved spectroscopies has been demonstrated to provide valuable information about the orientations of transition dipole moments [92, 105]. Pump probe anisotropy experiments pointed towards the possibility that electronic coherences were present in the light-harvesting pigment-protein complexes [27, 106]. In 2DES, four pulses are available for polarization control, which allows for a much broader range of polarization sequences compared to PP.

Each pathway represented by Feynman diagrams (see sec. 3.3) is associated with the orientational prefactor. It is proportional to the scalar product of the transition dipole moments involved and to the orientational prefactor, which depends on the relative orientations between individual laser pulses and the transition dipole moments. For the ensemble of isotropically oriented samples, it reads [107, 108]

$$\begin{aligned}\Omega_{ijkl}^{\alpha\beta\gamma\delta} = \frac{1}{30}[&\langle\cos\Theta_{\alpha\beta}\cos\Theta_{\gamma\delta}\rangle(4\cos\Theta_{ij}\cos\Theta_{kl}-\cos\Theta_{ik}\cos\Theta_{jl}-\cos\Theta_{il}\cos\Theta_{jk})+\\ &\langle\cos\Theta_{\alpha\gamma}\cos\Theta_{\beta\delta}\rangle(-\cos\Theta_{ij}\cos\Theta_{kl}+4\cos\Theta_{ik}\cos\Theta_{jl}-\cos\Theta_{il}\cos\Theta_{jk})+\\ &\langle\cos\Theta_{\alpha\delta}\cos\Theta_{\beta\gamma}\rangle(-\cos\Theta_{ij}\cos\Theta_{kl}-\cos\Theta_{ik}\cos\Theta_{jl}+4\cos\Theta_{il}\cos\Theta_{jk})]\end{aligned} \tag{3.9}$$

where i, j, k, l denote laser pulse polarizations and $\alpha, \beta, \gamma, \delta$ are the transition dipole moments of the system. The total prefactor determines the amplitude of each contribution (pathway) in the 2D spectrum.

The most relevant polarization sequence for separation of the vibrational and electronic coherence reads $(i, j, k, l) = (45°, -45°, 90°, 0°)$ or (CP) for short, for the isotropically oriented samples. E. g. for coupled non-parallel monomers A,B which form a dimer with two excitonic states, the only signal surviving the CP scheme is the electronic or mixed vibronic coherence.

To further elaborate, all the pathways can be divided into three groups according to the sequence of the transition dipole moments (either A or B) interacting with pulses 1–4. Firstly, all the interactions involve only one of the transition dipoles (AAAA) and skipping the symmetric pathways interacting with dipole B first. This case covers signals, corresponding to population relaxation and vibrational coherence. Secondly, the AABB interaction sequence describes the coupling and the energy transfer pathways between A and B. Finally, ABAB or ABBA sequences represent the excitonic and/or mixed coherence pathways. Using eq. 3.9, we can compare the orientational prefactors for all the above cases for standard all-parallel and CP 2DES, depending on the angle between A andB transitions (Fig. 3.6).

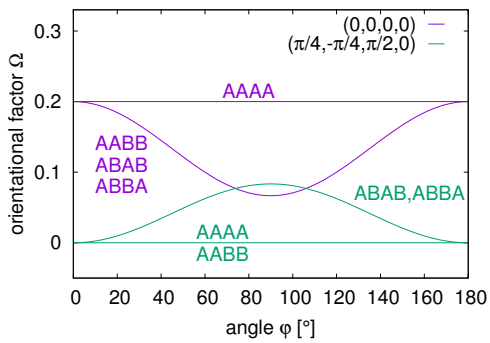

Figure 3.6: Orientational prefactor depending on the angle between the excitonic transitions of the dimer. All parallel measurement (purple) does not provide any strong selection and all pathways contribute to the overall signal. For the cross-polarized sequence (green) the only surviving signals are those, which alternate interactions with differently oriented transition dipoles for the two pairs of the excitation pulses (ABAB, ABBA). Population and vibrational coherence signals are completely suppressed for all angles between dipole moments.

Fig. 3.6 confirms that only electronic character coherences survive the CP measurement, and have the largest amplitude if the two excitonic state transition dipoles are mutually orthogonal. This is intuitive, since in the CP scheme the two pairs of interactions are also orthogonally polarized.

Vibronic mixing between vibrational and electronic degrees of freedom substantially complicate the analysis, which is discussed in Chapter 4, Papers IV,VII and [52, 109].

Experimental Implementation and leakage

Experimental implementation of the polarization resolved 2DES brings about several challenges. The CP scheme is very sensitive to accurate setting of the polarizations of the laser pulses. From eq. 3.9, we can calculate the ratio between the orientational prefactors of the desired electronic coherence pathway and possible leakage signal, for example the stationary diagonal peak, corresponding to population signal. Fig. 3.7 correlates the ratio to the angle between the two transitions A,B (φ) and detuning angle (θ_{err}) of the polarization of the first two laser pulses from the ideal CP scheme. The ratio of CP/AP signal strongly depends on the detuning angle and is only weakly dependent on the excitonic dipole moment orientations. Detuning just by 1° leads to a drop of the CP/AP ratio down to ~ 60, which is close to the typical value achievable in our experiments.

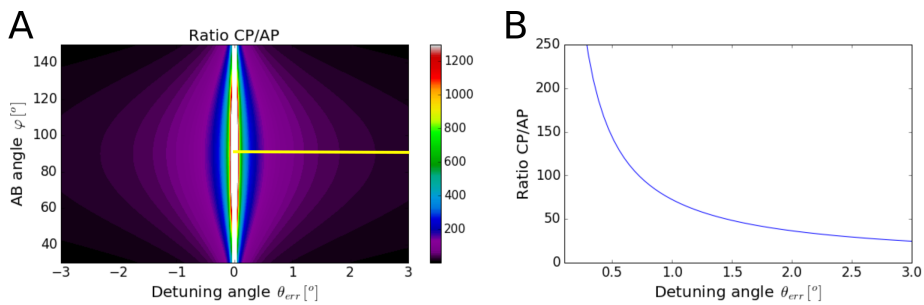

Figure 3.7: (A) Ratio between the cross-polarized (CP) and leaking all-parallel (AP) signal through the imperfectly set polarizers depends only weakly on the relative dipole moment orientation φ. However, detuning of the first laser pulse just by 1° leads to a drop of the CP/AP ratio down to ~ 60. (B) A cut along the yellow line of panel (A) for the case when the excitonic transitions are orthogonal to each other.

Another challenge in polarization-controlled 2DES is phasing of the CP data. Conventionally every 2D experiment has to be phased to a corresponding PP measurement, however this is fundamentally not possible for CP, because of the absence of corresponding PP experiment. In our work, we used the weak leakage signal to phase the CP measurements to the all-parallel PP. If we do not attempt to extract and compare the absolute phases of the coherent oscillations for the different points in the 2D spectrum, the slightly inaccurate phasing does not significantly affect the oscillation patterns.

Another complication that we have encountered is connected to the great selectivity of the CP sequence. During the pulse overlap, the pulse ordering is undefined and so excitation pulses may switch roles. This is a negligible effect for the all-parallel measurement, however switching the ordering of the pulses in the CP measurement destroys the selectivity. Since the non-selective wrong pulse ordering signal is much stronger compared to a very weak CP signal, it can

substantially affect even later population times beyond the pulse overlap region. For the case of the CP scheme, we found that wrong pulse ordering sequence will mostly hamper the lower cross-peak, which is usually investigated in relation to the coherent dynamics (see Paper VI).

3.6 Heterodyne Detected Transient Grating

Long lived coherences are readily observed in 2DES. However, the experiment is time-demanding and usually does not allow the sampling of the whole coherent dynamics due to the available time afforded by sample and laser stability. When comparing to PP, averaging over excitation frequency provides better signal to noise ratio in PP at the expense of spectral congestion (see Section 3.4). In between the two, there is heterodyne detected transient grating (TG), which provides both real and imaginary part of the response and allows for exactly the same polarization control as 2DES. However as in PP, the signal is integrated along ω_1 and it is not possible to separate the rephasing and non-rephasing signals. Implementation of TG is straightforward in the 2DES setup, the time-delay between the first two pulses is fixed to be 0 instead of scanning it to cover the system dephasing time (see Section 3.1).

Coinciding first two pulses in time is reminiscent of the pump pulse in PP, however, the beam geometry ensures the emission of the 3^{rd} order polarization is in the phase matching direction, which is in principle background free. No scanning of the t_1 delay saves time and enables longer population scans and averaging.

This allows for a clean and fast check of the coherent oscillations in the CP experiments, which provides better estimates of the dephasing times and accurate frequency resolution. In Paper V, we compared oscillation modes identified in CP-TG to the results obtained from 2DES and resonance Raman measurements and observed a good agreement between all of them.

Chapter 4

Energy Transfer Induced Coherence Shift

After absorption of a femtosecond laser pulse, molecular valence electrons get promoted to the higher lying orbitals. In light-harvesting proteins, the electronic transitions of the individual chromophores are coupled. The electronic transitions also couple to the intramolecular and protein vibrations (electron-phonon coupling). Since the excitation is coherent and spectrally broad, the evolution of all the states and their superpositions in all the molecules will be triggered in unison with the same quantum mechanical phase. The short pulse induces polarization oscillation in the molecules, which can be measured as optical signal oscillating in the time-resolved optical experiments. This is macroscopic manifestation of the evolution of the quantum mechanical superposition states denoted as coherences. Depending on the nature of the states in the superposition, the coherences can posses more vibrational or electronic character. The interaction of the excited states with the environment causes dephasing of this coherent motions by destroying the initial phase relationship. Since the nuclei are $\sim 1000\times$ heavier than electrons, much faster dephasing is expected for the electronic coherences [54].

Following the concepts of decoherence theory, there are in principle two ways how to observe the quantum coherence phenomena [110]. First, reducing the system-bath (environment) interaction decreases the dephasing rate of the coherences, hence extending their lifetime and facilitating their observation and possible utilization. This approach is typical for quantum computing schemes [111]. The second option is to employ femtosecond time resolution to observe the ultrafast dephasing rates in molecular and light-harvesting systems. 2DES takes mostly advantage of the latter, in addition, experiments are often done at low temperatures to reduce the bath influence on dephasing (see Chapter 3).

The first experiments observed the coherent motions of nuclei in the form of vibrational wavepackets in the ground electronic state [112]. During the course of 1980s, the field of femtochemistry was born. It became possible to observe not only the coherent motions of the nuclei in the ground state but

also in the excited state, which served as a probe of photo-induced chemical reactions of simple molecules [113]. These efforts culminated by two Nobel prizes awarded in chemistry for the development of ultrafast spectroscopies in 1986 and 1999. In contrast to simple molecules, the photosynthetic light-harvesting proteins are multichromophoric systems of huge complexity and many degrees of freedom [2]. Vibrational as well as electronic coherences have been observed in the PP experiment in both light-harvesting antennas [106] and reaction centers [26, 27, 41].

It was surprising when the long-lived oscillatory features detected in 2DES were assigned to purely electronic coherences both at 77 K and room temperature [114, 115], with dephasing times that were beyond any expectations [54]. Recent theoretical work on vibrational and mixed vibronic coherences has provided more viable explanation for the long-lived oscillations in the light-harvesting proteins [51, 52, 116]. However, these ideas were still lacking strong experimental support. To address these issues, we employed polarization-resolved 2DES (see Chapter 3) to separate purely vibrational coherences from the mixed vibronic and/or electronic ones in bacterial RC_{sph} (see Papers I). We found even more significant mismatch between the electronic-like coherence lifetime of a couple of picoseconds and the ~ 150 fs lifetime of the participating excited states. Eventually, the extended experiments and improved data analysis allowed us to solve the mismatch. We introduced a new photophysical process, responsible for the observed oscillatory patterns, which was termed Energy Transfer Induced Coherence Shift (ETICS). We show that by employing ETICS mechanism we are able to explain the observed coherent dynamics in RC_{sph}. In the following, the principles of the ETICS are described, which serves as an extension of Paper IV.

4.1 Model System

To illustrate ETICS features, the minimal model of a two-level system with a single vibrational level was employed (see Fig. 4.1A). We assume $\sim 230\,\mathrm{cm}^{-1}$ Gaussian line-width for the electronic transition, which is completely covered by the laser spectrum (see Fig. 4.1B). The entire analysis is performed for the rephasing part of the 2D spectra, since the non-rephasing part contains analogous information. Only the Liouville interaction pathways resulting in coherence, oscillating in population time t_2 are discussed (see Section 3.3, 3.4). To obtain analogous signals from the experimental data, the exponential population decay (contributions from the population pathways) should be subtracted and the remaining oscillating residuals correspond then to the coherence pathways. Additional Fourier transformation over t_2 for each point in 2D spectra allows to correlate coherent oscillation amplitude of a given oscillation frequency ω_2 to the excitation and detection frequency (ω_1, ω_3) spectrum, resulting in the so called "oscillation map" [104]. For each oscillatory pathway (see Section 3.4), complex oscillatory data with $\omega_2 = 600\,\mathrm{cm}^{-1}$ frequency was generated with the same $\sim 230\,\mathrm{cm}^{-1}$ Gaussian envelope as for the electronic transition. The initial amplitude of the oscillation is the same for both GSB and SE pathways. The

full t_2-window for the oscillations is 6 ps and their lifetime is set to 200 fs and 1500 fs for the SE and GSB, respectively. Depending on the peak position within 2D spectrum, the phase sweeps antidiagonally across the peak for the rephasing part of the response [116]:

$$\phi(\omega_1, \omega_3, \pm\omega_2) = \pm \arctan\left(\frac{\sigma(\omega_3 - \omega_1)}{-\omega_1\omega_3 - \sigma^2}\right) \tag{4.1}$$

where ϕ is the phase and σ is the width of the absorption band.

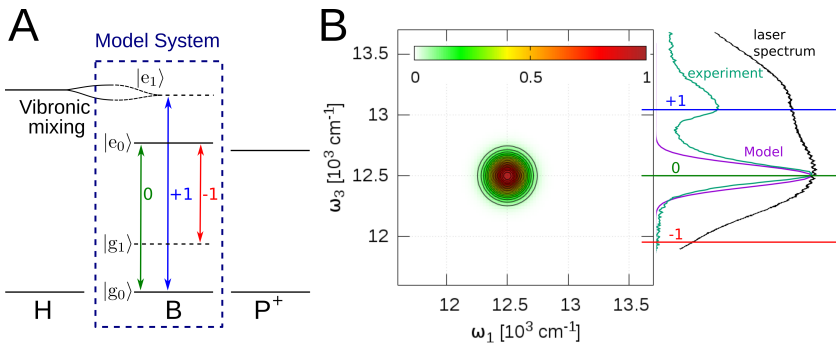

Figure 4.1: (A) Energy level diagram of the oxidized RC_{sph}. Blue rectangle shows the four-level model system used to simulate the B band. The purely electronic transition (green) and the transitions including ± 1 vibrational quantum (red and blue) are indicated. (B) Rephasing real part of the 2DES model spectrum showing the single Gaussian peak corresponding to the B band. Linear absorption of the model (magenta) and the RC_{sph} (green) is shown together with the experimental spectrum of the laser pulse considered for the theoretical analysis (black).

Even though the phenomenological model is very simple, it is related and to some extent comparable to the RC_{sph} measurements. In the experiments, we measured oxidized bacterial reaction centers from *Rba. sphaeroides* (see Section 2.3). The laser spectrum covers two bands of RC_{sph}, accessory BChl *a* (B) and BPheo *a* (H) (see Fig. 4.1B). Decay channel from the lower lying B state to the excitonic P^+ state of the oxidized special pair (P) is responsible for the rapid decay of B (Paper I, [26, 27]). Our model is surprisingly well suited for describing coherent dynamics of B. The oscillation mode $\omega_2 = 600\,\mathrm{cm}^{-1}$ is close to the excitonic gap between B–H ($\omega_2 = 620\,\mathrm{cm}^{-1}$), the most relevant candidate for potential electronic coherence (Fig. 4.1A, Paper I). Low Huang-Rhys (HR) factors (~ 0.01) describing the electron-phonon coupling, and limited laser spectrum ($\sim 1500\,\mathrm{cm}^{-1}$), precludes transitions including ± 2 vibrational quanta. In addition, 77 K temperature in the experiments ensures that molecules initially are in the vibrational ground state. This allows us to limit the model to single vibrational level in both the ground and excited states. Moreover, the selected lifetimes of 200 fs and 1500 fs correspond to the lifetime of the excited state of B and lifetime of the ground state coherence, respectively. No ESA pathways

present in the model correspond to the fact that the ESA in RC_{sph} is weak.

4.2 Coherence Pathways

Taking advantage of the heterodyne detection used in 2DES, both the real and imaginary part of the refractive index are obtained. If the complex FT is performed on a full data set, it is possible to separate oscillatory pathways evolving either with $-\omega_2$ for $e^{+i\omega_2 t_2}$ or $+\omega_2$ for $e^{-i\omega_2 t_2}$ during the population time t_2 (see Section 3.3). In other words, we separate the density matrix elements $|0\rangle\langle 1|$ and $|1\rangle\langle 0|$, where the $|1\rangle$ state lies higher in energy than $|0\rangle$. The sign of ω_2 is coded by color in all Feynman diagrams (see Fig. 4.2A). Instead of $|0\rangle$ and $|1\rangle$ we use $|e\rangle, |g\rangle$ for excited and ground state, respectively, with a subscript indicating occupation of the vibrational level.

Fig. 4.2A shows all the possible oscillatory pathways in the real rephasing part of the signal and how they appear in the experimental oscillation maps for the oxidized RC_{sph} at $\omega_2 = \pm 560\,cm^{-1}$. The complex FT further disentangles the oscillations according to the sign of ω_2 [104, 117]. Note that spectral separation of the peaks in the oscillation maps equals the vibrational quantum (or excitonic splitting in the case of electronic coherence). As illustrated in Fig. 4.2 and explained in Section 3.3, all the maps are accessible from the experimental data, hence allowing for direct comparison to the modeling results.

4.3 Reproducing Experiment

Fig. 4.3 illustrates the central problem of the coherent dynamics in RC_{sph} and its solution by introduction of the ETICS process. According to the experimental results, excited state lifetime is 150 fs and the dephasing of the ground state coherences takes a couple of picoseconds. However, the amplitude maps based on this observation using pathways showed in Fig. 4.2 yield clear mismatch with the experimental data (see Fig. 4.3). Including ETICS leads to the substantially improved match with the experimental data, as well as it provides better intuitive physical picture, justifying dephasing times, oscillation amplitude cancellations and phase shifts. Below we compare various model simulations in detail.

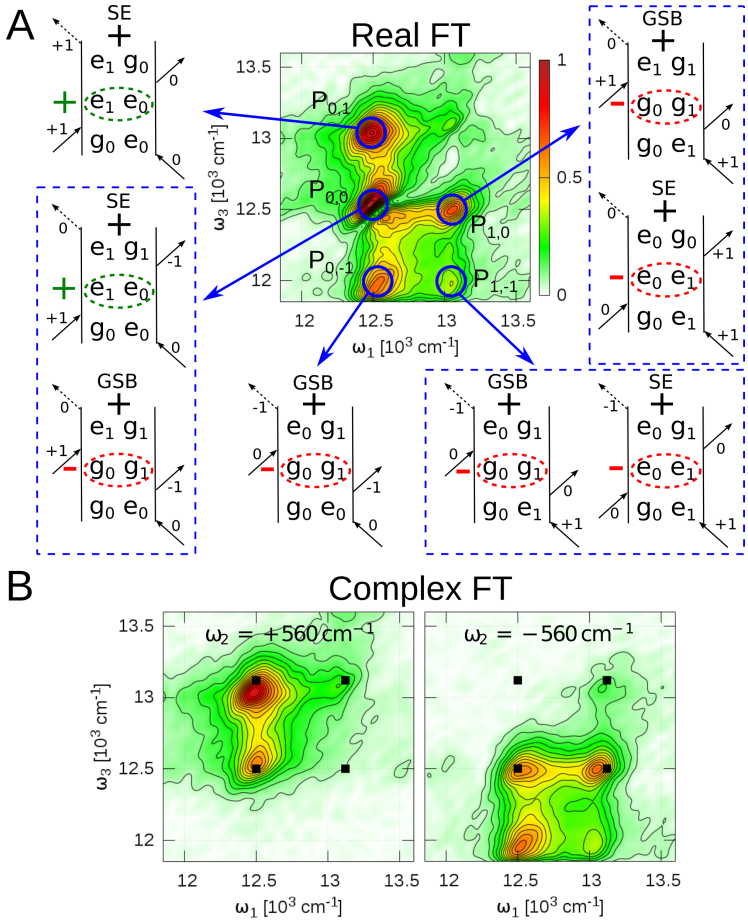

Figure 4.2: Oscillation maps of oxidized RC_{sph} extracted from the 2DES experiment. (A) Real FT oscillation map with all the pathways contributing to the oscillatory part of the signal. The pathways are sorted by the GSB or SE character, position in the oscillation map and sign of the evolution during t_2 ($+\omega_2$ in green, $-\omega_2$ in red). All pathways have positive overall sign (black) as explained in Section 3.3. $|e\rangle, |g\rangle$ mark the excited and the ground state, subscript indicating vibrational quantum. Numbers next to the interaction arrows mark the changes in vibrational quantum upon the transitions. Positions of the peaks are marked as $P_{i,j}$, where i, j denotes the vibrational quantum of the first and last transition, respectively. (B) Complex FT of the same data set allows to separate contributions from $\pm\omega_2$ pathways, following exactly the scheme in (A).

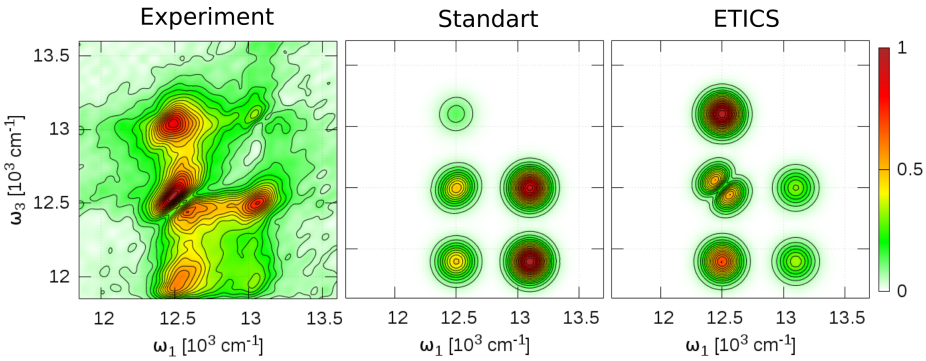

Figure 4.3: Comparison of the experimental (left) and simulated oscillation amplitude maps. Standard model based on the GSB and SE pathways (middle) leads to the mismatch with the experiment. Addition of the ETICS process and pathways (right) yields a good match with the experiment.

In order to correctly reproduce the oscillation maps, the effect of the laser spectrum has to be taken into account. As described in Section 4.1, the limited spectrum allows to restrict the model to single vibrational level at each electronic state. Moreover, Fig. 4.2A shows that each pathway is associated with a different sequence of interactions in terms of vibrational quanta, depending on the position where the pathway appears in the 2D spectrum. The positions are assigned in Fig. 4.2 and used throughout the text. In order to properly account for the pulse spectrum effect, it is important to realize that the measured interferogram is divided during the data treatment by the square root of the pulse spectrum intensity. That is analogous to division by the electric field of the last interaction or signal emission (dashed arrows in Fig. 4.2A). To allow the comparison to experimental oscillation maps, each model pathway is scaled by $\sqrt{I_i \cdot I_j \cdot I_k}$, where I is the spectral intensity of the pulse at the wavelength, corresponding to the given transition energy including vibrational quantum i, j, k.

The real and complex FT of the model oscillations along t_2 are performed exactly as in the experiment for the oscillatory residuals. If we assume the short-lived SE (200 fs) as compared to the lifetime of the GSB coherence (1500 fs), the amplitudes of the SE peaks in the oscillation maps will be substantially lower (Fig. 4.4A). Overall, the real FT oscillation map does not match the experimental one (Fig. 4.2), mainly due to the weak SE signal.

For the light-harvesting pigment-protein complexes, correlated fluctuations of the site energies have been suggested to prolong the lifetime of the SE coherences [50, 118]. Fig. 4.4B shows that even allowing the SE to have the same lifetime as the GSB coherence (1500 fs), the oscillation maps still do not match experimental observation. A very prominent feature in the experimental maps is the cancellation on the diagonal of the peak $P_{0,0}$ (see Fig. 4.2), which is completely missing in the modeled map. Moreover, the peaks $P_{1,0}$ and $P_{1,-1}$ in the model are too intense due to constructive interference of the SE and GSB pathways. Importantly, the long-lived SE is not physically feasible for RC_{sph}, since the

excited state lifetime of H and B is ~ 150 fs, which is much shorter than in the most other light-harvesting antennas. Therefore our first report on long–lived coherences with strong electronic character in RC_{sph} could not provide satisfactory enough interpretation (Paper I).

To introduce the ETICS process, we compare its pathways to the progenitor SE pathways; each ETICS pathway has the same first two interactions as one of the SE pathways leading to the excited state coherence in Fig. 4.5. The EET occurs in ~ 150 fs to an acceptor (P^+ state for the oxidized RC_{sph}), but the coherence is left behind on the donor, now evolving in the electronic ground state. This is the reason why the signals stemming from the ETICS pathways dephase on the picosecond timescale, even though originally the coherences were created in the short-lived excited state. The last two interactions are again the same as for the SE analogues. The only change is that the third pulse interacts from the left side of the density matrix (pathway diagrams in Fig. 4.5). All the ETICS pathways have therefore opposite overall sign (see Section 3.3) compared to the SE analogues (the overall sign of the signal or pathway should not be confused with the $\pm\omega_2$ sign, which remains the same in ETICS, see Fig. 4.5). We note that the overall sign also depends on Franck-Condon factors i.e. wavefunction overlaps, which is however not needed to consider here. Pathways appearing at the same positions in oscillation map have the same Franck-Condon factors and therefore, the oscillation map amplitudes do not change, including the constructive or destructive interference patterns.

The long dephasing time and changed sign of the ETICS pathways are crucial features. Since the frequency domain oscillation maps lack any time-resolution, the high amplitude of the SE-like signals observed in the experiment imply the long dephasing time. In contrast to the case of the long-lived SE, opposite sign of the ETICS leads to the destructive interference with GSB pathways at positions $P_{0,0}$, $P_{1,0}$, $P_{1,-1}$. If the initial amplitude of the oscillations is the same for excited state (ES) and ground state (GS), and 100 % of the SE is converted to the GS via ETICS, the cancellation of the $P_{1,0}$, $P_{1,-1}$ is complete as can be seen in Fig. 4.4C. The question arises, why the interference at $P_{0,0}$ shows the nodal line as observed in the experiment and not the complete cancellation as for the other two peaks. The explanation lies in the phase sweep associated with each of the oscillation peaks. The phase sweeps in the opposite direction for $+\omega_2$ and $-\omega_2$, respectively (Eq. 4.1). In positions $P_{1,0}$, $P_{1,-1}$ the interfering pathways are both $+\omega_2$, only the ETICS pathway has the opposite overall sign (the phase sweep remains the same though), therefore the oscillations cancel out perfectly. On the other hand at $P_{0,0}$ the ETICS pathway has $-\omega_2$ sign in contrast to the $+\omega_2$ sign of the GSB. Therefore the phase sweeps in opposite direction with the overall effect of the nodal line going diagonally through the $P_{0,0}$ peak center (see Fig. 4.4C).

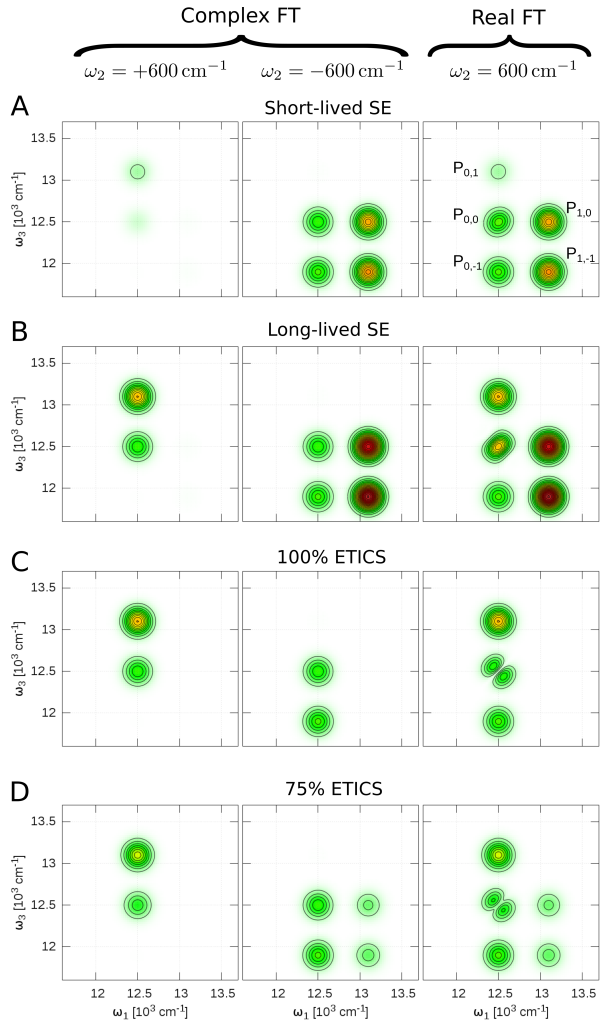

Figure 4.4: Simulated oscillation maps illustrate features of the ETICS mechanism. All the pathways are separately scaled by the excitation pulse intensity showed in Fig. 4.1. Left and middle panels show the complex FT amplitude maps for the $+\omega_2$ and $-\omega_2$ pathways, respectively. Right column shows the real FT transform combining $\pm\omega_2$ pathways together. No vibronic mixing effects are included here. (A) Short-lived SE compared to GSB yields a rectangular pattern mostly located below the diagonal. (B) Long-lived SE can not reproduce the cancellation on the diagonal and overestimates the amplitude at $P_{1,0}$, $P_{1,-1}$. (C) If the ETICS exhibits exactly the same oscillation amplitude as the GSB, resulting oscillation map shows perfect cancellation at $P_{1,0}$, $P_{1,-1}$ and ideal nodal line on the diagonal. (D) If the ETICS is only 75 % efficient, nodal line gradually loses contrast and peaks $P_{1,0}$, $P_{1,-1}$ reappear.

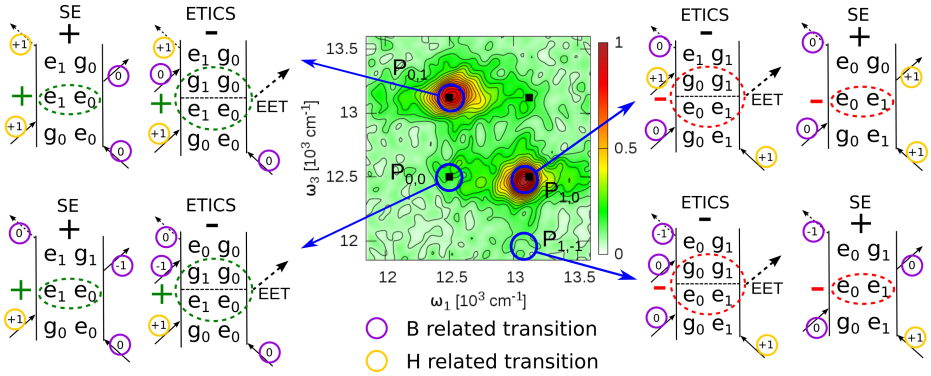

Figure 4.5: SE pathways together with their ETICS analogues. The only difference between them is that the third pulse interacts from the left side of the diagram, which ultimately leads to the opposite sign of the signal (in black). However, the ω_2 sign is conserved (in red and green). The laser interactions are divided according to the B or H character. These electronic transitions are favored compared to the vibronic transitions, due to the low HR factors of B. The oscillation map is extracted from the cross-polarized experiment (real part) for the $\omega_2 = 650\,\mathrm{cm}^{-1}$ which is strongly enhanced in cross-polarized measurement compared to the other modes. The pattern exactly follows the oscillations expected from the purely electronic coherences.

The last example in Fig. 4.4D shows the oscillation map in the case when ETICS signal has the 75 % amplitude as compared to the GSB contributions. This can be the situation when the coherence shift to the GS is not 100 % efficient. The corresponding effect on the oscillation map is that the nodal line has less contrast and peaks $P_{1,0}$, $P_{1,-1}$ do not show perfect cancellation.

Even though 75 % efficient ETICS reproduces the experimental oscillation maps well, the match is not perfect and 100 % efficient ETICS cannot be excluded. This is the case, because one important ingredient was omitted from the model, which is the effect of the vibronic mixing. From the experimental observations, we show that the vibronic mixing is necessary for the interpretation of data (Paper IV) and we evaluated it in Paper VII. However estimation is not completely robust without the system specific, detailed quantum mechanical modeling of the relevant part of the RC_{sph} protein. The vibronic mixing in relation to ETICS will be addressed in Section 4.5.

4.4 Additional Features of ETICS

As mentioned above, the initially created coherence in the ES is shifted to the GS gradually as the EET step proceeds. Hence before the EET is completed we expect contributions to the signal from both the purely SE and ETICS pathways. Since the ETICS pathways have the opposite overall sign, the decay of SE and rise of the ETICS signal implies gradual π-phaseshift in the time domain on the time

scale of the EET. This is exactly what we observed in both polarization-resolved 2DES and TG (Paper IV,V). The model presented in the previous section does not include the gradual shift from SE to ETICS. It corresponds to the analysis of the experimental data, where the first 216 fs were omitted from the FT, the timescale of the EET and the decay (rise) of SE (ETICS), i.e. π-phaseshift.

4.5 Vibronic Mixing

ETICS is a very general process, the only requirement is that the vibrational cooling or dephasing of the electronic coherence has to have comparable lifetime to the EET timescale. This is usually achieved by substantial coupling between donor and acceptor sites. In addition, the multitude of vibrational modes of the chromophores in the light-harvesting proteins leads to the vibronic mixing effects. The mixing arises from the coupling between electronic and vibrational degrees of freedom, mainly for the transitions that are close to resonance. The vibronic mixing was suggested to have a twofold effect on the coherent oscillations. First, the electronic part of the coherence extends the lifetime towards the vibrational dephasing time, as the vibrational coherence borrows the oscillator strength of the electronic transition [51]. Second, some of the purely GSB coherences are enhanced and can even survive the cross-polarization schemes designed to completely suppress them [52].

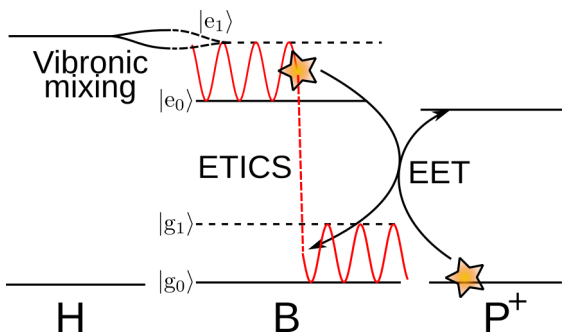

Figure 4.6: ETICS scheme for the oxidized RC_{sph}. Vibronically mixed excited state coherence is shifted to the ground state of B upon excitation energy transfer to P^+. Vibronic mixing causes the dual character of $|e_1\rangle$ state and therefore two ETICS pathways survive the cross-polarization measurement.

The vibronic mixing is essential to explain our observation of the ETICS process in the cross-polarized 2DES experiments (Papers IV,VI). In the case of RC_{sph}, the lowest electronic transition of H is close to resonance with the vibronic transitions of B with 560, 650 cm^{-1} vibrational modes, which leads to the vibronic mixing in the excitonic framework. P^+ plays the role of the efficient excitation energy acceptor from B, thus EET competes with the vibrational dephasing in the B excited state manifold. The full scheme of the ETICS process

is depicted in Fig. 4.6.

In our notation, the $|e_1\rangle$ state is a mixed state for the close-to-resonance mode, sharing the vibrational character of B and the electronic character of H. Therefore two orthogonally polarized pulses can sequentially probe both characters of the $|e_1\rangle$ state, which gives non-zero signal in cross-polarized measurement of the peaks $P_{0,1}$, $P_{1,0}$ (see Chapter 3, Fig. 4.5 and Paper IV). In other words, the two transitions experience slightly different angle of the transition dipole moment, which can be quantitatively evaluated (Paper VII). On the other hand the $|e_0\rangle$ state has a purely electronic character of B, and thus the pathways contributing to $P_{0,0}$, $P_{1,-1}$peaks do not survive the cross-polarized sequence. The pattern resulting from the ETICS process and observed in the cross-polarized measurement follows exactly the oscillation map pattern expected from the purely electronic coherence [116]. The long-lived ETICS coherent oscillations can be therefore easily mistaken for the electronic coherences that were claimed to be witnesses of the wave-like energy transfer in light-harvesting complexes [114, 115]. Proposition of the ETICS mechanism calls for the re-examination of such hypotheses.

4.6 ETICS Instruction Manual

In this section, the main features which identify the ETICS mechanism in the 2D spectra are presented:

1. Strong and unexpectedly long-lived signal at $P_{0,1}$ position where only the SE/ETICS contributes in the rephasing part of the 2D spectra (assuming that ESA contributions are weak).

2. Cancellation on the diagonal position $P_{0,0}$ in the rephasing oscillation map extracted from real part of the data.

3. π-phase shift observed on the time scale of the EET transfer, which is mostly visible at the crosspeaks. This can be difficult to observe if many modes beat over each other. Another complication can arise for lower frequency modes of $\leq 200\,\mathrm{cm}^{-1}$ since the spacing between the peaks is given by the mode's frequency and contributions from different pathways can overlap.

4. Considering the spectrum of the excitation pulse, the oscillation amplitudes on the position $P_{1,0}$, $P_{1,-1}$ are lower in intensity than expected.

4.7 ETICS and Incoherent Energy Transfer

Even though we observe ETICS process via coherent dynamics, it is relevant to incoherent EET between the population states too. So far, two mechanisms have been proposed on how the vibrational structure of the excited state can contribute to the EET efficiency. First, excited state vibrational levels increase the total

absorption cross-section by increasing the overall density of states available for absorption (Fig. 4.7, left). EET then proceeds from the vibrationally relaxed electronic state. Second, in analogy to the hot electron transfer, vibronically excited donor can transfer resonantly from unrelaxed state as suggested for the carotenoid to chlorophyll energy transfer [119] (Fig. 4.7, middle). Both mechanisms are independent of the vibrational structure of the ground state. ETICS however suggests that the ground state vibrational manifold can be equally important for the EET. The ETICS process implies resonant EET from unrelaxed donor to vibrationally relaxed acceptor (Fig. 4.7, right). This EET is followed by the vibrational cooling on the picosecond timescale in the ground state of the donor. If the EET is ultrafast, as in the RC_{sph}, the ETICS might be a very efficient way how to decouple the EET from the vibrational cooling.

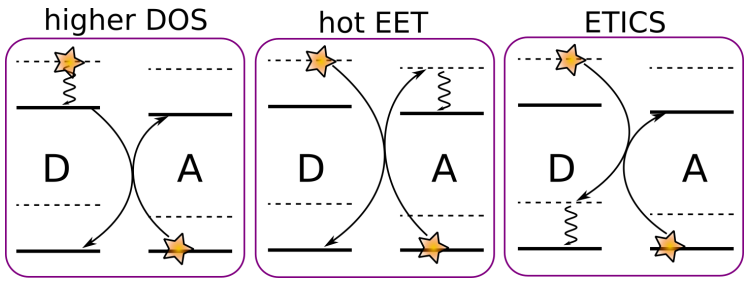

Figure 4.7: Schemes of how the vibrational structure can facilitate EET between the molecules with similar electronic transition energies. (Left) Higher density of states (DOS) increases the absorption cross section. (Middle) Hot EET from unrelaxed donor, followed by the vibrational relaxation in the excited state of the acceptor. (Right) ETICS allows for the resonant EET between unrelaxed donor and relaxed acceptor on the femtosecond timescale. The excessive energy is later dissipated within picoseconds via vibrational cooling of the donor ground state.

4.8 ETICS in Other experiments

At the moment, only a limited amount of publications contain detailed analysis of the oscillation dynamics in 2DES in form of oscillation maps. It is therefore difficult to judge if ETICS would be more adequate interpretation of the published experimental data. Regarding reaction centers, Fuller et al. investigated photosystem II RC and included theoretical modeling of the oscillation maps for the rephasing part of the 2D spectra [120]. Experimental observation indicates cancellation of the oscillation amplitude on the diagonal peak, one of the main features of the ETICS mechanism. Moreover the modeling can not reproduce this cancellation, another strong indication that ETICS might be at play.

Theoretically, very similar process to ETICS has been investigated and discarded for the case of chlorosomes [121].

4.9 Conclusion

In the cross-polarized 2DES experiments, ETICS signal serves as a witness of the vibronic mixing, which can be quantitatively evaluated (Paper VII). Even though in principle ETICS does not depend on the vibronic mixing, both effects are expected to coexist in the light-harvesting proteins. This is due to the interplay of the vibrational structure of the chromophores, electronic couplings and ultrafast EET timescales.

The only restriction for ETICS is that the dephasing of the coherent oscillations in the excited state is comparable to or longer than the EET timescale. We note that exactly the same condition is necessary for the proposed electronic coherence to potentially play any role in the light-harvesting processes. before drawing any conclusions about the effect of the quantum coherence in the light-harvesting, ETICS mechanism should be considered. We believe that only after the full understanding of the fundamental coherent processes and their interplay, the quantum coherence can be utilized in the new generation of functional materials. Nevertheless, the question of how important is the ETICS channel for the overall efficiency of the EET needs to be addressed in the future.

Bibliography

[1] Devens Gust, David Kramer, Ana Moore, Thomas a. Moore, and Wim Vermaas. Engineered and Artificial Photosynthesis: Human Ingenuity Enters the Game. *MRS Bull.*, 33:383–387, 2008.

[2] Robert E. Blankenship. *Molecular Mechanism of Photosynthesis*. Blackwell Science Ltd, 2002.

[3] Hans-Holger Rogner. *World Energy Assessment. Energy and the challenge of Sustainability*. UNDP, 2000.

[4] W B Whitman, D C Coleman, and W J Wiebe. Prokaryotes: the unseen majority. *Proc. Natl. Acad. Sci. USA*, 95(12):6578–6583, 1998.

[5] Michael T. Madigan and Deborah Jung. *The Purple Phototrophic Bacteria, chapter 1: An overview of Purple Bacteria Systematics, Physiology, and Habitats*. Springer Science, 2009. pp. 2–15.

[6] Theo A. Hansen and Hans van Gemerden. Sulfide utilization by purple nonsulfur bacteria. *Arch Mikrobiol.*, 86(1):49–56, 1972.

[7] J Imhoff. *Taxonomy and physiology of phototrophic purple bacteria and green sulfur bacteria*. 2004.

[8] H Gemerden and Jordi Mas. *Ecology of phototrophic sulfur bacteria*. 2004.

[9] LNM Duysens. Transfer of Light Energy Within the Pigment Systems Present in Photosenthesizing Cells. *Nature*, 168:548–550, 1951.

[10] Rienk van Grondelle and Hans van Gorkom. The birth of the photosynthetic reaction center: the story of lou duysens. *Photosynth. Res.*, 120(1-2):3–7, 2014.

[11] MK Sener, John D Olsen, C Neil Hunter, and Klaus Schulten. Atomic-level structural and functional model of a bacterial photosynthetic membrane vesicle. *Proc. Natl. Acad. Sci.*, 104(40):15723–28, 2007.

[12] Svetlana Bahatyrova, Raoul N Frese, C Alistair Siebert, John D Olsen, Kees O Van Der Werf, Rienk Van Grondelle, Robert a Niederman, Per a Bullough, Cees Otto, and C Neil Hunter. The native architecture of a photosynthetic membrane. *Nature*, 430(August):1058–1062, 2004.

[13] Margus Rätsep, Zheng Li Cai, Jeffrey R. Reimers, and Arvi Freiberg. Demonstration and interpretation of significant asymmetry in the low-resolution and high-resolution Qy fluorescence and absorption spectra of bacteriochlorophyll a. *J. Chem. Phys.*, 134(2), 2011.

[14] Bruno Robert, Richard J. Cogdell, and Rienk van Grondelle. *Light-Harvesting Antennas in Photosynthesis, chapter 5: The Light-harvesting System of Purple Bacteria.* Kluwer Academic Publishers, 2003. pp. 169–194.

[15] V Sundström, Tõnu Pullerits, and Rienk van Grondelle. Photosynthetic light-harvesting: reconciling dynamics and structure of purple bacterial LH2 reveals function of photosynthetic unit. *J. Phys. Chem. B*, 103:2327–2346, 1999.

[16] V. Sundström, R. van Grondelle, H. Bergström, E. øAkessonPOZOR, and T. Gillbro. Excitation-energy transport in the bacteriochlorophyll antenna systems of rhodospirillum rubrum and rhodobacter sphaeroides, studied by low-intensity picosecond absorption spectroscopy. *Biochimica et Biophysica Acta (BBA) - Bioenergetics*, 851(3):431–446, 1986.

[17] John T. M. Kennis, Alexandre M. Streltsov, Simone I. E. Vulto, Thijs J. Aartsma, Tsunenori Nozawa, , and Jan Amesz. Femtosecond dynamics in isolated lh2 complexes of various species of purple bacteria. *J. Phys. Chem. B*, 101(39):7827–7834, 1997.

[18] T Pullerits, M Chachisvilis, and V Sundström. Exciton delocalization length in the B850 antenna of Rhodobacter sphaeroides. *J. Phys. Chem.*, 100(95):10787–10792, 1996.

[19] S Hess, M Chachisvilis, K Timpmann, MR Jones, GJS Fowler, CN Hunter, and V Sundström. Temporally and spectrally resolved subpicosecond energy transfer within the peripheral antenna complex (lh2) and from lh2 to the core antenna complex in photosynthetic purple bacteria. *Proc. Natl. Acad. Sci.*, 92:12333–37, 1995.

[20] Tomáš Polívka and Villy Sundström. Ultrafast dynamics of carotenoid excited States-from solution to natural and artificial systems. *Chemical reviews*, 104(4):2021–71, April 2004.

[21] P Müller, X P Li, and K K Niyogi. Non-photochemical quenching. A response to excess light energy. *Plant Physiol.*, 125(4):1558–1566, 2001.

[22] Gernot Renger and Thomas Renger. Photosystem ii: The machinery of photosynthetic water splitting. *Photosynth. Res.*, 98(1-3):53–80, 2008.

[23] Kazuhiko Kinosita Jr. Real time imaging of rotating molecular machines. *FASEB J.*, 13(9002):s201–S208, 1999.

[24] JP Allen, G Feher, TO Yeates, H Komiya, and DC Rees. Structure of the reaction center from Rhodobacter sphaeroides R-26: The protein subunits. *Proc. Natl. Acad. Sci.*, 84:6162–66, August 1987.

[25] JP Allen, G Feher, TO Yeates, H Komiya, and DC Rees. Structure of the reaction center from Rhodobacter sphaeroides R-26: the cofactors. *Proc. Natl. Acad. Sci. USA*, 84(16):5730–4, August 1987.

[26] DM Jonas, MJ Lang, Yutaka Nagasawa, Taiha Joo, and Graham R. Fleming. Pump-probe polarization anisotropy study of femtosecond energy transfer within the photosynthetic reaction center of Rhodobacter sphaeroides R26. *J. Phys. Chem.*, 3654(100):12660–12673, 1996.

[27] David C Arnett, C C Moser, P L Dutton, and N F Scherer. The First Events in Photosynthesis: Electronic Coupling and Energy Transfer Dynamics in the Photosynthetic Reaction Center from Rhodobacter sphaeroides. *J. Phys. Chem. B*, 103:2014–2032, 1999.

[28] JA Jackson, Su Lin, AKW Taguchi, JC Williams, JP Allen, NW Woodbury, and NW Woodbury. Energy transfer in Rhodobacter sphaeroides reaction centers with the initial electron donor oxidized or missing. *J. Phys. Chem. B*, 101:5747–5754, 1997.

[29] C N Rafferty and R K Clayton. The orientations of reaction center transition moments in the chromatophore membrane of Rhodopseudomonas sphareroides, bases on new linear dichroism and photoselection measurements. *Biochim. Biophys. Acta - Bioenergetics*, 546(2):189–206, 1979.

[30] Thomas Renger. Theory of Optical Spectra Involving Charge Transfer States: Dynamic Localization Predicts a Temperature Dependent Optical Band Shift. *Phys. Rev. Lett.*, 93(18):188101, oct 2004.

[31] T Mar and G Gingras. Circular-dichroism spectra of oriented photoreaction center from Rhodospirillum rubrum. *Biochim. Biophys. Acta*, 764:86–92, 1984.

[32] Christine Kirmaier, Dewey Holten, and William W. Parson. Temperature and detection-wavelength dependence of the picosecond electron-transfer kinetics measured in Rhodopseudomonas sphaeroides reaction centers. Resolution of new spectral and kinetic components in the primary charge-separation process. *Biochim. Biophys. Acta*, 810:33–48, 1985.

[33] K D Philipson and K Sauer. Comparative study of the circular dichroism spectra of reaction centers from several photosynthetic bacteria. *Biochemistry*, 12(3):535–539, 1973.

[34] J L Martin, J Breton, a J Hoff, A Migus, and A Antonetti. Femtosecond spectroscopy of electron transfer in the reaction center of the photosynthetic bacterium Rhodopseudomonas sphaeroides R-26: Direct electron transfer from the dimeric bacteriochlorophyll primary donor to the bacteriopheophytin acceptor with a time constant of 2.8 $\pm$ 0.2 psec. *Proc. Natl. Acad. Sci. USA*, 83(4):957–61, 1986.

[35] W Holzapfel, U Finkele, W Kaiser, D Oesterhelt, H Scheer, H U Stilz, and W Zinth. Initial electron-transfer in the reaction center from Rhodobacter sphaeroides. *Proc. Natl. Acad. Sci.*, 87(13):5168–72, July 1990.

[36] W. Holzapfel, U. Finkele, W. Kaiser, D. Oesterhelt, H. Scheer, H.U. Stilz, and W. Zinth. Observation of a bacteriochlorophyll anion radical during the primary charge separation in a reaction center. *Chem. Phys. Lett.*, 160(1):1–7, 1989.

[37] M Bixon and Joshua Jortner. Electron transfer via bridges. *J. Chem. Phys.*, 107(13):5154–5170, 1997.

[38] Gerald J Small. On the validity of the standard model for primary charge separation in the bacterial reaction center: Photosynthesis and the Bacterial Reaction Center. *Chem. Phys.*, 197(3):239–257, 1995.

[39] William W. Parson and Arieh Warshel. Mechanism of Charge Separation in Purple Bacterial Reaction Centers. In C.Neil Hunter, Fevzi Daldal, MarionC. Thurnauer, and J.Thomas Beatty, editors, *The Purple Phototrophic Bacteria*, volume 28 of *Advances in Photosynthesis and Respiration*, pages 355–377. Springer Netherlands, Netherlands, 2008.

[40] W W Parson, Z T Chu, and A Warshel. Electrostatic control of charge separation in bacterial photosynthesis. *Biochim. Biophys. Acta*, 1017(3):251–272, 1990.

[41] MH Vos, MR Jones, CN Hunter, J Breton, JC Lambry, and JL Martin. Coherent dynamics during the primary electron-transfer reaction in membrane-bound reaction centers of Rhodobacter sphaeroides. *Biochemistry*, 33(22):6750–6757, 1994.

[42] G. R. Fleming, J. L. Martin, and J. Breton. Rates of primary electron transfer in photosynthetic reaction centres and their mechanistic implications. *Nature*, 333(6169):190–192, 1988.

[43] C K Chan, T J Dimagno, L X Q Chen, J R Norris, and G R Fleming. Mechanism of the Initial Charge Separation in Bacterial Photosynthetic Reaction Centers. *Proc. Natl. Acad. Sci. USA*, 88(24):11202–11206, 1991.

[44] D Kleinfeld, M. Y Okamura, and G Feher. Electron transfer in reaction centers of rhodopseudomonas sphaeroides. 1. determination of the charge recombination pathway of d+qaqb- and free-energy and kinetic relations between qa-qb and qaqb-. *Biochim. Biophys. Acta*, 766:126–140, 1984.

[45] M Leonhard and W Mäntele. Fourier transform infrared spectroscopy and electrochemistry of the primary electron donor in Rhodobacter sphaeroides and Rhodopseudomonas viridis reaction centers: vibrational modes of the pigments in situ and evidence for protein and water modes affecte. *Biochemistry*, 32(17):4532–4538, 1993.

[46] Ulrich Finkele, Christoph Lauterwasser, and Wolfgang Zinth. Role of tyrosine M210 in the initial charge separation of reaction centers of Rhodobacter sphaeroides. *Biochemistry*, 29(1985):8517–8521, 1990.

[47] K. J. Kaufmann, P. L. Dutton, T. L. Netzel, J. S. Leigh, and P. M. Rentzepis. Picosecond kinetics of events leading to reaction center bacteriochlorophyll oxidation. *Science*, 188(4195):1301–1304, 1975.

[48] MH Vos, F Rappaport, JC Lambry, J Breton, and JL Martin. Visualization of coherent nuclear motion in a membrane protein by femtosecond spectroscopy. *Nature*, 363:320–325, 1993.

[49] V.a Shuvalov and A.G Yakovlev. Coupling of nuclear wavepacket motion and charge separation in bacterial reaction centers. *FEBS Letters*, 540:26–34, April 2003.

[50] H Lee, YC Cheng, and GR Fleming. Coherence dynamics in photosynthesis: protein protection of excitonic coherence. *Science*, 1462, 2007.

[51] Niklas Christensson, Harald F Kauffmann, Tõnu Pullerits, and Tomáš Mančal. Origin of Long-Lived Coherences in Light-Harvesting Complexes. *J. Phys. Chem. B*, 116(25):7449–7454, June 2012.

[52] Vivek Tiwari, William K Peters, and David M Jonas. Electronic resonance with anticorrelated pigment vibrations drives photosynthetic energy transfer outside the adiabatic framework. *Proc. Natl. Acad. Sci.*, 110(4):1203–1208, January 2013.

[53] Neill Lambert, Yueh-Nan Chen, Yuan-Chung Cheng, Che-ming Li, Guang-Yin Chen, and Franco Nori. Quantum biology. *Nat. Phys.*, 9(1):10–18, December 2012.

[54] Volkhard May and Oliver Kühn. *Dynamics of Isolated and Open Quantum Systems*. Wiley-VCH Verlag GmbH & Co. KGaA, 2011.

[55] J Thomas Beatty, Jörg Overmann, Michael T Lince, Ann K Manske, Andrew S Lang, Robert E Blankenship, Cindy L Van Dover, Tracey a Martinson, and F Gerald Plumley. An obligately photosynthetic bacterial anaerobe from a deep-sea hydrothermal vent. *Proc. Natl. Acad. Sci. USA*, 102(26):9306–10, jun 2005.

[56] Niels-Ulrik Frigaard and Donald A. Bryant. *Complex Intracellular Structures in Prokaryotes*, volume 2 of *Microbiology Monographs*, chapter Chlorosomes: Antenna Organelles in Photosynthetic Green Bacteria, pages 79–114. Springer-Verlag Berlin Heidelberg, 2006.

[57] LA Staehelin, JR Golecki, RC Fuller, and Gerhart Drews. Visualization of the supramolecular architecture of chlorosomes (Chlorobium type vesicles) in freeze-fractured cells of Chloroflexus aurantiacus. *Arch. Microbiol.*, 277:269–277, 1978.

[58] Jakub Pšenčík, T. P. Ikonen, P. Laurinmaki, M.C. Merkel, S.J. Butcher, R.E.Serimaa, and R. Tuma. Lamellar organization of pigments in chlorosomes, the light harvesting complexes of green photosynthetic bacteria. *Biophys. J.*, 87:1165–1172, 2004.

[59] M.I. Bystrova, I.N. Malgosheva, and A.A. Krasnovskii. Study of molecular mechanism of self-assembly of aggregated forms of bacteriochlorophyll-c. *Molecular Biology*, 13(3):440–451, 1979.

[60] Masamitsu Hirota, Takeshi Moriyama, Keizo Shimada, Mette Miller, John M. Olson, and Katsumi Matsuura. The effect of detergent on the structure and composition of chlorosomes isolated from *chloroflexusaurantiacus*. *Biochim. Biophys. Acta*, 1099:271–274, 1992.

[61] Pavel Klinger, Juan B. Arellano, František Vácha, Jan Hála, and Jakub Pšenčík. Effects of carotenoids and monogalactosyl diclyceride on bacteriochlorophyll *c* aggregates in aqueous buffer: Implications for the self-assembly of chlorosomes. *Photochem. Photobiol.*, 80:572–578, 2004.

[62] Niels-Ulrik Frigaard, Shinichi Takaichi, Masamitsu Hirota, Keizo Shimada, and Katsumi Matsuura. Quinones in chlorosomes of green sulfur bacteria and their role in redox-dependent fluorescence studied in chlorosome-like bacteriochlorophyll *c* aggregates. *Arch. Microbiol.*, 167(2):343–349, 1997.

[63] NRS Reddy and GJ Small. *Spectral hole burning: Methods and Applications to photosynthesis*. Kluwer, 1996.

[64] Edwin E. Jelley. Spectral absorption and fluorescence of dyes in the molecular state. *Nature*, 138:1009–1010, 1936.

[65] G. Shcheibe. Über die veränderlichkeit der absorptionsspektren in lösungen und die nebenvalenzen als ihre ursache. *Angew. Chem.*, 50(11):212–219, 1937.

[66] Frank Würthner, Theo E Kaiser, and Chantu R Saha-Möller. J-aggregates: from serendipitous discovery to supramolecular engineering of functional dye materials. *Angewandte Chemie (International ed. in English)*, 50(15):3376–410, April 2011.

[67] G. Scheibe, F. Haimerl, and W. Hoppe. Über die ursache des cirkulardichroismus der reversibel polymeren des. *Tetrahedron Lett.*, 11(35):3067–3070, 1970.

[68] W Cooper. Multiple Structure of Aggregated States in 1,1'-diethyl-2,2'-Cyanine Dye. *Chem. Phys. Lett.*, 7(1), 1970.

[69] H von Berlepsch, C Bottcher, and L Dahne. Structure of j-aggregates of pseudoisocyanine dye in aqueous solution. *J. Phys. Chem. B*, 104(37):8792–8799, 2000.

[70] Mohamed M S Abdel-mottaleb, Mark Van Der Auweraer, and Mohamed S A Abdel-mottaleb. Photostability of J -aggregates adsorbed on TiO 2 nanoparticles and AFM imaging of J -aggregates on a glass surface. *Int. J. Photoenergy*, 06:2–6, 2004.

[71] Pierre-Antoine Bouit, Daniel Rauh, Stefan Neugebauer, Juan Luis Delgado, Emmanuel Di Piazza, Stéphane Rigaut, Olivier Maury, Chantal Andraud, Vladimir Dyakonov, and Nazario Martin. A "Cyanine-Cyanine" Salt Exhibiting Photovoltaic Properties. *Org. Lett.*, 11(21):4806–4809, nov 2009.

[72] G. Scheibe, A. Schöntag, and F. Katheder. Fluoreszenz und Energiefortleitung bei reversibel polymerisierten Farbstoffen. *Naturwiss.*, 29:499–501, 1939.

[73] V. Sundström, T. Gillbro, R. A. Gadonas, and A. Piskarskas. Annihilation of singlet excitons in J aggregates of pseudoisocyanine (PIC) studied by pico- and subpicosecond spectroscopy. *J. Chem. Phys.*, 89(5):2754, 1988.

[74] Scheblykin IG. *Temperature Dependence of Exciton Transport in J-aggregates*. World Scientific, 2012.

[75] E. W. Knapp. Lineshapes of molecular aggregates, exchange narrowing and intersite correlation. *Chem. Phys.*, 85(1):73–82, 1984.

[76] Henk Fidder, Jacob Terpstra, and Douwe a. Wiersma. Dynamics of Frenkel excitons in disordered molecular aggregates. *J. Chem. Phys.*, 94(10):6895–6907, 1991.

[77] Naoki Fukutake and Takayoshi Kobayashi. Size distribution of pseudoisocyanine (PIC) J-aggregates studied by near-field absorption spectroscopy. *Chem. Phy. Lett.*, 356(3-4):368, 2002.

[78] Stefan Kirstein and Siegfried Daehne. J-aggregates of amphiphilic cyanine dyes: Self-organization of artificial light harvesting complexes. *Int. J. Photoenergy*, 2006:1–21, 2006.

[79] H. von Berlepsch, C. Böttcher, A Ouart, C. Burger, S. Dähne, and S. Kirstein. Supramolecular Structures of J -Aggregates of Carbocyanine Dyes in Solution. *J. Phys. Chem. B*, 104:5255–5262, 2000.

[80] Kristen C. Hannah and Bruce A. Armitage. DNA-templated assembly of helical cyanine dye aggregates: A supramolecular chain polymerization. *Acc. Chem. Res.*, 37(11):845–853, 2004.

[81] K. E. Achyuthan, T. S. Bergstedt, L. Chen, R. M. Jones, S. Kumaraswamy, S. A. Kushon, K. D. Ley, L. Lu, D. McBranch, H. Mukundan, F. Rininsland, X. Shi, W. Xia, and D. G. Whitten. Fluorescence superquenching of conjugated polyelectrolytes: applications for biosensing and drug discovery. *J. Mater. Chem.*, 15:2648–2656, 2005.

[82] Cătălin Didraga, Audrius Pugžlys, P. Ralph Hania, Hans Von Berlepsch, Koos Duppen, and Jasper Knoester. Structure, spectroscopy, and microscopic model of tubular carbocyanine dye aggregates. *J. Phys. Chem. B*, 108(39):14976–14985, 2004.

[83] S. S. Lampoura, C. Spitz, S. Dähne, J. Knoester, and K. Duppen. The Optical Dynamics of Excitons in Cylindrical J-Aggregates. *J. Phys. Chem. B*, 106(12):3103–3111, 2002.

[84] Franz Milota, Valentyn I Prokhorenko, Tomáš Mančal, Hans von Berlepsch, Oliver Bixner, Harald F Kauffmann, and Jürgen Hauer. Vibronic and vibrational coherences in two-dimensional electronic spectra of supramolecular J-aggregates. *J. Phys. Chem. A*, 117(29):6007–14, July 2013.

[85] L Mandelstam and I Tamm. The Uncertainty Relation Between Energy and Time in Non-relativistic Quantum Mechanics. *Journal of Physics*, 9(4):249–254, 1945.

[86] L. Lepetit, G. Chériaux, and M. Joffre. Linear techniques of phase measurement by femtosecond spectral interferometry for applications in spectroscopy. *J. Opt. Soc. Am. B*, 12(12):2467, dec 1995.

[87] L Lepetit and M Joffre. Two-dimensional nonlinear optics using Fourier-transform spectral interferometry. *Opt. Lett.*, 21(8):564–6, apr 1996.

[88] JD Hybl, AW Albrecht, Sarah M. Gallagher Faeder, and David M. Jonas. Two-dimensional electronic spectroscopy. *Chem. Phy. Lett.*, 297(November):307–313, 1998.

[89] Sarah M. Gallagher, Allison W Albrecht, John D Hybl, Brett L Landin, Bhavani Rajaram, and David M Jonas. Heterodyne detection of the complete electric field of femtosecond four-wave mixing signals. *J. Opt. Soc. Am. B*, 15(8):2338–45, aug 1998.

[90] Tobias Brixner, Jens Stenger, Harsha M Vaswani, Minhaeng Cho, Robert E Blankenship, and Graham R Fleming. Two-dimensional spectroscopy of electronic couplings in photosynthesis. *Nature*, 434(7033):625–8, mar 2005.

[91] Jakub Dostál. *Photosynthetic Apparatus of Green Sulfur Bacteria Studied by Coherent Two-Dimensional Electronic Spectroscopy.* PhD thesis, Lund University, Charles University in Prague, 2014.

[92] Rudi Berera, Rienk van Grondelle, and John T M Kennis. Ultrafast transient absorption spectroscopy: principles and application to photosynthetic systems. *Photosynth. Res.*, 101(2-3):105–118, 2009.

[93] Martin Aeschlimann, Tobias Brixner, Alexander Fischer, Christian Kramer, Pascal Melchior, Walter Pfeiffer, Christian Schneider, Christian Strüber, Philip Tuchscherer, and Dmitri V Voronine. Coherent two-dimensional nanoscopy. *Science*, 333(6050):1723–6, sep 2011.

[94] Patrick F Tekavec, Geoffrey a Lott, and Andrew H Marcus. Fluorescence-detected two-dimensional electronic coherence spectroscopy by acousto-optic phase modulation. *J. Chem. Phys.*, 127(21):214307, dec 2007.

[95] David M Jonas. Two-dimensional femtosecond spectroscopy. *Annu. Rev. Phys. Chem.*, 54(1):425–463, January 2003.

[96] Sang-Hee Shim and Martin T Zanni. How to turn your pump-probe instrument into a multidimensional spectrometer: 2D IR and Vis spectroscopies via pulse shaping. *Phys. Chem. Chem. Phys.*, 11(5):748–61, feb 2009.

[97] Tobias Brixner, Tomáš Mančal, Igor V Stiopkin, and Graham R Fleming. Phase-stabilized two-dimensional electronic spectroscopy. *J. Chem. Phys.*, 121(9):4221–4236, September 2004.

[98] Ramũnas Augulis and Donatas Zigmantas. Two-dimensional electronic spectroscopy with double modulation lock-in detection: enhancement of sensitivity and noise resistance. *Optics express*, 19(14):13126–33, July 2011.

[99] S. (Shaul) Mukamel. *Principles of nonlinear optical spectroscopy.* New York : Oxford University Press, 1995. Includes bibliographical references and index.

[100] P Hamm and M Zanni. *Concepts and Methods of 2D Infrared Spectroscopy.* 2011.

[101] N. A. Kurnit, I. D. Abella, and S. R. Hartmann. Observation of a photon echo. *Phys. Rev. Lett.*, 13(19):567–568, 1964.

[102] Richard G. Brewer and R.L. Shoemaker. Optical free induction decay. *Phys. Rev. A*, 6(6):2001–07, 1972.

[103] C. Cohen-Tannoudji and A. Kastler. *Optical pumping.* North-Holland, 1966. pp. 3-81.

[104] Hebin Li, Alan D Bristow, Mark E Siemens, Galan Moody, and Steven T Cundiff. Unraveling quantum pathways using optical 3D Fourier-transform spectroscopy. *Nat Commun.*, 4(1390), January 2013.

[105] Andreas C. Albrecht. Polarizations and assignments of transitions: The method of photoselection. *J. Mol. Spectrosc.*, 6:84–108, 1961.

[106] Sergei Savikhin, Daniel R. Buck, and Walter S. Struve. Oscillating anisotropies in a bacteriochlorophyll protein: Evidence for quantum beating between exciton levels. *Chem. Phys.*, 223(2-3):303–312, 1997.

[107] RM Hochstrasser. Two-dimensional IR-spectroscopy: polarization anisotropy effects. *Chem. Phys.*, 266:273–284, 2001.

[108] M T Zanni, N H Ge, Y S Kim, and R M Hochstrasser. Two-dimensional IR spectroscopy can be designed to eliminate the diagonal peaks and expose only the crosspeaks needed for structure determination. *Proc. Natl. Acad. Sci. USA*, 98(20):11265–70, sep 2001.

[109] Vytautas Butkus, Donatas Zigmantas, Darius Abramavicius, and Leonas Valkunas. Distinctive character of electronic and vibrational coherences in disordered molecular aggregates. *Chem. Phys. Lett.*, 587:93–98, 2013.

[110] Maxilian A Schlosshauer. *Decoherence and the Quantum-to-Classical Transition*, volume 1. Springer, Berlin, 2007.

[111] T D Ladd, F Jelezko, R Laflamme, Y Nakamura, C Monroe, and J L O'Brien. Quantum computers. *Nature*, 464(7285):45–53, 2010.

[112] D. von der Linde, A. Laubereau, and W. Kaiser. Molecular vibration in liquids: Direct Measurement of the Molecular Daphasing Time; Determination of the Shape of Picosecond Light Pulses. *Phys. Rev. Lett.*, 26(16):954, 1971.

[113] A. Mokhtari, P. Cong, J. L. Herek, and A. H. Zewail. Direct femtosecond mapping of trajectories in a chemical reaction. *Nature*, 348(6298):225–227, 1990.

[114] Elisabetta Collini, Cathy Y Wong, Krystyna E Wilk, Paul M G Curmi, Paul Brumer, and Gregory D Scholes. Coherently wired light-harvesting in photosynthetic marine algae at ambient temperature. *Nature*, 463(7281):644–647, February 2010.

[115] Gregory S Engel, Tessa R Calhoun, Elizabeth L Read, Tae-Kyu Ahn, Tomáš Mančal, Yuan-Chung Cheng, Robert E Blankenship, and Graham R Fleming. Evidence for wavelike energy transfer through quantum coherence in photosynthetic systems. *Nature*, 446(7137):782–786, April 2007.

[116] Vytautas Butkus, Donatas Zigmantas, Leonas Valkunas, and Darius Abramavicius. Vibrational vs. electronic coherences in 2D spectrum of molecular systems. *Chem. Phys. Lett.*, 545:40–43, August 2012.

[117] Joachim Seibt, Thorsten Hansen, and Tõnu Pullerits. 3D Spectroscopy of Vibrational Coherences in Quantum Dots: Theory. *J. Phys. Chem. B*, 117(38):11124–11133, September 2013.

[118] Johan Strümpfer and Klaus Schulten. The effect of correlated bath fluctuations on exciton transfer. *J. Chem. Phys.*, 095102:1–9, 2011.

[119] Peter J. Walla, Patricia A. Linden, Kaoru Ohta, and Graham R. Fleming. Excited-state kinetics of the carotenoid S_1 state in LHC II and two-photon excitation spectra of lutein and betacarotene in solution: Efficient Car $S_1 - >$Chl electronic energy transfer via hot S_1 states? *J. Phys. Chem. A*, 106(10):1909–1916, 2002.

[120] Franklin D. Fuller, Jie Pan, Andrius Gelzinis, Vytautas Butkus, S. Seckin Senlik, Daniel E. Wilcox, Charles F. Yocum, Leonas Valkunas, Darius Abramavicius, and Jennifer P. Ogilvie. Vibronic coherence in oxygenic photosynthesis. *Nat. Chem.*, 6(July):706–711, 2014.

[121] Tomáš Mančal, Jakub Dostál, Jakub Pšenčík, and Donatas Zigmantas. Transfer of vibrational coherence through incoherent energy transfer process in Förster limit. *Can. J. Chem.*, 92(2):135–143, 2014.

Paper I

J. Am. Chem. Soc. • 2012 • Vol. 134, pp. 16484–16487 Paper I

Coherent Picosecond Exciton Dynamics in a Photosynthetic Reaction Center

[1*]Sebastian Westenhoff, [2,3*]David Paleček, [1]Petra Edlund, [1]Philip Smith and [2]Donatas Zigmantas

[1] *Department of Chemistry and Molecular Biology, University of Gothenburg, Box 462, SE-40530 Gothenburg, Sweden*

[2] *Department of Chemical Physics, Lund University, P.O. Box 124, SE-22100 Lund, Sweden*

westenho@chem.gu.se; donatas.zigmantas@chemphys.lu.se

*Contributed equaly

Abstract

Photosynthetic reaction centers convert sunlight into a transmembrane electrochemical potential difference, providing chemical energy to almost all life on earth. Light energy is efficiently transferred through chromophore cofactors to the sites, where charge separation occurs. We applied two-dimensional electronic spectroscopy to assess the role of coherences in the photoresponse of the bacterial reaction center of Rhodobacter sphaeroides. By controlling the polarization of the laser beams, we were able to assign unambiguously the oscillatory dynamics to electronic (intermolecular) coherences. The data show that these coherences are sustained for more than 1 ps, indicating that the protein coherently retains some excitation energy on this time scale. Our finding provides a mechanism for effective delocalization of the excitations on the picosecond time scale by electronic coherence, setting the stage for efficient charge separation.

Photosynthesis provides energy to most life on earth by conversion of sunlight into chemical energy. The light is absorbed by pigment-rich antenna proteins and transferred to reaction-center proteins, where charge separation occurs. All photosynthetic reaction centers contain a conserved functional core, which in this study is represented by the reaction center of the purple bacteria *Rhodobacter sphaeroides* (RC_{sph}). The RC_{sph} comprises, among other cofactors, four bacteriochlorophylls and two bacteriopheophytins. These chromophores form an assembly (see Figure 1a) and give rise to three distinctive absorption bands peaking at 760, 805, and 860 nm, respectively (Figure 1b, red line). We use H, B, and P to denote the excitonic states that give rise to these bands and whose major contributions are from the bacteriopheophytins, the accessory bacteriochlorophylls, and the dimeric bacteriochlorophylls (spatial pair), respectively. It is generally accepted that the photoexcitations are transferred from H over B to P within 200 fs [1]. Subsequently, charge separation occurs within a few picoseconds [2].

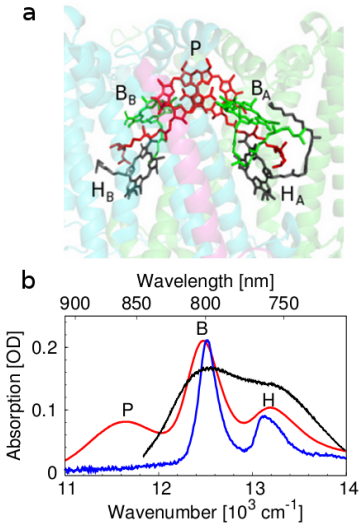

Figure 1: *Structure and absorption spectra of* RC_{sph}. *(a) Molecular arrangement of H, B, and P (see text for abbreviations) in the* RC_{sph} *binding pocket. (b) Linear absorption spectra of* RC_{sph} *at 294 K (red) and* RC_{sph} *with oxidized P at 80 K (blue) and the laser spectrum (black).*

To elucidate further the photoresponse of photosynthetic reaction centers, it is important to assess the role of quantum coherences (superpositions) between the excited states. This has been made possible by the advent of two-dimensional (2D) optical spectroscopy in the visible spectral range [3, 4]. Excited state coherences, which were first studied in photosynthetic antenna proteins, have been shown to live for several hundred femtoseconds in complexes from bacteria [5, 6], higher plants [7] and marine algae [8]. The implications of these findings for the photophysical function of the proteins are today vividly debated. Some theoretical studies suggest that coherent, wavelike motion of the excitations may be responsible for the high quantum yield of excitation energy transfer among the antenna pigments [9, 10], but the mechanism causing the long-lived quantum coherences is not well understood at present [11–16]. For reaction-center proteins, information on quantum-coher- ence dynamics is sparse. In the reaction center of photosystem II, electronic coherences could not be assigned unambiguously by 2D electronic spectroscopy [17]. For RC sph , a two-color photon echo experiment indicated a decay time of 440 fs for the coherent interaction between the B and H excitons at 77 K [18], but direct observation of the electronic coherence by oscillatory dynamics has remained elusive. It is therefore highly desirable to assess directly the electronic coherences in reaction-center proteins.

In this work, we used 2D electronic spectroscopy to probe simultaneously the population and coherence dynamics of excitations in detergent-solubilized RC_{sph} with a chemically oxidized P at 80 K. The absorption spectrum of this sample is shown by the blue line in Figure 1b. The chemical modification blocks the charge transfer and strongly reduces the absorption strength of P but leaves B, H, and the energy transfer to P unaffected [19, 20]. A typical 2D spectroscopy map at a waiting time $t_2 = 40$ fs is shown in Figure 2a. The B and H bands are clearly visible on the diagonal, as is the cross-peak below the diagonal (marked "HB").The corresponding upper cross-peak is masked by the negative excited-state absorption signal from B.

The 2D spectroscopy experiment can probe the evolution of populations, vibrational (intramolecular) co-

herences, or electronic (intermolecular) coherences as a function of t_2. Population dynamics gives rise to smoothly evolving signals, whereas coherences are observed as oscillatory signals. Typically, this leads to convoluted traces where vibrational and electronic coherences as well as population dynamics contribute, making assignments difficult. An example is shown in Figure 2b, where the t_2 dependencies of the diagonal H and B peaks and the lower HB cross-peak (under all-parallel polarization conditions) reveal a decay of populations overlaid with small oscillatory signals.

To identify coherences with electronic character, we used a special combination of linearly polarized pulses that dramatically suppresses all of the signals except the oscillating intermolecular ones [7]. This strategy was borrowed from 2D IR spectroscopy, where a number of polarization schemes are used to suppress or enhance certain pathways [21, 22]. In our configuration, the polarization orientation of pulses 1 to 4 was set to ($\pi/4$, $-\pi/4$, $\pi/2$, and 0), respectively. This selects, after orientational averaging, only those interaction pathways that evolve during t_2 as a superposition of two excited states with different transition dipole moment orientations, which we term "intermolecular" or "electronic" coherences in the remainder of the manuscript. The configuration strongly suppresses the population dynamics contributions and the coherences between vibrational states, which are termed "intramolecular" or "vibrational" coherences, because populations and vibrational coherences are prepared by the transitions with parallel dipole moments.

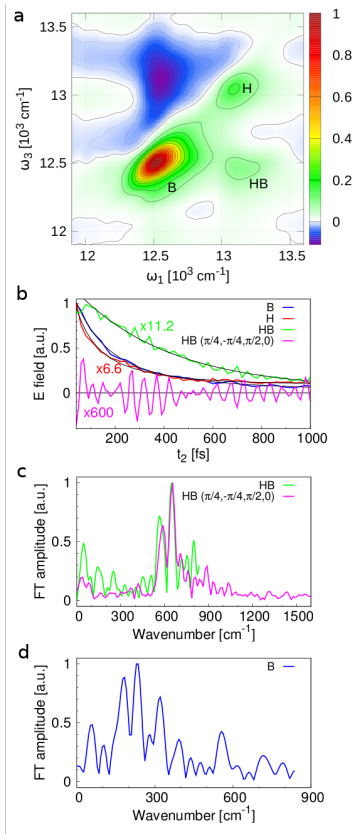

Figure 2: *2D absorption spectroscopy of oxidized* RC_{sph} *at 80 K. (a) Representative 2D spectrum at a waiting time* $t_2 =$ 40 fs. ω_1 *and* ω_3 *are the Fourier transform frequencies corresponding to the coherence and detection times* t_1 *and* t_3*, respectively. (b) Intensities of the diagonal peaks H and B and the cross-peak HB as functions of* t_2*. The gray lines are fits of multiexponential decay functions to the data. The effective decay times calculated from the two major decay rates are 94 and 151 fs for H and B, respectively. (c) Fourier spectra of the* t_2 *dependence of the lower cross-peak HB for the all-parallel and* ($\pi/4$, $-\pi/4$, $\pi/2$, 0) *polarization conditions. (d) Fourier spectrum of the* t_2 *dependence of the diagonal peak B. In all of the panels, unless indicated otherwise in the figure legend, the beams were polarized in parallel.*

Taking into account all of the experimental considerations in the measurements discussed here, we estimate the suppression ratio of the population dynamics and vibrational coherences to be ∼85 in the ($\pi/4$, $-\pi/4$, $\pi/2$, 0) polarization configuration relative to the all-parallel configuration.

The effectiveness of this acquisition strategy is documented in Figure 2b, where the t_2 dependences of the HB cross-peak for the ($\pi/4$, $-\pi/4$, $\pi/2$, 0) and all-parallel polarization configurations are shown as magenta and green traces, respectively. Clearly, population dynamics are suppressed in case of the ($\pi/4$, $-\pi/4$, $\pi/2$, 0) configuration and an offset-free oscillating signal is observed. This signal must be from a coherence that involves two excited states with different transition dipole orientations, and we therefore assign it to coherences with electronic character. Furthermore, the Fourier transforms of these kinetic traces (Figure 2c) reveal 645 cm^{-1} as the major frequency component for both the ($\pi/4$, $-\pi/4$, $\pi/2$, 0) and all-parallel polarization conditions. This frequency corresponds exactly to the difference between the transition energies of B and H, further strengthening our assignment.

Figure 2d shows the Fourier transform amplitude of the oscillatory signals in the decay of the diagonal peak B measured with all-parallel pulse polarizations. Oscillations are observed at 90, 190, 220, 310, 390, and 710 cm^{-1} . All of these modes have vibrational origin, as they match quite well the published resonance Raman frequencies of B [23]. The peak at 575 cm^{-1} is observed in all of the measurements presented in Figure 2c,d and is thus likely of mixed vibrational and electronic origin [12]. A more detailed analysis of these vibrational coherences will be presented in a forthcoming publication.

In summary this analysis shows that the t_2 dependence of the lower cross-peak HB measured with the ($\pi/4$, $-\pi/4$, $\pi/2$, 0) polarization conditions is a direct and clean signature of coherence beatings between H and B with electronic character. Remarkably, this coherence lives significantly longer than the 1 ps time window probed here (Figure 2b, magenta trace), and its lifetime exceeds the previously reported value of 440 fs based on the two-color photon echo experiment [18, 24]. Figure 2b also illustrates that in contrast to the long-lived coherence between H and B, most of the populations on H and B decay with effective time constants of ∼94 and ∼151 fs, respectively, in agreement with previous reports [20]. Clearly, the observed coherence between H and B has a much longer decay time than the population dynamics of H and B.

This finding is unexpected. When the total molecular system dynamics is considered in terms of population relaxation rates (γ_H and γ_B) and coherence dephasing rates, the total HB coherence dephasing rate is given by

$$\Gamma_{BH} = \frac{1}{2}(\gamma_H + \gamma_B) + \Gamma_{HB}^{pure} \qquad (1)$$

where is the pure electronic dephasing rate of the electronic coherence between H and B. From this argument, it follows that the observed long-lived coherence between H and B cannot survive without corresponding excitation populations on H and B. We note that this statement reflects a very general property of the reduced density matrix of molecular aggregates, σ_{ij}, where

off-diagonal and diagonal elements represent coherences and populations, respectively, on sites i and j. By definition,

$$\sqrt{\sigma_{ii}\sigma_{jj}} \geq |\sigma_{ij}| \qquad (2)$$

further demonstrating that coherences cannot exist without corresponding populations [25].

Indeed, close inspection of the population decays (Figure 2b; also see Figure 2 in ref [20]) reveals small but long-lived (more than 1 ps) population components on both H and B. This behavior is surprising because the driving force for excitation energy transfer from H to B and P vastly exceeds the available thermal energy. Within the framework of incoherent excitation energy transfer, Boltzmann statistics would therefore predict negligible back-transfer from P to H and B, and the populations of H and B should decay to zero within the time window probed. This shows that excitation energy transfer to P is incomplete. Taken together with our finding of the long-lived coherences between H and B, we conclude that the reaction center coherently retains some excitation energy in higher- energy chromophores on a picosecond time scale.

For molecular aggregates in the weak or intermediate coupling regime, electronic coherence effectively delocalizes excitations over one or several chromophores, whereas dephasing leads to localization of the energy. This is exemplified in multichromophoric light-harvesting proteins, where long-lived electronic coherences have previously been observed [5–8]. In contrast to the findings for antenna proteins, we have found in the present work that electronic coherences apparently outlive the majority of the excitation populations and that this leads to incomplete energy transfer. We therefore suggest that the reaction center protein uses long-lived electronic coherences to delocalize excitation energy over H, B, and likely P on picosecond time scales. This mechanism is in agreement with efficient charge generation in wild-type RC_{sph} because intermolecular excited-state delocalization benefits efficient charge transfer.

Associated content

Experimental details and the protocol for the overproduction and purification of RC_{sph}. This material is available free of charge via the Internet at http://pubs.acs.org.

Author information

Corresponding Author
westenho@chem.gu.se
donatas.zigmantas@chemphys.lu.se
Author Contributions
S.W. and D.P. contributed equally.
Notes
The authors declare no competing financial interest.

Acknowledgments

S.W. and D.Z. acknowledge financial support from the Swedish Research Council. S.W. and P.E. acknowledge support from the Stiftelsen Olle Engkvist Byggmästare. The authors thank Prof. R. Neutze for access to the SweGen protein production facilities and the protocols for the overproduction procedure.

References

[1] Xanthipe J. Jordanides, Gregory D. Scholes, and Graham R. Fleming. The Mechanism of Energy Transfer in the Bacterial Photosynthetic Reaction Center. *J. Phys. Chem. B*, 105(8):1652–1669, March 2001.

[2] H Wang, S Lin, JP Allen, JC Williams, S Blankert, Christa Laser, and Neal W Woodbury. Protein dynamics control the kinetics of initial electron transfer in photosynthesis. *Science*, 316(5825):747–50, 2007.

[3] JD Hybl, AW Albrecht, Sarah M. Gallagher Faeder, and David M. Jonas. Two-dimensional electronic spectroscopy. *Chem. Phy. Lett.*, 297(November):307–313, 1998.

[4] Tobias Brixner, Jens Stenger, Harsha M Vaswani, Minhaeng Cho, Robert E Blankenship, and Graham R Fleming. Two-dimensional spectroscopy of electronic couplings in photosynthesis. *Nature*, 434(7033):625–8, mar 2005.

[5] Gregory S Engel, Tessa R Calhoun, Elizabeth L Read, Tae-Kyu Ahn, Tomáš Mančal, Yuan-Chung Cheng, Robert E Blankenship, and Graham R Fleming. Evidence for wavelike energy transfer through quantum coherence in photosynthetic systems. *Nature*, 446(7137):782–786, April 2007.

[6] Gitt Panitchayangkoon, Dmitri V Voronine, Darius Abramavicius, Justin R Caram, Nicholas H C Lewis, Shaul Mukamel, and Gregory S Engel. Direct evidence of quantum transport in photosynthetic light-harvesting complexes. *Proc. Natl. Acad. Sci. USA*, 108(52):20908–12, dec 2011.

[7] Gabriela S Schlau-Cohen, Akihito Ishizaki, Tessa R Calhoun, Naomi S Ginsberg, Matteo Ballottari, Roberto Bassi, and Graham R Fleming. Elucidation of the timescales and origins of quantum electronic coherence in LHCII. *Nat. Chem.*, 4(5):389–395, 2012.

[8] Elisabetta Collini, Cathy Y Wong, Krystyna E Wilk, Paul M G Curmi, Paul Brumer, and Gregory D Scholes. Coherently wired light-harvesting in photosynthetic marine algae at ambient temperature. *Nature*, 463(7281):644–647, February 2010.

[9] M. B. Plenio and S. F. Huelga. Dephasing-assisted transport: quantum networks and biomolecules. *New J. Phys.*, 10(11):113019, 2008.

[10] Masoud Mohseni, Patrick Rebentrost, Seth Lloyd, and Alán Aspuru-Guzik. Environment-assisted quantum walks in photosynthetic energy transfer. *J. Chem. Phys.*, 129(17):174106, 2008.

[11] Darius Abramavicius and Shaul Mukamel. Exciton dynamics in chromophore aggregates with correlated environment fluctuations. *J. Chem. Phys.*, 134(17):174504, 2011.

[12] Niklas Christensson, Harald F Kauffmann, Tõnu Pullerits, and Tomáš Mančal. Origin of Long-Lived Coherences in Light-Harvesting Complexes. *J. Phys. Chem. B*, 116(25):7449–7454, June 2012.

[13] A. W. Chin, J. Prior, R. Rosenbach, F. Caycedo-Soler, S. F. Huelga, and M. B. Plenio. The role of non-equilibrium vibrational structures in electronic coherence and recoherence in pigment-protein complexes. *Nat. Phys.*, 9(2):113–118, 2013.

[14] Akihito Ishizaki and Graham R Fleming. Theoretical examination of quantum coherence in a photosynthetic system at physiological temperature. *Proc. Natl. Acad. Sci. USA*, 106(41):17255–60, 2009.

[15] Sangwoo Shim, Patrick Rebentrost, Stéphanie Valleau, and Alán Aspuru-Guzik. Atomistic Study of the Long-Lived Quantum Coherences in the Fenna-Matthews-Olson Complex. *Biophys. J.*, 102(3):649–660, 2012.

[16] Hyun Woo Kim, Aaron Kelly, Jae Woo Park, and Young Min Rhee. All-atom semiclassical dynamics study of quantum coherence in photosynthetic Fenna-Matthews-Olson complex. *J. Am. Chem. Soc.*, 134:11640–11651, 2012.

[17] Kristin L. M. Lewis and Jennifer P. Ogilvie. Probing Photosynthetic Energy and Charge Transfer with Two-Dimensional Electronic Spectroscopy. *J. Phys. Chem. Lett*, 3(4):503–510, 2012.

[18] H Lee, YC Cheng, and GR Fleming. Coherence dynamics in photosynthesis: protein protection of excitonic coherence. *Science*, 1462, 2007.

[19] Jacques Breton. Orientation of the chromophores in the reaction center of rhodopseudomonas viridis. comparison of low-temperature linear dichroism spectra with a model derived from x-ray crystallography. *Biochim. Biophys. Acta*, 810(2):235 – 245, 1985.

[20] JA Jackson, Su Lin, AKW Taguchi, JC Williams, JP Allen, NW Woodbury, and NW Woodbury. Energy transfer in Rhodobacter sphaeroides reaction centers with the initial electron donor oxidized or missing. *J. Phys. Chem. B*, 101:5747–5754, 1997.

[21] RM Hochstrasser. Two-dimensional IR-spectroscopy: polarization anisotropy effects. *Chem. Phys.*, 266:273–284, 2001.

[22] M T Zanni, N H Ge, Y S Kim, and R M Hochstrasser. Two-dimensional IR spectroscopy can be designed to eliminate the diagonal peaks and expose only the crosspeaks needed for structure determination. *Proc. Natl. Acad. Sci. USA*, 98(20):11265–70, sep 2001.

[23] NJ Cherepy, AP Shreve, LJ Moore, SG Boxer, and A R Mathies. Temperature dependence of the Qy resonance Raman spectra of bacteriochlorophylls, the primary electron donor, and bacteriopheophytins in the bacterial photosynthetic reaction center. *Biochemistry*, 2960(97):8559–8566, 1997.

[24] We note that in the earlier experiment reported in ref [18], an accurate determination of the coherence time was more difficult because the measured signal was composed of a signal from the coherence between B and H convoluted with oscillating signals stemming from low-frequency vibrational modes.

[25] S. (Shaul) Mukamel. *Principles of nonlinear optical spectroscopy.* New York : Oxford University Press, 1995. Includes bibliographical references and index.

Paper II

Photosynth. Res. • 2014 • Vol. 119(3), pp. 331–338 Paper II

Low Temperature Spectroscopy of Bacteriochlorophyll *c* Aggregates

[1,2]David Paleček, [1]Roman Dědic, [1]Jan Alster, [1]Jan Hála

[1] *Department of Chemical Physics and Optics, Faculty of Mathematics and Physics, Charles University, Prague, Czech Republic*

[2] *Department of Chemical Physics, Lund University, Getingevägen 60, 221 00 Lund, Sweden*

david@stanka.de

Abstract

Chlorosomes from green photosynthetic bacteria belong to the most effective light-harvesting antennas found in nature. Quinones incorporated in bacterichlorophyll (BChl) *c* aggregates inside chlorosomes play an important redox-dependent photo-protection role against oxidative damage of bacterial reaction centers. Artificial BChl *c* aggregates with and without quinones were prepared. We applied hole-burning spectroscopy and steady state absorption and emission techniques at 1.9 K and two different redox potentials to investigate the role of quinones and redox potential on BChl *c* aggregates at low temperatures. We show that quinones quench the excitation energy in a similar manner as at room temperature, yet the quenching process is not as efficient as for chlorosomes. Interestingly, our data suggests that excitation quenching partially proceeds from higher excitonic states competing with ultrafast exciton relaxation. Moreover, we obtained structure-related parameters such as reorganization energies and inhomogeneous broadening of the lowest excited state, providing experimental ground for theoretical studies aiming at designing plausible large scale model for BChl *c* aggregates including disorder.

1. Introduction

Capturing the sunlight photons and converting them into usable energy in the most efficient way is one of the great challenges in energy science for the 21st century [1]. Understanding and mimicking natural light-harvesting processes is one of the possible ways to follow. Despite similar concepts and structural universality of reaction centers of the photosynthetic machinery across the nature [2], light harvesting antennas vary greatly, adapting organisms to diverse environments, light intensities, and solar spectrum densities.

Green photosynthetic bacteria typically occur in stratified lakes and microbial mats [3]. They can be even found in depths up to 100 m in the Black Sea [4], thanks to unique light-harvesting antennae called chlorosomes (for review see [5, 6]). Chlorosomes are the largest and the most efficient light-harvesting antenna systems found in nature. They contain mainly bacteriochlorophylls (BChl) *c*, *d*, and *e* (depending on species), carotenoids, and quinones forming together aggre-

gates which are encapsulated in a lipid-protein monolayer. Minor portion of BChl *a* is present in a paracrystalline protein array called baseplate connecting the chlorosomes to a reaction center through FMO pigment protein complex or B806-866 complex, depending on species [7]. Unlike in other light-harvesting complexes where pigment-protein interaction prevails, BChls in chlorosomes are organized in a self-assembly manner, employing a strong pigment-pigment interaction with no need for protein scaffold [6]. This makes it possible to prepare artificial BChl *c* aggregates *in vitro* as suitable candidates for artificial light-harvesting applications. For example solar cells sensitized by artificial self-assembling zinc porphyrins have been studied [8].

Aggregates of BChl *c* with optical properties in absorption, fluorescence, circular and linear dichroism spectra similar to those of chlorosomes [9–11] can be prepared in non-polar solvents [12, 13] and aqueous buffers [14] (for review see [15, 16]). Hydrophobic interactions between BChl *c* chlorin rings drive the aggregation in non-polar solvents, whereas non-polar molecules such as lipids, carotenoids and isoprenoid quinones induce aggregation in aqueous buffers due to interaction with non-polar hydrocarbon tails of BChls [17, 18]. Strong excitonic coupling between closely packed pigments leads to a significant red-shift of the Q_y absorption band of BChls in the aggregates.

Green sulfur bacteria are strictly anoxygenic organisms in which excitation energy (EE) is quenched in the presence of oxygen in isolated chlorosomes, as well as in whole cells [19, 20], preventing photo-damage of the low potential electron acceptors in reaction centers by reactive oxygen species [6]. Quinones and redox potential play a major role in this process [11, 19]. Similar EE quenching is observed for artificially prepared aggregates (mixture of BChl *c* with monogalactosyl diglyceride or lecithin) at room temperature (RT) if the quinones are present [11, 18].

This study presents the very first low temperature spectroscopic investigation of BChl *c* aggregates prepared *in vitro* with and without isoprenoid quinone (vitamin K2) at both reduced and oxidized conditions. We employed low temperature absorption, fluorescence, and persistent hole-burning (HB) spectroscopies to assign the role of quinones in redox dependent excitation quenching at liquid helium temperatures. These methods provide information on static and dynamic contributions to disorder, together with structural parameters useful for designing plausible large scale model for BChl *c* aggregates and/or the chlorosomes. We also discuss possible implications of our spectroscopic results for the nature of quenching process and organization of artificial BChl *c* aggregates.

2. Materials and Methods

Artificial BChl *c* aggregates were prepared as described before [17, 18]. Our aggregation inducing agent was either lipid lecithin (95 % L-α-phosphatidyl choline, Avanti Polar Lipids) or menaquinone-4 (vitamin K2 , Sigma, V9378). More specifically, lecithin (quinone) sample was prepared by mixing 20 µl of 25 mM lecithin (menaquinone-4) in ethanol with 25 µl

of 25 mM solution of BChl *c* in ethanol. Resulted mixtures were vigorously injected into 1.25 ml 50 mM Tris-HCl buffer of pH 8.0 and stored for 4 days in dark to let aggregates fully develop. After that, 0.3 ml of aggregate suspensions were mixed with 0.4 ml of 100% glycerol to ensure formation of a homogeneous glassy matrix when freezed in a 1 mm thick low-temperature cuvette. To achieve desired optical density of ∼0.5 in 1 mm cuvette for HB experiment, 0.4 mM concentration of BChl *c* was used compared to 0.01–0.02 mM used in previous RT studies [17, 18]. The samples prepared in normal atmosphere without using any reducing agents are considered oxidized and denoted as Lec_{ox} and $K2_{\mathrm{ox}}$. We also prepared reduced versions of both the samples (denoted Lec_{red} and $K2_{\mathrm{red}}$) by adding ∼4 µl of 600 mM sodium dithionite during the process of filling cuvettes resulting in ∼15 mM dithionite concentration. Incubation time of dithionite was 45 min, during which the presence of dithionite in the samples was monitored by its absorption around 300 nm.

RT absorption spectra were recorded on UV/VIS spectrometer (Specord 250, Analytik Jena). Low temperature steady state absorption spectra were acquired using 250 W tungsten lamp (Oriel) as an irradiation source. Output light was sent through double-grating monochromator (Jobin Yvon HRD 1) and focused into the cryostat (SVT-300, Janis Research) filled with liquid helium (LHe). Peltier cooled photomultiplier (Hamamatsu R943-02) was used for signal detection. Adjusting monochromator slits, spectral resolution was varied between 2.6 cm^{-1} and 1.3 cm^{-1} for broad-band steady state and HB measurements, respectively. Second reference channel with a photomultiplier of the same type was used to correct for the longer-term instabilities caused by temperature fluctuations of the lamp filament. Low temperature absorption spectra were corrected for scattering by matching their absorption profile to those at RT in spectral region of 830–850 nm. Low temperature fluorescence was excited by 457 nm line of Ar^+ ion laser (Sabre Innova, Coherent) while the same double-grating monochromator with the same photomultiplier on the exit slit was used for detection. Spectra were corrected for excitation laser intensity fluctuations and spectral sensitivity of apparatus.

In HB experiment one compares absorption before and after irradiation of the sample with narrow band laser. For this purpose, we used diode laser (TEC 500, Sacher Lasertechnik) tunable in the range ∼765–800 nm with the bandwidth of < 1 GHz. Size of the laser spot was ∼1 mm, completely overlapping the light-spot from the probing lamp. Lock-in detection scheme was used to separate very weak signals from the noise. Besides temperature dependencies of hole widths, all measurements were realized below the Lambda point of LHe at 1.9 K which reduces noise from LHe evaporating in the optical path through the cryostat.

HB action spectra in absorption, often related to site distribution function (SDF) of the lowest excited states (LES) in the systems with non-interacting pigments or ultrafast energy transfer, are measured as the dependence of hole-depth on the burning wavelength using constant low burning energy. For this purpose, we used continuous titanium-sapphire laser (TiC, Avesta Ltd.) tunable over

broad spectral range between $\sim 700 - 1000$ nm with the spectral bandwidth of < 2 GHz. Laser power of 50 mW for 100 s resulting in 500 J cm^{-2} was used for burning. For the $K2_{ox}$ sample which exhibited lowest burning efficiency, 100 mW burning power was used instead, resulting in 1000 J cm^{-2} burning dose.

3. Results and Discussion

3.1. Steady state absorption

Formation of BChl *c* aggregates can be monitored by red-shift of BChl *c* Q_y absorption band. Figure 1 and Table 1 demonstrate spectral evolution (red-shift of Q_y, narrowing, increasing absorption coefficient) of the samples upon cooling from the RT to 1.9 K. Lecithin samples (Lec_{ox} and Lec_{red}) exhibit very similar behaviour regarding red-shift of their Q_y bands and increase of the absorption cross-section. Absorption peak around 667 nm is likely caused by absorption of monomeric BChl *c* embedded in lecithin micelles which is supported by accompanied fluorescence at $\sim$ 685 nm reflecting isolation of the BChl *c* monomers from the aggregates (see Figure 3).

Although the overall red-shift is approximately the same for all the samples, quinone samples exhibit more pronounced aggregation induced red-shift at RT, whereas lecithin samples exhibit larger red-shift upon cooling. Aggregation induced red-shift is found to be $\sim$ 100 nm and $\sim$ 85 nm in respect to monomers for quinone and lecithin samples, respectively. The red-shifts are significantly larger than $\sim$ 60 nm and $\sim$ 75 nm reported before for quinone and lecithin aggregates [18]. We relate the more pronounced red-shift of the Q_y band to approximately 20 times higher concentration of BChl *c* needed for HB spectroscopy compared to $\sim$ 20 µM that was used previously [18]. The higher BChl *c* concentration gives rise to formation of physically larger clusters of non-interacting aggregates, as well as it increases the probability of formation larger strongly coupled domains within individual aggregates. Specific and nonspecific scattering on the larger aggregate clusters is one of the causes of the absorption red-shift [21]. The stronger excitonic interaction is the other source of the red-shift of the Q_y band. However, it remains a challenge for the future studies to quantify the contribution of each of them. Note that for native chlorosomes from *Chlorobaculum tepidum*, red-shift of the Q_y band depends on the growth conditions being in the range between $\sim 85 - 93$ nm [22], which is in good agreement with our data presented here. X-ray scattering experiments showed the structural resemblance between the BChl *c* aggregates in hexane and the native chlorosomes [23]. Moreover, dependence of the Q_y red-shifts on concentration of the aggregation inducing agents is gradual which means that only the number of pigments participating in the strongly coupled domain changes, not the basic structural unit [18].

Increasing absorption cross-section and narrowing of the Q_y bands upon cooling demonstrate decreasing dynamic disorder in the aggregates. The red-most Qy bands around 760 nm therefore split into two discernible bands, whereas the higher energy bands remain unchanged (see Table 1). To explain the difference in the cooling red-shifts between quinone and lecithin

samples, one can speculate that quinone stabilizes short-range order more than lecithin. This would also lead to formation of larger well-ordered domains with lower dynamic disorder in the quinone aggregates at RT, implying smaller red-shift upon cooling, as well as larger aggregation induced red-shift as discussed above.

Quinone samples ($K2_{ox}$ and $K2_{red}$) differ from each other in absorption profile due to a band near 722 nm present only for $K2_{ox}$ sample. The band in the similar region ($\sim$ 710 – 715 nm at RT) has been previously assigned to BChl *c* anti-parallel dimers in aqueous buffer [24]. Nevertheless, theoretical calculations suggest that several other dimer-based structural units provide similar stabilization energies for optimized structures [25]. However, the precise determination of the basic structural unit is beyond the capability of the experimental methods employed in this study. Anyway, the specific structural motive of the aggregate does not effect conclusions drawn here.

Figure 1 shows the time evolution of the linear absorption after addition of dithionite during preparation of $K2_{red}$ sample at RT. The band around 722 nm disappears within 5 min, accompanied by simultaneous absorption increase in the region around 680 nm. This suggests that sodium dithionite disrupts the dimeric form in the $K2_{red}$ sample.

Table 1: *Absorption peak maxima at RT (λ_{RT}) and* 1.9 K *($\lambda_{1.9\,K}$) and their spectral shifts due to aggregation (Δ_{RT}, in respect to monomer absorption at* 667 nm*) and cooling to* 1.9 K *($\Delta_{1.9\,K}$). Peak maxima were identified from second derivative of absorption spectra. The experimental errors are up to* 2 nm.

Sample	λ_{RT}	Δ_{RT}	$\lambda_{1.9\,K}$	$\Delta_{1.9\,K}$
$K2_{ox}$	766	**99**	773	**7**
	-	-	758	-
	722	**55**	722	**0**
$K2_{red}$	768	**101**	773	**5**
	-	-	757	-
	667	**0**	671	**4**
Lec_{ox}	751	**84**	769	**18**
	-	-	754	-
	667	**0**	667	**0**
Lec_{red}	751	**84**	769	**18**
	-	-	754	-
	667	**0**	669	**2**

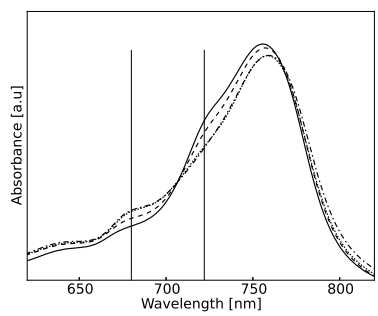

Figure 1: *Evolution of $K2_{red}$ absorption at RT with time after addition of sodium dithionite,* 1 min *(dashed line),* 5 min *(dotted line),* 45 min *(dash-dotted line), $K2_{ox}$ sample without dithionite (solid line). Vertical lines indicate absorption at* 680 nm *and* 722 nm*, respectively.*

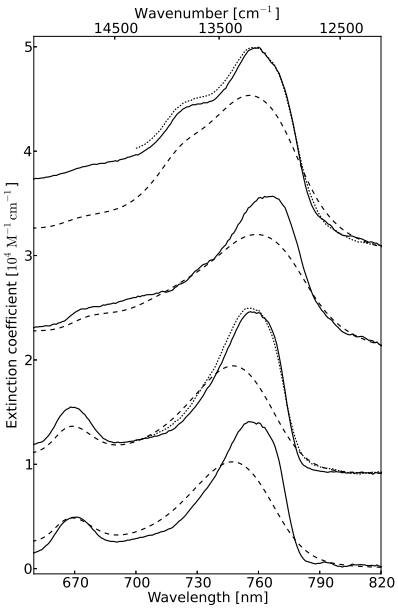

Figure 2: *Steady state absorption of the samples at RT (dashed line), at* 77 K *(dotted line) and* 1.9 K *(solid line) for* $K2_{\mathrm{ox}}$ *(top),* $K2_{\mathrm{red}}$ *(second),* Lec_{ox} *(third) and* Lec_{red} *(bottom) samples. Each set of lines is offset by* $0.9{\cdot}10^4\ \mathrm{M^{-1}\,cm^{-1}}$ *for clarity.*

3.2. Steady state fluorescence

Fluorescence measurements provide additional information about the excitonic structure of the aggregates. Moreover, quenching of the fluorescence intensity reflects shortening of the excited state lifetime as an additional deexcitation channel competes with the fluorescence. Normalized fluorescence spectra of all samples are depicted in Figure 3. Fluorescence spectral profiles can be fitted by a linear combination of skewed Gaussian functions of the form ([26] and references therein):

$$F(\nu) = \sum_i A_i \exp\left[\left(\frac{\nu-\mu_\mathrm{i}}{\sigma_\mathrm{i}}\right)^2\right]\left[1+\mathrm{erf}\left(\alpha_\mathrm{i}\frac{\nu-\mu_\mathrm{i}}{\sigma_\mathrm{i}}\right)\right] \quad (1)$$

where ν is wavenumber, A_i is the amplitude, μ_i is the central energy, σ_i is the width and α_i is the skewness of the i-th Gaussian peak. Two skewed Gaussians were needed to obtain sufficient fits to the data. Widths of the main emission band together with other fluorescence parameters are summarized in Table 2.

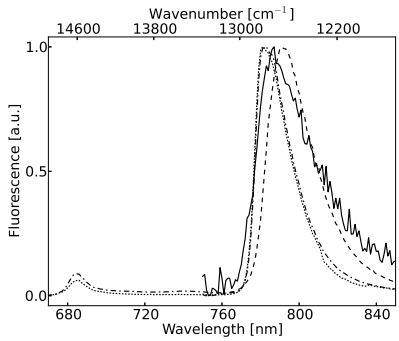

Figure 3: *Normalized fluorescence spectra of all samples at* 1.9 K *excited at* 457 nm, $K2_{\mathrm{ox}}$ *(solid line),* $K2_{\mathrm{red}}$ *(dashed line),* Lec_{ox} *(dotted line),* Lec_{red} *(dash-dotted line).*

Table 2: *Low temperature fluorescence parameters for all samples, Stokes shift (S), bandwidths (W) of the main emission band obtained from the fit, fluorescence quenching ratio (Q, see text for details).*

Sample	S [nm]/[cm^{-1}]	W [cm^{-1}]	Q
$K2_{\mathrm{ox}}$	28/470	303	8.7
$K2_{\mathrm{red}}$	30/490	299	
Lec_{ox}	24/410	246	2
Lec_{red}	24/410	247	

Lecithin samples exhibit significantly smaller Stoke's shift of 24 nm

compared to 28 nm (30 nm) for the $K2_{ox}$ ($K2_{red}$) samples respectively as first measured at low temperature for the BChl *c* aggregates. These values are close to 26 nm obtained for chlorosomes at various growth conditions [22]. Further discussion of Stoke's shift in relation to the results of HB experiments is in Section 3.4. We observe no dependence of the fluorescence spectral shapes on the excitation wavelength in the range 457–514 nm. Moreover, neither absorption nor fluorescence spectra exhibit temperature dependencies in the range 1.9–100 K. However, different behaviour was observed previously for chlorosomes where mainly fluorescence band became narrower and red-shifted after cooling the whole cells from 65 K down to 5 K [20]. The difference in the red-shift can be caused by the fact that chlorosomes in the whole cells are embedded in the cytoplasm which varies optical properties after freezing. No temperature induced narrowing of the fluorescence bands suggest the lower relative contribution of the dynamic disorder in artificial aggregates compared to the static contribution.

3.3. Fluorescence Quenching

Quenching ratio is defined as the ratio of fluorescence intensity of the sample under reduced conditions to the fluorescence of the sample in the oxidized state. For the first time, the quenching ratio is obtained for BChl *c* aggregates at 1.9 K, 2.0 for lecithin and 8.7 for quinone samples. For the latter, the quenching ratio is slightly higher compared to 5.8 and 7 published previously for BChl *c* aggregates at RT [11, 18]. Observed small quenching for lecithin samples suggests, that there exists a complementary redox-dependent mechanism for EE quenching other to quinones related. One possible explanation is self-quenching by BChl *c* radicals proposed for chlorosomes [27]. Molar ratio of quinone to BChl *c* was ∼0.8 (mol/mol) in our experiments, which is optimal concentration for studying the role of quinones in EE quenching based on the previous study [18]. Natural molar ratio found in native chlorosomes of *Chlorobaculum tepidum* is ∼0.1 (mol/mol) with observed quenching ratio of 11, i.e. quenching in chlorosomes is more efficient [11]. However, chlorosomes from *Chlorobaculum tepidum* contain chlorobium quinone, which is known to be more efficient quencher of EE [11]. Unlike in chlorosomes, quinones in BChl *c* aggregates play important structural role apart from being redox dependent quenchers, which could effectively lower the concentration of quinones involved in the quenching process [18]. The quinones are integrated into the nonpolar inter-lamellar space of the aggregate where the close contact and interaction between the polar head of the quinone and porphyrin ring of the BChl *c* is assumed to be essential for the quenching process. The same type of interaction was showed to be responsible for EE transfer between structurally similar carotenoids and BChl *c* in the chlorosomes [28].

3.4. Hole-burning experiments

Using HB spectroscopy, one can access the information obscured by inhomogeneous broadening, especially about the LES in the system and its couplings to the environment (for review see [29]). Width of the zero phonon hole (ZPH) is indirectly proportional to the excited

state lifetime according to the relation:

$$\delta_{\mathrm{h}} = \frac{1}{2\pi \mathrm{c} \mathrm{T}_1} + \frac{1}{\pi \mathrm{c} \mathrm{T}_2^*} \qquad (2)$$

where δ_{h} is homogeneous hole width, c is the speed of light, T_1 is the excited state lifetime and T_2^* is the pure dephasing time [30]. HB spectroscopy is therefore in this respect complementary spectroscopic method to pump-probe, since one obtains excited state lifetime indirectly in frequency domain. Additional features in hole-burned spectra such as phonon side-holes then reflect the electron-phonon coupling due to the interaction with environment (glass, protein etc.) [29]. Spectral dependence of the relative hole-depth at constant burning fluence provide information about the LES distribution within the $\mathrm{Q_y}$ band [31]. Relating SDF directly to the distribution of the LES in absorption is valid for BChl *c* aggregate under assumption that EE transfer (excitonic relaxation in this case) is much faster than the lifetime of LES. The assumption holds for chlorosome-like aggregates since the initial energy transfer is happening on the sub-100 fs timescale [32].

Figure 4 shows the typical spectral hole burnt to Lec_{ox} sample at 1.9 K. The hole spectrum is dominated by the ZPH with no discernible phonon sidebands which is a general feature of our data. The reason lies in a very low coupling to glassy matrix since BChl *c* mostly couple to neighbouring closely packed BChls. Antiholes on both sides of the ZPH confirm the photophysical HB process. No temperature dependence of the width of ZPH justify neglecting T_2^* in Equation 2 since the pure dephasing time is temperature-dependent [33]. All the presented values of the ZPL widths were extrapolated to zero burning energy. These extrapolated values were used to obtain excited state lifetimes according to Equation 2. In general, holes are shallow with relative depths in the maximum of SDF strongly dependent on the sample as summarized in Table 3. All these facts are in accordance with the results obtained for chlorosomes and provide further support for their resemblance to BChl *c* aggregates.

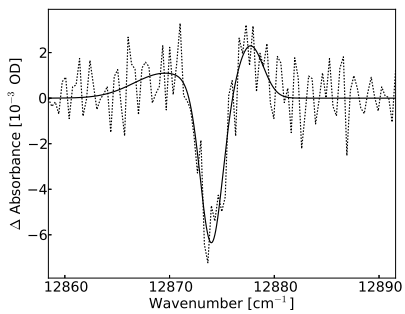

Figure 4: *Typical spectral hole burnt into Lec_{ox} sample (dotted line) at* $12\,868\,\mathrm{cm}^{-1}$ *(*777.1 nm*). The hole profile is fitted with a sum of three independent Gaussian functions (solid line).*

None of the samples exhibits dependence of spectral hole-width (LES lifetime) on the burning wavelength. In other words, we do not see any evidence for quenching of higher energy states by lower-laying ones within margins of our experimental error, although we cannot completely exclude it. This confirms the assumption that initial excitonic relaxation is extremely fast (see above). The averaged lifetimes determined from HB experiment are almost identical under oxidized and reduced conditions for both materials. Namely, lecithin samples exhibit the lifetimes of (4.3 ± 0.3) ps under ox-

idized and (4.5 ± 0.1) ps under reduced conditions. Similarly, the lifetime of (3.5 ± 0.3) ps and (3.7 ± 0.2) ps are obtained for quinone sample at oxidized and reduced conditions, respectively. Weak trend towards shortening of lifetimes under oxidized conditions can be discerned. Surprisingly, this trend is much smaller than that for chlorosomes from whole cells where the lifetime shortens from 5.75 ps at reduced conditions to 2.65 ps at oxidized conditions [20]. Nevertheless, in both cases lifetime shortening cannot fully explain observed quenching of fluorescence intensity (see Section 3.3). Possible explanation might be that EE quenching involves also other states than those accessible through HB experiment. This idea is supported by higher burning efficiency for lecithin samples and after addition of sodium dithionite in our experiments (see Table 3). It implies that excitation quenching competes on its timescales with exciton relaxation and would be therefore ultrafast on several 100 fs timescale, which was not resolved in time-resolved studies up to date [20, 27].

Important result in relation to quinone induced quenching in artificial BChl *c* aggregates is the appreciably shorter lifetime of LES in quinone samples compared to lecithin ones, meaning stronger quenching in the case of quinone samples even at reduced conditions. This is also well documented by 10 times smaller intensity of fluorescence of $K2_{\mathrm{red}}$ sample compared to Lec_{red}.

Position of SDF provides insight into the overestimated reorganization energies if determined as a half of the Stoke's shift. Calculation based on the values of Stoke's shift in Table 2 yields reorganization energies in range of 200–250 cm^{-1}. Using SDF instead of Q_y band maximum to determine the reorganization energies provide values of 30–50 cm^{-1}. These values are in a good agreement with values published for BChl *c* in solution (35–90 cm^{-1}, [34]) and for chlorosomes (20–30 cm^{-1} determined from SDF analysis, [33]).

Table 3: *Summary of parameters obtained from the fits of SDF by Gaussian function, central energy of SDF (ν_{SDF}), width of the SDF ($\mathrm{W}_{\mathrm{SDF}}$) and relative hole-depth (D).*

Sample	ν_{SDF} [cm^{-1}]	$\mathrm{W}_{\mathrm{SDF}}$ [cm^{-1}]	D [%]
$K2_{\mathrm{ox}}$	$12\,764 \pm 16$	52 ± 17	1.6
$K2_{\mathrm{red}}$	—	—	1.9
Lec_{ox}	$12\,828 \pm 8$	51 ± 6	4.2
Lec_{red}	$12\,862 \pm 12$	62 ± 9	4.3

Width of the SDF function reflects the inhomogeneous broadening of the LES. To our best knowledge, this is the first report of SDF in absorption for BChl *c* aggregates (see Table 3 and Figure 5). We observe significantly narrower distribution of LES in the range 50–60 cm^{-1} for artificial aggregates compared to 90–140 cm^{-1} published for native chlorosomes using HB in fluorescence [33, 35]. SDF related parameters have to be considered when designing plausible models for long-range organization of BChl *c* aggregates including disorder.

4. Conclusions

The spectroscopic properties of BChl *c* aggregates strongly resembles native chlorosomes, even at low temperatures. Experiments confirmed the role of isoprenoid quinones in redox dependent oxidation quenching at low temperatures. However, the quenching is not so efficient as for chlorosomes. I

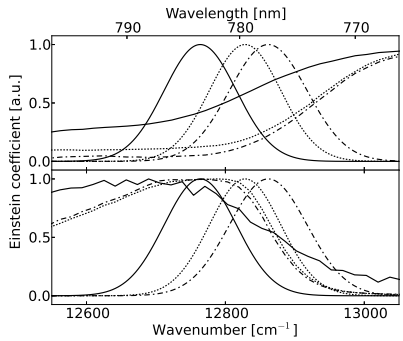

Figure 5: *Gaussian fits to SDF obtained from HB experiments in absorption together with absorption (upper panel) and fluorescence (lower panel) spectra for* $K2_{\mathrm{ox}}$ *(solid line),* Lec_{ox} *(dotted line) and* Lec_{red} *(dash-dotted line). All spectra are normalized.*

nterestingly, HB results suggest that quenching mechanism involves higher excitonic states than those examined by HB. It means that excitation quenching competes with the ultrafast excitonic relaxation. Moreover, quinone containing artificial BChl *c* aggregates quench the EE even at reduced conditions. Low temperature results provide information about static disorder and exclude low-frequency electron-phonon coupling. Together with structural parameters, the results can serve for designing plausible large scale model for BChl *c* aggregates.

Acknowledgements

The work was supported by project number 87010 from Grant Agency of Charles University (GAUK), grant number SVV 267304 from Charles University and project number P501/12/G055 from the Czech Science Foundation (GAČR).

References

[1] Graham R. Fleming and Mark A. Ratner. Grand challenges in basic energy sciences. *Phys Today*, 61(7):28–33, 2008.

[2] Robert E. Blankenship. *Molecular Mechanisms of Photosynthesis*, volume 1, chapter Photosynthetic Organisms and Organelles, pages 11–25. Blackwell Science, London, 2002.

[3] Hans Van Gemerden and Jordi Mas. *Anoxygenic Photosynthetic Bacteria*, volume 2, chapter Ecology of Phototrophic Sulfur Bacteria, pages 50–79. Kluwer Academic Publishers, Dordrecht, 1995.

[4] DJ Repeta, DJ Simpson, BB Jorgensen, and HW Jannasch. Evidence for anoxygenic photosynthesis from the distribution of bacterio-chlorophylls in the Black Sea. *Nature*, 342(2):69–72, nov 1989.

[5] Niels-Ulrik Frigaard and Donald A. Bryant. *In: Shively JM (eds) Complex Intracellular Structures in Prokaryotes*, volume 2 of *Microbiology Monographs*, chapter Chlorosomes: antenna organelles in photosynthetic green bacteria, pages 79–114. Springer, Berlin, 2006.

[6] Robert E. Blankeship and Katsumi Matsuura. *In: Green BR and Parson WW (eds) Light-harvesting antennas in photosynthesis*, volume 13, chapter

Antenna Complexes from Green Photosynthetic Bacteria, pages 195–217. Kluwer Academic Publishers, Dordrecht, 2003.

[7] Yueyong Xin, Su Lin, Gabriel a Montaño, and Robert E Blankenship. Purification and characterization of the B808-866 light-harvesting complex from green filamentous bacterium *Chloroflexus aurantiacus*. *Photosynth res*, 86(1-2):155–63, November 2005.

[8] Annemarie Huijser, Peter L. Marek, Tom J. Savenije, Laurens D.A. Siebbeles, Torsten Scherer, Robert Hauschild, Jędrzej Szmytkowski, Heinz Kalt, Horst Hahn, and Teodor Silviu Balaban. Photosensitization of TiO_2 and SnO_2 by artificial self-assembling mimics of the natural chlorosomal bacteriochlorophylls. *J Phys Chem C*, 111(31):11726–11733, 2007.

[9] Stephan CM Otte, Jos C van der Heiden, Norbert Pfenning, and Jan Amesz. A comparative study of the optical characteristics of intact cells of photosynthetic green sulfur bacteria containing bacteriochlorophyll *c*, *d* or *e*. *Photosynth Res*, 28:77–87, 1991.

[10] Mette Miller, Tomas Gillbro, and John M. Olson. Aqueous aggregates of bacteriochlorophyll *c* as a model for pigment organization in chlorosomes. *Photochem and Photobiol*, 57(1):98–102, 1993.

[11] Niels-Ulrik Frigaard, Shinichi Takaichi, Masamitsu Hirota, Keizo Shimada, and Katsumi Matsuura. Quinones in chlorosomes of green sulfur bacteria and their role in redox-dependent fluorescence studied in chlorosome-like bacteriochlorophyll *c* aggregates. *Arch Microbiol*, 167(2):343–349, 1997.

[12] M.I. Bystrova, I.N. Malgosheva, and A.A. Krasnovskii. Study of molecular mechanism of self-assembly of aggregated forms of bacteriochlorophyll *c*. *Mol Biol*, 13(3):440–451, 1979.

[13] A.A. Krasnovsky and M.I. Bystrova. Self-assembly of chlorophyll aggregated structures. *BioSystems*, 12:181–194, 1980.

[14] Masamitsu Hirota, Takeshi Moriyama, Keizo Shimada, Mette Miller, John M. Olson, and Katsumi Matsuura. The effect of detergent on the structure and composition of chlorosomes isolated from *Chloroflexus aurantiacus*. *Biochim Biophys Acta*, 1099:271–274, 1992.

[15] Teodor Silviu Balaban. Tailoring porphyrins and chlorins for self-assembly in biomimetic artificial antenna systems. *Accounts Chem Res*, 38:612–623, 2005.

[16] Tomohiro Miyatake and Hitoshi Tamiaki. Self-aggregates of natural chlorophylls and their synthetic analogues in aqueous media for making light-harvesting systems. *Coordin Chem Rev*, 254(21-22):2593–2602, November 2010.

[17] Pavel Klinger, Juan B. Arellano, Frantiek Vácha, Jan Hála, and Jakub Pšenčík. Effects of carotenoids and monogalactosyl diclyceride on bacteriochlorophyll *c* aggregates in aqueous buffer: implications for the self-assembly of chlorosomes. *Photochem and Photobiol*, 80:572–578, 2004.

[18] Jan Alster, A. Župčánová, F. Vácha, and J. Pšenčík. Effects of quinones on formation and properties of bacteriochlorophyll aggregates. *Photosynth Res*, 95:183–189, 2008.

[19] R. E. Blankenship, P. Cheng, T. P. Causgrove, D. C. Brune, S.H.H. Wang, J.U. Choh, and J. Wang. Redox regulation of energy transfer efficiency in antennas of green photosynthetic bacteria. *Photochem Photobiol*, 57:103–107, 1993.

[20] Jakub Pšenčík, Tomáš Polívka, Petr Němec, Juraj Dian, Jakub Kudrna, Petr Malý, and Jan Hála. Fast energy transfer and exciton dynamics in chlorosomes of the green sulphur bacterium *Chlorobium tepidum*. *J Phys Chem A*, 102:4392–4398, 1998.

[21] K Razi Naqvi, M N Merzlyak, and T B Melø. Absorption and scattering of light by suspensions of cells and subcellular particles: an analysis in terms of Kramers-Kronig relations. *Photochem. Photobiol. Sci*, 3(1):132–7, January 2004.

[22] Carles M. Borrego, Paolo D. Gerola, Mette Miller, and Raymond P. Cox. Light intensity effects on pigment composition and organisation in the green sulfur bacterium *Chlorobium tepidum*. *Photosynth Res*, 59:159–166, 1999.

[23] Jakub Pšenčík, Mika Torkkeli, Anita Zupčanová, František Vácha, Ritva E Serimaa, and Roman Tuma. The lamellar spacing in self-assembling bacteriochlorophyll aggregates is proportional to the length of the esterifying alcohol. *Photosynth Res*, 104(2-3):211–9, June 2010.

[24] Mitsuo Umetsu, Ryoichi Seki, Tomoyuki Kadota, Zheng-Yu Wang, Tadafumi Adschiri, and Tsunenori Nozawa. Dynamic exchange properties of the antiparallel bacteriochlorophyll *c* dimers. *J Phys Chem B*, 107:9876–9882, 2003.

[25] J. Alster, M. Kabeláč, R. Tuma, J. Pšenčík, and J.V. Burda. Computational study of short-range interactions in bacteriochlorophyll aggregates. *Comput Theor Chem*, 998:87–97, October 2012.

[26] Yutaka Shibata, Yoshitaka Saga, Hitoshi Tamiaki, and Shigeru Itoh. Low-temperature fluorescence from single chlorosomes, photosynthetic antenna complexes of green filamentous and sulfur bacteria. *Biophys J*, 91:3787–3796, 2006.

[27] Paula van Noort, Yinwen Zhu, Russell LoBrutto, , and Robert E. Blankenship. Redox effects on the excited-state lifetime in chlorosomes and bacteriochlorophyll *c* oligomers. *Biophys J*, 72:316–325, 1997.

[28] Jakub Pšenčík, Juan B Arellano, Aaron M Collins, Pasi Laurinmäki, Mika Torkkeli, Benita Löflund, Ritva E Serimaa, Robert E Blankenship, Roman Tuma, and Sarah J Butcher. Structural and functional roles of carotenoids in chlorosomes. *J Bacteriol*, 195(8):1727–34, April 2013.

[29] Ryszard Jankowiak, Mike Reppert, Valter Zazubovich, Jörg Pieper, and Tonu Reinot. Site selective and single complex laser-based spectroscopies: a window on excited state electronic structure, excitation energy transfer, and electron-phonon coupling of selected photosynthetic complexes. *Chem Rev*, 111(8):4546–98, August 2011.

[30] Josef Fridrich and Dietrich Haarer. Photochemical hole burning: a spectroscopic study of relaxation processes in polymers and glasses. *Angew Chem*, 23(2):113–140, 1984.

[31] NRS Reddy, R Picorel, and GJ Small. B896 and B870 components of the *Rhodobacter sphaeroides* antenna: a hole burning study. *J Phys Chem*, pages 6458–6464, 1992.

[32] Jakub Dostál, Tomáš Mančal, Ramunas Augulis, František Vácha, Jakub Pšenčík, and Donatas Zigmantas. Two-dimensional electronic spectroscopy reveals ultrafast energy diffusion in chlorosomes. *J Am Chem Soc*, 134(28):11611–7, July 2012.

[33] Jakub Pšenčík, Martin Vácha, František Adamec, Milan Ambrož, Juraj Dian, Jan Boček, and Jan Hála. Hole burning study of excited state structure and energy transfer dynamics of bacteriochlorophyll *c* in chlorosomes of green sulphur photosynthetic bacteria. *Photosynth Res*, 42:1–8, 1994.

[34] D C Brune, R E Blankenship, and G R Seely. Fluorescence quantum yields and lifetimes for bacteriochlorophyll *c*. *Photochem and photobiol*, 47(5):759–63, May 1988.

[35] ZG Fetisova and K Mauring. Experimental evidence of oligomeric organization of antenna bacteriochlorophyll *c* in green bacterium *Chloroflexus aurantiacus* by spectral hole. *FEBS lett*, 307(3):371–374, 1992.

Paper III

Vibronic origin of long-lived coherence in an artificial molecular light harvester

[1*]James Lim, [2,3*]David Paleček, [1]Felipe Caycedo-Soler, [4]Craig N. Lincoln [5]Javier Prior, [6]Hans von Berlepsch, [1]Susana F. Huelga, [1]Martin B. Plenio, [2]Donatas Zigmantas and [4]Jürgen Hauer

[1] *Institut für Theoretische Physik, Universität Ulm, Albert-Einstein Allee 11, 89069 Ulm, Germany*

[2] *Department of Chemical Physics, Lund University, P.O. Box 124, SE-22100 Lund, Sweden*

[3] *Department of Chemical Physics, Charles University in Prague, Ke Karlovu 3, 121 16 Praha 2, Czech Republic*

[4] *Photonics Institute, Vienna University of Technology, Gusshausstrasse 27, 1040 Vienna, Austria*

[5] *Departamento de Física Aplicada, Universidad Politécnica de Cartagena, Cartagena 30202, Spain*

[6] *Forschungszentrum für Elektronenmikroskopie, Institut für Chemie und Biochemie, Freie Universität Berlin, Fabeckstrasse 36a, D-14195 Berlin, Germany*

*Contributed equaly

juergen.hauer@tuwien.ac.at

Abstract

Natural and artificial light-harvesting processes have recently gained new interest. Signatures of long-lasting coherence in spectroscopic signals of biological systems have been repeatedly observed, albeit their origin is a matter of ongoing debate, as it is unclear how the loss of coherence due to interaction with the noisy environments in such systems is averted. Here we report experimental and theoretical verification of coherent exciton-vibrational (vibronic) coupling as the origin of long-lasting coherence in an artificial light harvester, a molecular J-aggregate. In this macroscopically aligned tubular system, polarization-controlled 2D spectroscopy delivers an uncongested and specific optical response as an ideal foundation for an in-depth theoretical description. We derive analytical expressions that show under which general conditions vibronic coupling leads to prolonged excited-state coherence.

The remarkably high efficiency in photosynthesis, where nine out of ten absorbed photons reach the reaction centre, is a fascinating field of modern research. In such photosynthetic complexes, structure, dynamics and function are inextricably linked. A conserved building block comprises strongly absorbing pigments arranged in close proximity to one another sup-

ported by the surrounding protein scaffold [1, 2]. Typical inter-pigment distances are of order of 10 Å and photon absorption leads to the formation of delocalized excited electronic states (excitons) shared by two or more pigment molecules. Exciton creation, migration and trapping are central to the functionality of a photosynthetic apparatus. The controlled and adjustable arrangement of the pigments tunes the electronic network and the properties of its interaction with the vibrational environment that is associated with either the pigments or the protein. The detailed balance of these properties determines the efficiency of light-harvesting systems [3, 4].

Exciton dynamics can be efficiently probed by two-dimensional (2D) electronic spectroscopy [5]. This technique revealed oscillatory signals in the spectral response of a wide variety of photosynthetic aggregates [6, 7]. Initially ascribed to excitonic beatings, oscillations have been found to persist up to several hundreds of femtoseconds at room temperature [8–10]. This timescale exceeds typical dephasing rates in the condensed phase and becomes comparable to exciton transfer times [1], thus posing the question of the nature and functional relevance of these coherences [4]. Unfortunately, the complex structure of 2D signals makes the unambiguous identification of the underlying mechanisms that support such long-lived coherences a challenging task and several hypotheses to explain them have been formulated [11–21]. The different approaches can be classified into theories including coherent interaction of excitons with intra-pigment vibrations [11–15] and theories focusing on incoherent exciton-protein interaction such as correlated fluctuations [16–18]. It is possible that some of these mechanisms may coexist on certain timescales and that one or another may become dominant depending on the system under consideration.

In this work, we show that the relatively simple excitonic structure of a molecular J-aggregate provides an ideal test case to identify the microscopic mechanism behind long-lived oscillations in electronic 2D signals. The investigated J-aggregate is tubular and aligns along the sample's flow direction when in solution. In addition, the J-aggregate exhibits excitonic bands with roughly orthogonal transition dipole moments. It is this combination of perpendicular excitonic transitions and macroscopic alignment that makes electronic 2D spectroscopy with polarization-controlled excitation pulses an ideal tool to study coherence effects between the excitonic bands. This approach significantly reduces the complexity of retrieved 2D signals, leading to only two peaks with oscillatory components in specific regions of the 2D maps, that is, one on the diagonal and one as a cross-peak for nonrephasing and rephasing signal components, respectively. Employing a vibronic model, we derive analytical expressions that show how system parameters such as electronic decoherence rates and exciton-vibrational resonance determine the amplitude and lifetime of oscillatory signals. Fitting the analytical expressions to measured data, the vibronic model achieves quantitative agreement with experimental observations. Concerning potential functional relevance of the observed oscillations, we show that the long-lived oscillatory signals in our system are dominated by excited-state coherence rather

than ground-state coherence.

Results

The system

J-aggregates of cyanine dyes are promising candidates for artificial antenna systems [22–26]. They are chemically versatile and self-assemble into various extended supramolecular structures in aqueous solution [27]. Here a system that can be considered a macroscopically aligned synthetic light harvester was studied, namely a molecular J-aggregate of C8O3-monomers whose aggregation behaviour is well known [28, 29]. As revealed by cryogenic transmission electron microscopy [30], the aggregate structure is best described as a double-layered nanotube with outer diameter $\sim 11\,\mathrm{nm}$ and lamellar spacing of $\sim 2.2\,\mathrm{nm}$ between the chromophore layers. In addition, superhelical bundles of these tubes can also form though the addition of polyvinyl alcohol inhibits this process and thereby avoids single-layered tube formation [22] and maintains a stable solution over several weeks [31]. A drawing of the J-aggregate under investigation, from here on referred to as C8O3, is shown in Fig. 1a. The bilayer configuration of C8O3 allows the effect of different decoherence rates to be studied as the outer solvent-exposed layer shows faster decoherence than the inner protected layer.

The structural properties of the aggregate are remarkable: the 11 nm outer diameter is contrasted by a length of several micrometres. Circulating solvated C8O3 with a wire-guided jet (Fig. 1a) leads to a macroscopic orientation of the tubes because the longitudinal axis preferentially aligns along the flow direction.

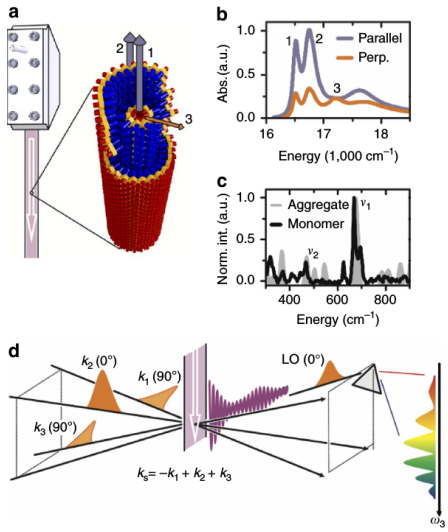

Figure 1: *C8O3 and polarization-controlled 2D spectroscopy. (a) Wire-guided window-free jet used for sample circulation, along with a schematic of the double-layered structure of the C8O3 aggregate. The aggregates align along the flow direction (white arrow). The transition dipole directions of bands 1–3 are displayed by arrows, which are mainly polarized along the tube axis (bands 1 and 2 shown in blue) or perpendicular to the axis (band 3 shown in orange). (b) Absorption spectra in arbitrary units, Abs. (a. u.), with light polarized parallel (blue) and perpendicular (perp.; orange) to the flow direction. (c) Non-resonant Raman spectra of the C8O3 monomer (black line) and aggregate (grey area). The vibrational frequencies ν_1 and ν_2 are close to the exciton energy splitting between bands 1 and 3 and bands 2 and 3, respectively. (d) Polarization-controlled 2D spectroscopy with three excitation pulses (k_1 to k_3) and a local oscillator (LO) for heterodyne detection of the signal field, depicted as an oscillating line. Polarization orientation (0°or 90°) is given with respect to the longitudinal axis of aligned C8O3.*

This creates anisotropy for linearly polarized light, as shown in Fig. 1b. Linear dichroism measurements [31]. A drawing of the J-aggregate under investigation, from here on referred to as C8O3, is sho and redox-chemistry studies [32] assign bands 1 and 2 to longitudinal transitions localized on the inner and outer cylinders, respectively (Fig. 1a). Transitions to band 3 are preferentially polarized perpendicular to the long axis of C8O3 and are shared by both layers. A detailed description of sample-preparation methods and band assignments is given in the Supplementary Notes 1 and 2.

Fitting the well-defined absorption peaks of C8O3 with Lorentzian functions (see Supplementary Note 2) reveals an exciton energy difference between bands 1 and 3 of $\Delta\Omega_{31} \approx 690\,\mathrm{cm}^{-1}$ and $\Delta\Omega_{32} \approx 460\,\mathrm{cm}^{-1}$ for bands 2 and 3. Both exciton energy splittings are close to vibrational frequencies $\nu_1 \approx 668\,\mathrm{cm}^{-1}$ and $\nu_2 \approx 470\,\mathrm{cm}^{-1}$ observed in non-resonant Raman spectra [33] (Fig. 1c). These vibrational frequencies are measured in both the monomer and aggregate Raman spectra, that is, they are not aggregation-induced Raman bands. Strongly enhanced modes at similar energies were observed in resonant Raman spectra of a related cyanine dye, and can be assigned to out-of-plane vibrations [34]. Such out-of-plane vibrations were shown to couple strongly to excitons [35]. The quasi-resonance between the vibrational frequencies ν_1 and ν_2 and exciton energy splittings $\Delta\Omega_{31}$ and $\Delta\Omega_{32}$ provides us with an interesting scenario of possible coherent interaction between bands (excitons) and vibrations [11, 13, 14, 21, 36]. Such exciton–vibrational coupling induces vibronic [12] and vibrational coherences [15], which can both lead to long-lived beating signals in 2D spectra. Here we emphasize that coherence in the electronic excited-state manifold is referred to as vibronic and in the ground-state manifold as vibrational. Identifying the dominant contribution is of fundamental importance because only vibronic coherence, which manifests in excited-state dynamics, can enhance exciton transport and thus support light-harvesting function [37–39].

Experimental results

The absorption spectrum of a light-harvesting system may be heavily congested because of overlapping excitonic bands and the resulting 2D signal would exhibit significant overlap between diagonal and cross-peaks, thereby impeding further analysis. It has been suggested to employ laser pulses of different relative polarization to selectively address relevant excitation pathways to obtain a clearer 2D signal [40]. However, the advantage of polarization-controlled 2D spectroscopy has been limited by the isotropic nature of the investigated samples (an ensemble). In the experiment presented here, these problems are circumvented by the measurement of the macroscopically aligned C8O3. The transition dipole moments of bands 1 and 2 are preferentially parallel to the longitudinal axis while band 3 is orthogonal, thus allowing for optimal polarization selectivity. This combination reduces the obtained 2D maps to only two relevant peaks with negligible overlap and an up to 30 times stronger signal intensity as compared with the isotropic case [41].

The ideal pulse sequence to iso-

late beating signals between states with orthogonal transition dipole moments, that is, bands 1 and 3 in the present case, is depicted in Fig. 1d, where the phase-matched direction for measuring rephasing spectra is displayed: non-rephasing spectra can be measured along the same phase-matched signal direction by changing the order of the first two pulses (see Methods). After subtraction of the non-oscillatory background, we performed a Fourier transformation along waiting time t_2 for all points on the 2D (ω_1, ω_3) map. The resulting ω_2 plots allow the lineshape of beating signal with frequency ω_2 to be visualized as a function of position in (ω_1, ω_3) space. The slice at the exciton energy splitting between bands 1 and 3 ($\omega_2 = 705 \pm 20\,\mathrm{cm}^{-1}$ with the experimental resolution of $\pm 20\,\mathrm{cm}^{-1}$) reveals a non-rephasing diagonal peak N11 and a rephasing cross-peak R31 as shown in Fig. 2a,b, respectively. N11 is centred at (ω_1, ω_3)= (Ω_1, Ω_1) with exciton energy $\Omega_1 \approx 16,405\,\mathrm{cm}^{-1}$ of band 1 and a symmetric linewidth $2\Gamma_{g1} \approx 130\,\mathrm{cm}^{-1}$ along both ω_1 and ω_3 axes (Fig. 2a). The centre of R31 is located at (ω_1, ω_3)= (Ω_3, Ω_1) with exciton energy $\Omega_3 \approx 17,125\,\mathrm{cm}^{-1}$ of band 3 and asymmetric linewidths $2\Gamma_{g3} \approx 300\,\mathrm{cm}^{-1}$ and $2\Gamma_{g1} \approx 130\,\mathrm{cm}^{-1}$ along ω_1 and ω_3 axes, respectively (Fig. 2b). In peak amplitude, R31 is $\sim 30\,\%$ of N11. Turning to the ω_2 slice corresponding to the energy splitting between bands 2 and 3 ($\omega_2 = 462 \pm 20\,\mathrm{cm}^{-1}$), Fig. 2e,f reveal a diagonal non-rephasing peak N22, which is centred at (ω_1, ω_3)=(Ω_2, Ω_2) with the exciton energy $\Omega_2 \approx 16,672\,\mathrm{cm}^{-1}$ of band 2 and a symmetric linewidth $2\Gamma_{g2} \approx 225\,\mathrm{cm}^{-1}$ along ω_1 and ω_3 axes. The amplitude of N22 is only $5\,\%$ of N11.

Theoretical model

To describe the long-lived oscillations in N11 and R31, a vibronic model is employed that describes the coupling of bands 1 and 3 to a quasi-resonant vibrational mode with frequency ν_1. Consider a system with electronic ground state $|g_k\rangle$ and excited states for bands 1 and 3, denoted by $|1_k\rangle$ and $|3_k\rangle$, respectively, where $k = 0$ and 1 denote the vibrational ground and excited states, respectively (Fig. 3a). The vibronic coupling between the quasi-resonant states $|3_0\rangle$ and $|1_1\rangle$ leads to unnormalized vibronic eigenstates $\langle\tilde{3}_0| = \langle 3_0| + \epsilon\,\langle 1_1|$ and $\langle\tilde{1}_1| = \langle 1_1| + \epsilon\,\langle 3_0|$. Here ϵ represents the degree of vibronic mixing defined by

$$\epsilon = i\nu_1\sqrt{\mathrm{S}_1}(i\Delta\nu_1 - \Gamma_{13})^{-1} \quad (1)$$

where $\Delta\nu_1 = (\Omega_3 - \Omega_1) - \nu_1$ denotes the detuning between $|3_0\rangle$ and $|1_1\rangle$, that is, between the exciton energy splitting and vibrational frequency, and S_1 denotes the Huang-Rhys factor of the vibrational mode, which in turn quantifies the strength of the vibronic coupling (see Supplementary Note 2 for details of the derivation). The electronic decoherence rate Γ_{gk} describes the exponential decay rate of the coherence between electronic ground state and band k, while Γ_{13} represents the overall exponential decay rate of the inter-exciton coherence between bands 1 and 3. In our model, we do not consider inhomogeneous broadening, which is justified by the observation that the experimentally measured absorption spectrum is well matched to a sum of Lorentzian functions with the linewidths $2\Gamma_{gk}$ (see Supplementary Note 2).

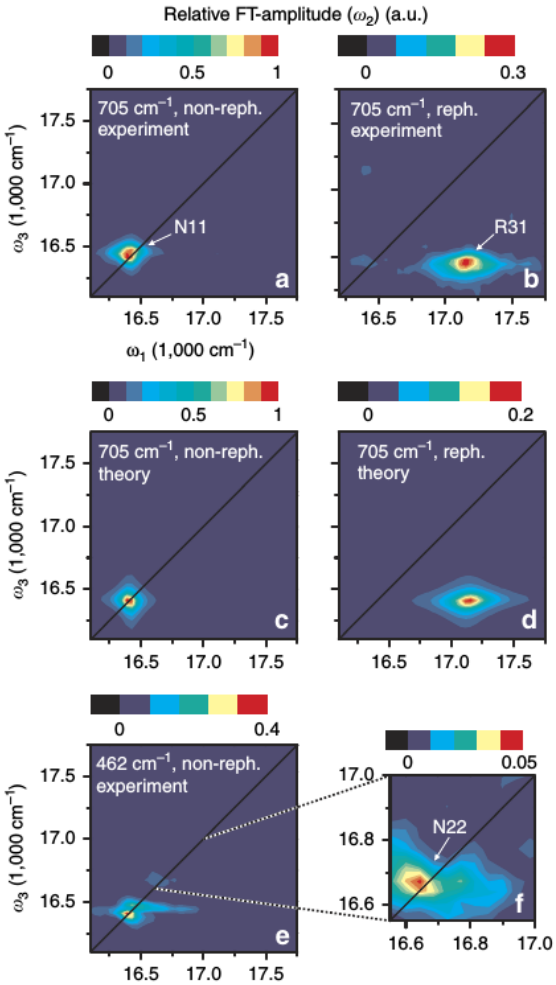

Figure 2: *Experimental and theoretical 2D spectra. (a,b) The Fourier-transform (FT) amplitude maps of non-rephasing (non-reph.) and rephasing (reph.) spectra at* $\omega_2 = 705 \pm 20\,\mathrm{cm}^{-1}$*, which reveal the presence of a non-rephasing diagonal peak N11 and a rephasing cross-peak R31. These peaks stem from the coherent interaction of bands 1 and 3 with the quasi-resonant vibrational mode with frequency* $\nu_1 \approx 668\,\mathrm{cm}^{-1}$ *. The amplitude of N11 is about three times larger than R31. The lineshape of N11 is symmetric along both* ω_1 *and* ω_3 *axes, while that of R31 is elongated along* ω_1 *axis. (c,d) The simulated spectra at* $\omega_2 = 705\,\mathrm{cm}^{-1}$ *with N11 and R31. (e) The FT amplitude map at* $\omega_2 = 462 \pm 20\,\mathrm{cm}^{-1}$ *reveals coherent interaction of bands 2 and 3 with the quasi-resonant vibrational mode with frequency* $\nu_2 \approx 470\,\mathrm{cm}^{-1}$*. However, as depicted in (f) the associated non-rephasing peak N22 at* $\omega_{1,3} \approx 16,670\,\mathrm{cm}^{-1}$ *is weak and only amounts to 5% of N11 at* $\omega_2 = 705 \pm 20\,\mathrm{cm}^{-1}$ *(see a). The diagonal peak at* $\omega_{1,3} \approx 16,400\,\mathrm{cm}^{-1}$ *in e stems from N11, with a peak centred at* $\omega_2 = 705 \pm 20\,\mathrm{cm}^{-1}$*, but broad enough to appear at* $\omega_2 = 462 \pm 20\,\mathrm{cm}^{-1}$*. All measurements were carried out at room temperature.*

This is valid when homogeneous broadening dominates the linewidths and the Huang-Rhys factors are sufficiently small, as is the case here. In addition, the lineshape of N11 (Fig. 2a) is not elongated along the diagonal $\omega_1 = \omega_3$, implying our 2D signal is dominated by homogeneous broadening. The same conclusion is reached from analysing 2D correlation spectra [33].

In nonlinear spectroscopy, the molecular response to laser excitation is described by response functions [42]. According to the vibronic model described above, the response function for the oscillatory signals in N11 reads

$$\mathcal{R}_{\mathrm{N11}} = \mu_1^2\mu_3^2\Gamma_{g1}^{-2}(\mathrm{e}^{[\mathrm{i}(\Delta\Omega_{31}+\delta\omega)-\Gamma_{13}]t_2} + \mathrm{e}^{[i(\nu_1-\delta\omega)-\gamma_\nu]t_2}\epsilon^2), \quad (2)$$

with μ_1 and μ_3 denoting the transition dipole moment of bands 1 and 3, respectively. The prefactor Γ_{g1}^{-2} stems from the lineshape of N11, γ_ν denotes the dissipation rate of the vibrations and do stands for the frequency shift of the vibronic eigenstates $\langle\tilde{3}_0|$ and $\langle\tilde{1}_1|$ relative to the uncoupled states $\langle 3_0|$ and $\langle 1_1|$ due to the vibronic coupling (see Fig. 3a and Supplementary Note 2 for further details). The coupling was found to be sufficiently strong to induce non-negligible vibronic mixing $|\epsilon|^2 \approx 0.03$, which leads to a long-lived beating signal in N11 up to $t_2 \approx 800$ fs, as shown in Fig. 3b. These results imply that the initial excitonic part of $|1_0\rangle\langle\tilde{3}_0|$ decays rapidly with $1/e$ decay time of $\Gamma_{13}^{-1} \approx 66$ fs while the vibronic coherence $|1_0\rangle\langle\tilde{1}_1|$ explains a long-lived oscillatory signal in N11: here $|1_0\rangle\langle\tilde{3}_0|$ ($|1_0\rangle\langle\tilde{1}_1|$) represents coherence between two vibronic states $|1_0\rangle$ and $|\tilde{3}_0\rangle$ ($|1_0\rangle$ and $\langle\tilde{1}_1|$), respectively.

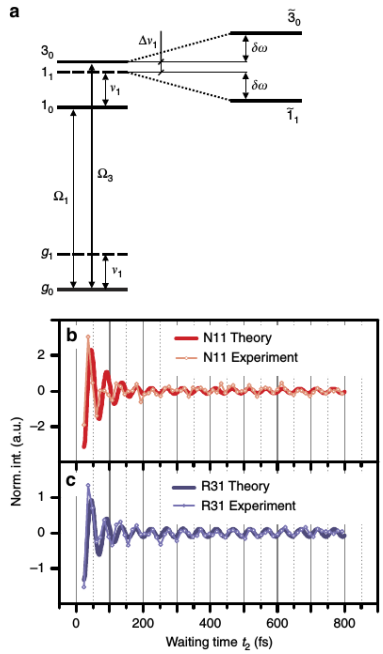

Figure 3: *Vibronic model. (a) We consider a vibronic model for bands 1 and 3 coupled to a vibrational mode with frequency* $\nu_1 \approx 668\,\mathrm{cm}^{-1}$ *(see Supplementary Note 2). The vibronic states* $|k_0\rangle$ *and* $|k_1\rangle$ *denote the vibrational ground and first excited states of an electronic state* $|k\rangle$*, respectively, with the single index states* $|g\rangle$*,* $|1\rangle$ *and* $|3\rangle$ *denoting the electronic ground state and bands 1 and 3, respectively. The exciton energy splitting* $\Delta\Omega_{31} = \Omega_3 - \Omega_1$ *between bands 1 and 3 is quasi-resonant with the vibrational frequency* ν_1*, where the detuning is denoted by* $\Delta\nu_1 = \Delta\Omega_{31} - \nu_1$*. The exciton–vibrational coupling between uncoupled states* $|3_0\rangle$ *and* $|1_1\rangle$ *leads to vibronic eigenstates* $\langle\tilde{3}_0|$ *and* $\langle\tilde{1}_1|$*, each of which is a superposition of* $|3_0\rangle$ *and* $|1_1\rangle$*, leading to an energy-level shifting by* $\delta\omega$*. (b) The time trace of N11 in normalized intensity (Norm. Int.) against waiting time* t_2*, where the experimental results are shown as light red circles and the theoretical simulation is shown as a full red line. (c) The time trace of R31 where the experimental results are shown as light blue circles and the simulated data are depicted as a full blue line. The root mean squared deviation between the experimental results and theoretical simulation in b and c is 0.92 and 0.59, respectively.*

The response function for the oscillatory contributions to R31 is given by

$$\begin{aligned}\mathcal{R}_{\mathrm{R31}} &= \mu_1^2\mu_3^2\Gamma_{g3}^{-1}\Gamma_{g1}^{-1} \\ &\times(\mathrm{e}^{[\mathrm{i}(\Delta\Omega_{31}+\delta\omega)-\Gamma_{13}]\mathrm{t}_2}+ \\ &\mathrm{e}^{[i(\nu_1-\delta\omega)-\gamma_\nu]t_2}\epsilon^2\left(\eta_e-\eta_g\right)),\end{aligned} \quad (3)$$

where $\Gamma_{g3}^{-1}\Gamma_{g1}^{-1}$ derives from the asymmetric lineshape of R31 (see Fig. 2b,d). Here η_e and η_g represent the contribution of excited-state vibronic coherence $|1_0\rangle\langle\tilde{1}_1|$ and ground-state vibrational coherence $|g_0\rangle\langle g_1|$, respectively, to the long-lived beating signal in R31 (see Supplementary Note 2). The vibrational coherence in the electronic ground-state manifold does not play a role in exciton transfer dynamics, but nonetheless modulates the 2D spectra. A fit of model parameters to experimental results (Fig. 3c) shows that $|\eta_e| \approx 2.5|\eta_g|$. This means the long-lived beating signal in R31 is dominated by the excited-state coherence $|1_0\rangle\langle\tilde{1}_1|$. The short-lived beating signal in R31 is induced by $|1_0\rangle\langle\tilde{3}_0|$, as is the case for N11. We note that the signal at N11, with approximately three times the amplitude of R31, is exclusively determined by excited-state contributions. Details of this vibronic model and the corresponding Feynman diagrams for the spectral components N11 and R31 are discussed in the Supplementary Note 2.

These results demonstrate how an excitonic system within a noisy environment can exhibit long-lasting coherent features: the observed long-lived oscillations are the result of coherent interaction of excitonic bands with an underdamped, quasiresonant vibration. This vibronic mechanism requires the vibrational dissipation rate γ_ν to be much slower than the electronic decoherence rate Γ_{13}, which is the case for C8O3, where $\gamma_\nu(1\,\mathrm{ps})^{-1}$ and $\Gamma_{13} \approx (66\,\mathrm{fs})^{-1}$. The differencein electronic and vibrational decoherence rates can be rationalized from the fact that excitons and vibrations are related to the motion of electrons and nuclei, respectively. The lower mass of electrons as compared with nuclei makes excitons more mobile and therefore more sensitive to environmental fluctuations, such as local electric fields, than vibrations. We note that the vibronic mixing leading to long-lived beating signals in 2D electronic spectra is described by a vibronic coupling that induces coherent energy exchange between excitons and quasi-resonant vibrations (see Supplementary Note 2 for further details):

$$H_{e-v} = \nu_1\sqrt{\mathrm{S}_1}\left(|3_0\rangle\langle 1_1| + |1_1\rangle\langle 3_0|\right). \quad (4)$$

This implies that the vibronic coupling not only induces long-lasting electronic excited-state coherences but also can mediate population transfer between excitonic bands. In a combination with thermal relaxation of exciton populations, the vibronic coupling may further enhance exciton population transfer and as a result could, in principle, have functional relevance in exciton transport [14, 38, 43–45].

Interestingly, the different decoherence rates $\Gamma_{g3} \approx 2\Gamma_{g1}$ of bands 1 and 3 lead to different amplitudes of the short-lived beating signals in N11 and R31 (Fig. 3b, c), which are determined by prefactors Γ_{g1}^{-2} and $\Gamma_{g3}^{-1}\Gamma_{g1}^{-1}$ and, respectively. The lower decoherence rate of band 1 can be explained by band 1 being localized on the inner layer, while band 3 is delocalized over both the inner and outer layers [46]. As shown by the response func-

tions for N11 and R31, the overall strength of the beating signals is proportional to the inverse of the electronic decoherence rates. It is therefore expected that the beating signal amplitude would diminish with an increase of the decoherence rate. This is the case for N22, where the physical situation in terms of exciton-vibrational resonance ($\Delta\Omega_{32} \approx \nu_2 \approx 470\,\mathrm{cm}^{-1}$) is equivalent to N11 ($\Delta\Omega_{31} \approx \nu_1 \approx 668\,\mathrm{cm}^{-1}$). The crucial difference is that band 2 has a higher decoherence rate than band 1, as band 2 is localized on the outer layer exposed to solvent [46]. This explains the broader linewidth of band 2 in absorption and 2D spectra. Using an estimated value of $\Gamma_{g2} \approx (47\,\mathrm{fs})^{-1}$, the presented theory predicts the strength of N22 to be 5 % of N11 (see Supplementary Note 2), which is in line with the experimental observations (Fig. 2f). These results indicate that the experimentally observed long-lived beating signals, induced by vibronic mixing, require adequately low electronic decoherence rates, highlighting that resonance between exciton energy splitting and vibrational frequency alone is not sufficient [47].

The presented vibronic model achieves quantitative agreement with the experimental observations. Crucially, the constraints imposed by the observed asymmetric decoherence rates $\Gamma_{g3} \approx 2\Gamma_{g1}$ and fast relaxation of exciton population in C8O3 on subpicosecond timescales[33] rule out incoherent models, where long-lived oscillations are sustained by Markovian correlated fluctuations (see Supplementary Note 3 for a detailed analysis). This further supports our conclusion that the observed experimental data provide evidence for vibronic mixing being the mechanism at play in our system.

We note that our results do not imply that correlated fluctuations can be universally ruled out, as this mechanism could be in place in certain pigment-protein complexes. The notion of correlated fluctuations has been developed for photosynthetic complexes where pigments are embedded in a protein scaffold. The protein has been considered as the potential source of correlated fluctuations in natural light harvesters [16, 17]. For C8O3, a structural frame such as a protein scaffold is absent and therefore correlated fluctuations are unlikely to induce long-lived oscillatory 2D signals, which is in line with our observations.

Discussion

We have verified, theoretically and experimentally, that coherent vibronic coupling in the electronic excited-state manifold is responsible for the long-lived beating signals observed in 2D spectra of an artificial light harvester. The relatively simple electronic and vibrational structure of the investigated molecular aggregate along with its macroscopic alignment allowed us to rule out the presence of correlated fluctuations. The specific geometry of our system allowed us to gain further insights by illustrating the conditions under which intra-pigment vibrations can prolong electronic coherent effects. The moderately low decoherence rate of band 1, localized on the inner layer and protected from solvent, is the basis for exciton-vibrational coupling as the source of long-lived beating signals. The outer band 2, even though resonantly coupled to a vibration, exhibits

a higher decoherence rate and therefore fails to produce observable oscillations. We conclude that the mere resonance between excitons and vibrations does not suffice to explain long-lived beating signals. An adequately low electronic decoherence rate, determined by the interaction between system and bath, is an equally important prerequisite.

The influence of vibronic coupling on energy transport in molecular aggregates has been extensively studied in the past, as recently reviewed [44]. The vibronic coupling has recently gained new interest (see ref. 48 for a recent tutorial overview), as it was suggested as a feasible mechanism to explain long-lived oscillations in the 2D spectra of several natural light-harvesting complexes and a photosynthetic reaction centre [9, 10]. The requirement of exciton-vibrational resonance is readily satisfied in such systems, given their numerous excitonic bands and rich vibrational structures. Incoherent models based on correlated fluctuations were not ruled out though. Our work provides a quantum mechanical foundation for enhanced energy transfer based on vibronic coupling. As recently demonstrated, this mechanism is not limited to natural light harvesting, vibronic coupling is also of key importance in photovoltaic devices [48].

Methods

Polarization-controlled 2D electronic spectroscopy

In 2D electronic spectroscopy, three ultrashort laser pulses generate an optical response of a molecular ensemble, which is spectrally resolved along both absorption (ω_1) and detection (ω_3) frequencies within the laser pulse spectrum. The absorption frequency ω_1 is obtained by precise scanning of the time delay between the first two pulses and subsequent Fourier transformation ($t_1 \rightarrow \omega_1$). In detection, the signal is spectrally dispersed, leading directly to the detection frequency ω_3. Varying time delay t_2 between pulses 2 and 3 provides information about evolution of the system on a femtosecond timescale [49–51]. To retrieve the purely absorptive part, the signal induced by pulses 1-3 is detected in a heterodyned fashion by interfering it with a phase-stable local oscillator pulse. Polarization control is achieved by the combination of $\lambda/4$ wave plates and wire grid polarizers for each of the laser beams to select the desired polarization with high accuracy. Polarization-resolved 2D experiments change the relative contributions of distinct pathways depending on the polarization of the laser pulses, orientation of the transition dipole moments and isotropy of the sample [40]. Rephasing spectra were acquired with a polarization sequence of $(90°, 0°, 90°, 0°)$ for pulses $(1, 2, 3,$ local oscillator$)$, in contrast to non- rephasing spectra, where the time ordering of the first two pulses is reversed, leading to a polarization sequence of $(0°, 90°, 90°, 0°)$. The polarization scheme used for rephasing spectra (Fig. 1d) shows 0° was defined to be parallel to the sample flow direction, depicted as a white arrow in Fig. 1a. For a macroscopically aligned sample, this particular polarization sequence selects pathways stemming from interband coherences and vibronic mixing [12, 15], discussed throughout the paper, while pathways with all-parallel transition dipole moments such as ground-state bleach, stimulated emission, excited-state absorption and also

vibrational wave packet excitation are suppressed. For the details regarding the experimental methods, see Supplementary Note 1. To subtract the non-oscillatory signals from 2D spectra, we employed a decay-associated spectra analysis [33], where the population decays were fitted by a sum of three 2D spectra with individual decay constants. The ω_2 maps in Fig. 2 were obtained using Fourier transformation ($t_2 \rightarrow \omega_2$) with zero-padding up to 2^7 data points. All measurements were carried out at room temperature.

Additional information

Supplementary Information accompanies this paper at http://www.nature.com/naturecommunications.

Author contributions

D.P., D.Z. and J.H. designed and conducted experiments; H.v.B. was responsible for sample preparation, structural characterization and Raman measurements; J.L., F.C.-S., C.N.L., D.P., J.P. and J.H. analysed the data; J.L., F.C.-S., S.F.H., J.H. and M.B.P. developed theory; all authors discussed the results and wrote the manuscript.

Acknowledgments

Acknowledgements We thank Valentyn I. Prokhorenko for help in 2D-DAS analysis. C.N.L. and J.H. acknowledge funding by the Austrian Science Fund (FWF): START project Y 631-N27 and by COST Action CM1202-PERSPECT-H2O. J.L., F.C.-S., S.F.H. and M.B.P. acknowledge funding by the EU STREP PAPETS and QUCHIP, the ERC Synergy Grant BioQ, the Deutsche Forschungsgemeinschaft (DFG) within the SFB/TRR21 and an Alexander von Humboldt Professorship. J.P. acknowledges funding by the Spanish Ministerio de Economía y Competitividad under Project No. FIS2012-30625. D.P. and D.Z. acknowledge funding by the Swedish Research Council and Knut and Alice Wallenberg Foundation.

References

[1] H. van Amerongen, L. Valkunas, and R. van Grondelle. *Photosynthetic Excitons*. World Scientific, 2000.

[2] Robert E. Blankenship. *Molecular Mechanism of Photosynthesis*. Blackwell Science Ltd, 2002.

[3] Thomas Renger, Volkhard May, and Oliver Kühn. Ultrafast excitation energy transfer dynamics in photosynthetic pigment–protein complexes. *Phys. reports*, 343(3):137–254, 2001.

[4] S. F. Huelga and M. B. Plenio. Vibrations, Quanta and Biology. *Contemporary Physics*, 54(27 June):181–207, 2013.

[5] David M Jonas. Two-dimensional femtosecond spectroscopy. *Annu. Rev. Phys. Chem.*, 54(1):425–463, January 2003.

[6] Gregory S Engel, Tessa R Calhoun, Elizabeth L Read, Tae-Kyu Ahn, Tomáš Mančal, Yuan-Chung Cheng, Robert E Blankenship, and Graham R Fleming. Evidence for wavelike energy transfer through quantum coherence in photosynthetic systems. *Nature*, 446(7137):782–786, April 2007.

[7] Jakub Dostál, Tomáš Mančal, František Vácha, Jakub Pšenčík, and Donatas Zigmantas. Unraveling the nature of coherent beatings in chlorosomes. *J. Chem. Phys.*, 140(11):115103, 2014.

[8] Elisabetta Collini, Cathy Y Wong, Krystyna E Wilk, Paul M G Curmi, Paul Brumer, and Gregory D Scholes. Coherently wired light-harvesting in photosynthetic marine algae at ambient temperature. *Nature*, 463(7281):644–647, February 2010.

[9] Elisabet Romero, Ramunas Augulis, Vladimir I Novoderezhkin, Marco Ferretti, Jos Thieme, Donatas Zigmantas, and Rienk van Grondelle. Quantum coherence in photosynthesis for efficient solar-energy conversion. *Nature Phys.*, 10, 2014.

[10] Franklin D. Fuller, Jie Pan, Andrius Gelzinis, Vytautas Butkus, S. Seckin Senlik, Daniel E. Wilcox, Charles F. Yocum, Leonas Valkunas, Darius Abramavicius, and Jennifer P. Ogilvie. Vibronic coherence in oxygenic photosynthesis. *Nat. Chem.*, 6(July):706–711, 2014.

[11] A. W. Chin, J. Prior, R. Rosenbach, F. Caycedo-Soler, S. F. Huelga, and M. B. Plenio. The role of non-equilibrium vibrational structures in electronic coherence and recoherence in pigment-protein complexes. *Nat. Phys.*, 9(2):113–118, 2013.

[12] M B Plenio, J Almeida, and S F Huelga. Origin of long-lived oscillations in 2D-spectra of a quantum vibronic model: electronic versus vibrational coherence. *J. Chem. Phys.*, 139(23):235102, 2013.

[13] A. W. Chin, S. F. Huelga, and M. B. Plenio. Coherence and decoherence in biological systems: principles of noise-assisted transport and the origin of long-lived coherences. *Phil. Trans. R. Soc. A*, 370(1972):3638–3657, 2012.

[14] Avinash Kolli, Edward J. O'Reilly, Gregory D. Scholes, and Alexandra Olaya-Castro. The fundamental role of quantized vibrations in coherent light harvesting by cryptophyte algae. *J. Chem. Phys.*, 137(17):174109, 2012.

[15] Vivek Tiwari, William K Peters, and David M Jonas. Electronic resonance with anticorrelated pigment vibrations drives photosynthetic energy transfer outside the adiabatic framework. *Proc. Natl. Acad. Sci.*, 110(4):1203–1208, January 2013.

[16] H Lee, YC Cheng, and GR Fleming. Coherence dynamics in photosynthesis: protein protection of excitonic coherence. *Science*, 1462, 2007.

[17] Akihito Ishizaki, Tessa R. Calhoun, Gabriela S. Schlau-Cohen, and Graham R. Fleming. Quantum coherence and its interplay with protein environments in photosynthetic electronic energy transfer. *Phys. Chem. Chem. Phys.*, 12(27):7319, 2010.

[18] Dugan Hayes, Graham B Griffin, and Gregory S Engel. Engineering Coherence Among Excited States in Synthetic Heterodimer Systems. *Science*, (April), apr 2013.

[19] N. Christensson, F. Milota, J. Hauer, J. Sperling, O. Bixner, A. Nemeth, and H. F. Kauffmann. High frequency vibrational modulations in two-dimensional electronic spectra and their resemblance to electronic coherence signatures. *J. Phys. Chem. B*, 115(18):5383–5391, 2011.

[20] Felipe Caycedo-Soler, Alex W. Chin, Javier Almeida, Susana F. Huelga, and Martin B. Plenio. The nature of the low energy band of the Fenna-Matthews-Olson complex: vibronic signatures. *J. Chem. Phys.*, 136(15):155102, 2012.

[21] Niklas Christensson, Harald F Kauffmann, Tõnu Pullerits, and Tomáš Mančal. Origin of Long-Lived Coherences in Light-Harvesting Complexes. *J. Phys. Chem. B*, 116(25):7449–7454, June 2012.

[22] Dirk J. Heijs, Arend G. Dijkstra, and Jasper Knoester. Ultrafast pump-probe spectroscopy of linear molecular aggregates: Effects of exciton coherence and thermal dephasing. *Chem. Phys.*, 341(1-3):230–239, 2007.

[23] Frank Würthner, Theo E Kaiser, and Chantu R Saha-Möller. J-aggregates: from serendipitous discovery to supramolecular engineering of functional dye materials. *Angewandte Chemie (International ed. in English)*, 50(15):3376–410, April 2011.

[24] D M Eisele, D H Arias, X F Fu, E A Bloemsma, C P Steiner, R A Jensen, P Rebentrost, H Eisele, A Tokmakoff, S Lloyd, K A Nelson, D Nicastro, J Knoester, and M G Bawendi. Robust excitons inhabit soft supramolecular nanotubes. *Proc. Natl. Acad. Sci. USA*, 111(33):E3367–E3375, 2014.

[25] Joel Yuen-Zhou, Dylan H. Arias, Dorthe M. Eisele, Colby P. Steiner, Jacob J. Krich, Moungi G. Bawendi, Keith A. Nelson, and Alán Aspuru-Guzik. Coherent Exciton Dynamics in Supramolecular Light-Harvesting Nanotubes Revealed by Ultrafast Quantum Process Tomography. *ACS Nano*, 8(6):5527–5534, 2014.

[26] Yan Qiao, Frank Polzer, Holm Kirmse, Egon Steeg, Sergei Kühn, Sebastian Friede, Stefan Kirstein, and Jürgen P Rabe. Nanotubular J-aggregates and quantum dots coupled for efficient resonance excitation energy transfer. *ACS Nano*, 9(2):1552–60, 2015.

[27] H von Berlepsch. *J-Aggregates, chapter 4.* World Scientific, 2012.

[28] H. Von Berlepsch, S. Kirstein, and C. Böttcher. Effect of alcohols on J-aggregation of a carbocyanine dye. *Langmuir*, 18(20):7699–7705, 2002.

[29] Hans Von Berlepsch. Controlling the helicity of tubular J-aggregates by chiral alcohols. *J. Phys. Chem.*, pages 9646–9654, 2003.

[30] H. von Berlepsch, C. Böttcher, A Ouart, C. Burger, S. Dähne, and S. Kirstein. Supramolecular Structures of J -Aggregates of Carbocyanine Dyes in Solution. *J. Phys. Chem. B*, 104:5255–5262, 2000.

[31] Hans Von Berlepsch, Stefan Kirstein, Ralph Hania, and Christoph Bo. Stabilization of Individual Tubular J -Aggregates by Poly (vinyl alcohol). *J. Phys. Chem. B*, 2003(107):14176–14184, 2003.

[32] Dörthe M Eisele, C W Cone, E A Bloemsma, S M Vlaming, C G F van der Kwaak, R J Silbey, Moungi G Bawendi, Jasper Knoester, J P Rabe, and D A Vanden Bout. Utilizing redox-chemistry to elucidate the nature of exciton transitions in supramolecular dye nanotubes. *Nat. Chem.*, 4(8):655–662, 2012.

[33] Franz Milota, Valentyn I Prokhorenko, Tomáš Mančal, Hans von Berlepsch, Oliver Bixner, Harald F Kauffmann, and Jürgen Hauer. Vibronic and vibrational coherences in two-dimensional electronic spectra of supramolecular J-aggregates. *J. Phys. Chem. A*, 117(29):6007–14, July 2013.

[34] Metin Aydin, Özge Dede, and Daniel L Akins. Density functional theory and Raman spectroscopy applied to structure and vibrational mode analysis of 1,1',3,3'-tetraethyl-5,5',6,6'-tetrachloro- benzimidazolocarbocyanine iodide and its aggregate. *J. Chem. Phys.*, 134(6):064325, 2011.

[35] Christopher C. Rich and Jeanne L. McHale. Resonance Raman Spectra of Individual Excitonically Coupled Chromophore Aggregates. *J. Phys. Chem. C*, 117(20):10856–10865, 2013.

[36] Vytautas Butkus, Donatas Zigmantas, Darius Abramavicius, and Leonas Valkunas. Distinctive character of electronic and vibrational coherences in disordered molecular aggregates. *Chem. Phys. Lett.*, 587:93–98, 2013.

[37] Jordan M Womick and Andrew M Moran. Exciton coherence and energy transport in the light-harvesting dimers of allophycocyanin. *J. Phys. Chem. B*, 113(48):15747–59, dec 2009.

[38] Jordan M Womick and Andrew M Moran. Vibronic enhancement of exciton sizes and energy transport in photosynthetic complexes. *J. Phys. CHem. B*, 115(6):1347–1356, 2011.

[39] Marco Del Rey, Alex W. Chin, Susana F. Huelga, and Martin B. Plenio. Exploiting structured environments for efficient energy transfer: The phonon antenna mechanism. *J. Phys. Chem. Lett*, 4(6):903–907, 2013.

[40] RM Hochstrasser. Two-dimensional IR-spectroscopy: polarization anisotropy effects. *Chem. Phys.*, 266:273–284, 2001.

[41] Elizabeth L Read, Gregory S Engel, Tessa R Calhoun, Tomás Mancal, Tae Kyu Ahn, Robert E Blankenship, and Graham R Fleming. Cross-peak-specific two-dimensional electronic spectroscopy. *Proc. Natl. Acad. Sci. USA*, 104(36):14203–8, sep 2007.

[42] S. (Shaul) Mukamel. *Principles of nonlinear optical spectroscopy*. New York : Oxford University Press, 1995. Includes bibliographical references and index.

[43] Václav Perlík, Joachim Seibt, Laura J. Cranston, Richard J. Cogdell, Craig N. Lincoln, Janne Savolainen, František Šanda, Tomáš Mančal, and Jürgen Hauer. Vibronic coupling explains the ultrafast carotenoid-to-bacteriochlorophyll energy transfer in natural and artificial light harvesters. *J. Chem. Phys.*, 142(21):212434, 2015.

[44] M. Schröter, S.D. Ivanov, J. Schulze, S.P. Polyutov, Y. Yan, T. Pullerits, and O. Kühn. Exciton–vibrational coupling in the dynamics and spectroscopy of Frenkel excitons in molecular aggregates. *Physics Reports*, 567:1–78, 2015.

[45] Nathan Killoran, Susana F. Huelga, and Martin B. Plenio. Enhancing light-harvesting power with coherent vibrational interactions: a quantum heat engine picture. *ArXiv*, pages 1–12, 2015.

[46] Cătălin Didraga, Audrius Pugžlys, P. Ralph Hania, Hans Von Berlepsch, Koos Duppen, and Jasper Knoester. Structure, spectroscopy, and microscopic model of tubular carbocyanine dye aggregates. *J. Phys. Chem. B*, 108(39):14976–14985, 2004.

[47] Alexei Halpin, Philip J. M. Johnson, Roel Tempelaar, R. Scott Murphy, Jasper Knoester, Thomas L. C. Jansen, and R. J. Dwayne Miller. Two-dimensional spectroscopy of a molecular dimer unveils the effects of vibronic coupling on exciton coherences. *Nat. Chem.*, 6(3):196–201, 2014.

[48] Sarah Maria Falke, Carlo Andrea Rozzi, Daniele Brida, Margherita Maiuri, Michele Amato, Ephraim Sommer, Antonietta De Sio, Angel Rubio, Giulio Cerullo, Elisa Molinari, Christoph Lienau, and Others. Coherent ultrafast charge transfer in an organic photovoltaic blend. *Science*, 344(6187):1001–1005, 2014.

[49] Tobias Brixner, Tomáš Mančal, Igor V Stiopkin, and Graham R Fleming. Phase-stabilized two-dimensional electronic spectroscopy. *J. Chem. Phys.*, 121(9):4221–4236, September 2004.

[50] Ramũnas Augulis and Donatas Zigmantas. Two-dimensional electronic spectroscopy with double modulation lock-in detection: enhancement of sensitivity and noise resistance. *Optics express*, 19(14):13126–33, July 2011.

[51] Ramūnas Augulis and Donatas Zigmantas. Detector and dispersive delay calibration issues in broadband 2D electronic spectroscopy. *JOSA B*, 30(6):1770, May 2013.

Paper IV

Quantum Coherence as a Witness of Vibronically Hot Energy Transfer in Bacterial Reaction Centre.

[1,2]David Paleček, [3]Petra Edlund, [3]Sebastian Westenhoff and [1]Donatas Zigmantas and

[1] *Department of Chemical Physics, Lund University, P.O. Box 124, SE-22100 Lund, Sweden*

[2] *Department of Chemical Physics, Charles University in Prague, Ke Karlovu 3, 121 16 Praha 2, Czech Republic*

[3] *Department of Chemistry and Molecular Biology, University of Gothenburg, Box 462, SE-40530 Gothenburg, Sweden*

donatas.zigmantas@chemphys.lu.se

Abstract

Photosynthetic proteins have evolved over billions of years for optimal energy transfer to the sites where charges are generated. Based on spectroscopically detected quantum coherences, it has been suggested that this energy transfer is partially wave-like. This conclusion critically depends on the assignment of the coherences to the evolution of excitonic superpositions. Here we demonstrate for a bacterial reaction centre that the long-lived coherent spectroscopic oscillations, which bear canonical signatures of excitonic superpositions, are due to vibrational coherences transferred to the ground state of the chromophores. We directly show that appearance of these coherences is caused by release of the electronic energy during the energy transfer. Proposed photophysical mechanism is general and may explain long-lived oscillations in other photosynthetic proteins. Furthermore, our findings supports the idea of protein tuning vibrational properties of chromophores for the energy transfer optimisation.

1. Introduction

For efficient photosynthesis, energy migrates through large chromophore assemblies to the active site of charge generation. This transfer is generally downhill in energy, but every energy transfer step must obey the law of energy conversation. This means that vibrational modes take up excess energy of each transfer step. The identification of these critical modes is difficult, since they are not readily observable in conjunction with energy transfer by current spectroscopies.

Absorption of light by a molecule excites its valence electrons and its nuclei readjust their positions. Subsequently, the electron cloud and the atoms oscillate coherently across all excited molecules; an electronic and vibrational coherence is established. Coupling to the environment, for instance to solvent molecules or to the

protein binding pocket, leads to dephasing of these coherence between different molecules.

Vibrational wave packets have been readily observed in photosynthetic proteins using femtosecond transient spectroscopic experiments in the visible, and near infrared spectral regions [1, 2]. In addition, polarisation resolved transient femtosecond absorption experiments provided early evidence for electronic coherences in photosynthetic proteins [3, 4]. The advent of two-dimensional electronic spectroscopy (2DES) opened a new avenue to study electronic and vibrational coherence [5–8]. The higher dimensionality of the data leads to less spectral congestion hence enabling more detailed insight [9, 10].

In the 2DES experiment a sequence of three ultrashort pulses (with time delays t_1 and t_2 between them) excites the sample. The resulting signal field is detected with a fourth pulse at t_3 after the last laser excitation pulse. The evolution of the excited states is then detected in two-dimensional correlation spectra relating excitation (ω_1) and detection frequencies (ω_3), which are Fourier transform (FT) conjugates of the t_1 and t_3 time delays [5]. The spectroscopy detects coherences between photophysical states as oscillatory signals along t_2. It is difficult to distinguish between electronic or vibrational coherence in the spectra. However polarisation resolved 2DES [11–14], an additional FT over population time t_2 [14–16], and theoretical analyses [10, 17] have been developed to this end.

The first reports on 2D electronic spectra of light-harvesting proteins created excitement, because it was concluded that electronic coherences live for more than a picosecond [7, 8, 11, 13, 18]. This would suggest that energy can migrate wave-like through photosynthetic proteins. This far-reaching conclusion relies on the correct assignment of the observed oscillation to an electronic coherence. Fundamentally, electronic coherences surviving on picosecond time scales in proteins seem unrealistic, because an electron weighs only a fraction of an atom. Electronic coherences should decay much faster than vibrational coherences, which typically dephase within a few picoseconds.

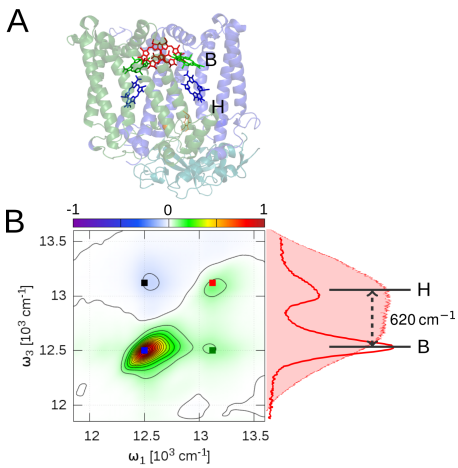

Figure 1: *(A) The structure of* RC_{sph}. *The special pair is coloured red, the associated bacteriochlorophylls green, the bacteriopheophytins blue. (B) 2D spectrum of the oxidised BRC at* $t_2 = 24$ fs, *at* 77 K *temperature together with the absorption spectrum and shaded laser spectrum. The energy gap between the excitonic bands is* $\sim 620\,\mathrm{cm}^{-1}$. *The chromophores form a spectroscopic aggregate and give rise to two excitonic absorption bands which are denoted as B, and H, respectively. The absorption of* P^+ *is not observed.*

We performed 2DES experiments on RC_{sph} grown from the carotenoid-

less R-26 strain. The protein comprises two strongly coupled bacteriochlorophyll *a* molecules, forming the special pair, two accessory bacteriochlorophylls *a*, and two bacteriopheophytins *a* (Fig. 1A). To enable the use of 2DES spectroscopy at a high repetition rate (20 kHz), we used RC_{sph} with a chemically oxidised special pair (P^+) at 77 K. This shortens the photocycle considerably by preventing charge separation, but the time constant of excitation energy transfer to the special pair is not altered [19].

A linear absorption spectrum of the reaction centre protein at 77 K (Fig. 1B) shows two distinct peaks. The peaks are separated by $\sim 620\,cm^{-1}$ and are associated with the excitons B and H (Fig. 1B). A 2D absorption spectra measured at $t_2 = 24$ fs matches these absorptions on the diagonal (Fig. 1B). We did not observe any distinct features of the two branches of RC_{sph} in the 2DES data. The positive cross-peak below the diagonal indicates coupling and excitation energy transfer (EET) between H and B. The negative-valued region above the diagonal arises from the excited state absorption of B. This absorption also masks the positive upper cross-peak.

Along t_2, all features in the 2D spectra decay smoothly and have oscillatory components (data not shown) [13]. The former reports on the *populations* of excited states and the latter indicates *coherences*. The integrated oscillatory features across the 2D spectra reveal frequencies of $195, 325, 560, 650, 725, 890$ and $1150\,cm^{-1}$ (Fig. 2A, blue line, "all-parallel" measurement). All of these frequencies can be identified as peaks in resonance Raman spectra of B [20, 21].

To assign the coherences, we performed two experiments. Firstly, we used a particular cross-polarisation scheme (relative polarization of $\pi/4, -\pi/4, \pi/2, 0$ for laser pulses 1 to 4), with which signals from purely vibrational coherences are suppressed [11, 13]. Indeed, the measurement shows that amplitudes of the frequencies at $195, 325, 725, 890$ and $1150\,cm^{-1}$ are decreased relative to frequencies at $560, 620\,cm^{-1}$ (Fig. 2A, red line, "cross-polarised"). The sustained frequencies are close to the energy difference between B and H ($620\,cm^{-1}$, see Fig. 1B). We and others have so far considered this degeneracy as evidence for an electronic contribution to the coherence [7, 8, 11, 13]. Secondly, we Fourier transformed the complex-valued 2DES data along t_2. This yields coherence amplitude maps of $+\omega_2$ and $-\omega_2$, with the positive and negative frequency separating the system response evolving as $e^{-i\omega_2 t_2}$ or $e^{+i\omega_2 t_2}$during the population time t_2. The coherent amplitude maps at $\omega_2 = -560\,cm^{-1}$ and $\omega_2 = +560\,cm^{-1}$, measured with a cross-polarised pulse sequence, show peaks on the off-diagonal (rephasing pulse order) and diagonal (non-rephasing pulse order). A similar pattern is observed for the coherence at $\omega_2 = \pm 650\,cm^{-1}$ (see Fig. SI2B). This pattern is as expected for electronic coherence between two interacting excitonic states [10].

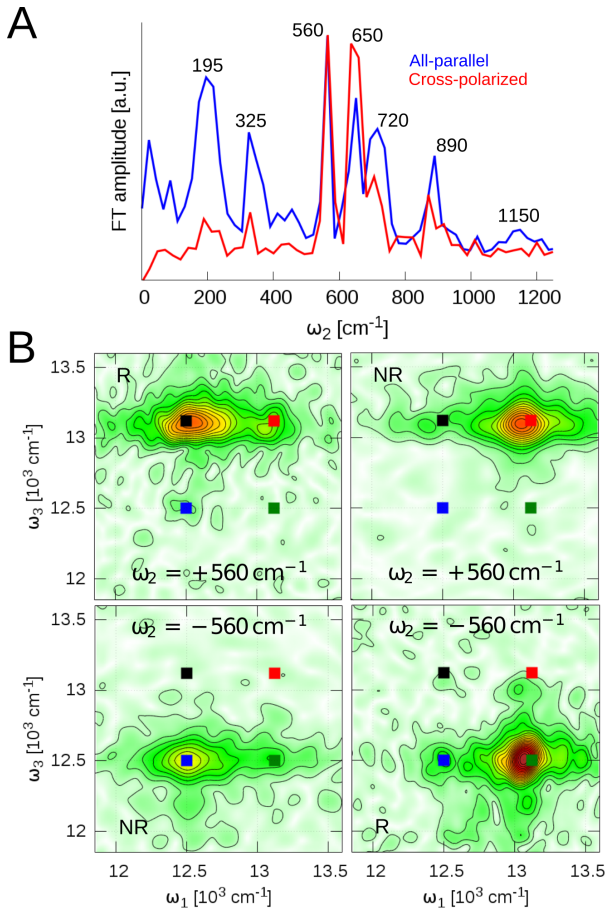

Figure 2: *Suppression of vibrational coherences by polarization resolved 2DES. (A) Integrated 2D oscillation maps show all the beating frequencies present in all-parallel and cross-polarised measurements. The spectra are normalised to the* $560\,\mathrm{cm}^{-1}$ *amplitude). (B) 2D slices at* $\omega_2 = 560\,\mathrm{cm}^{-1}$ *extracted from the cross-polarised spectra measured between* $216 - 1620\,\mathrm{fs}$*; the rephasing part oscillates exclusively off-diagonal and the non-rephasing part oscillates on diagonal only. The colour rectangles depict positions of the main peaks in the 2D spectrum.*

Thus, the the coherences at 560 and $650\,\mathrm{cm}^{-1}$ for $\mathrm{RC}_{\mathrm{sph}}$, interpreted with the current understanding of molecular electronic response, can be assigned to be electronic. However, electronic coherences can only exist when the excited states are populated. We determined the lifetime of the two coherences to be 1.5 ps and 2.5 ps, respectively (see SI, Fig SI5), although the underlying states, B and H, live only for ≤ 200 fs. Since coherences cannot outlive populations, an unsettling mismatch between spectral observation and fundamental quantum mechanical principle arises.

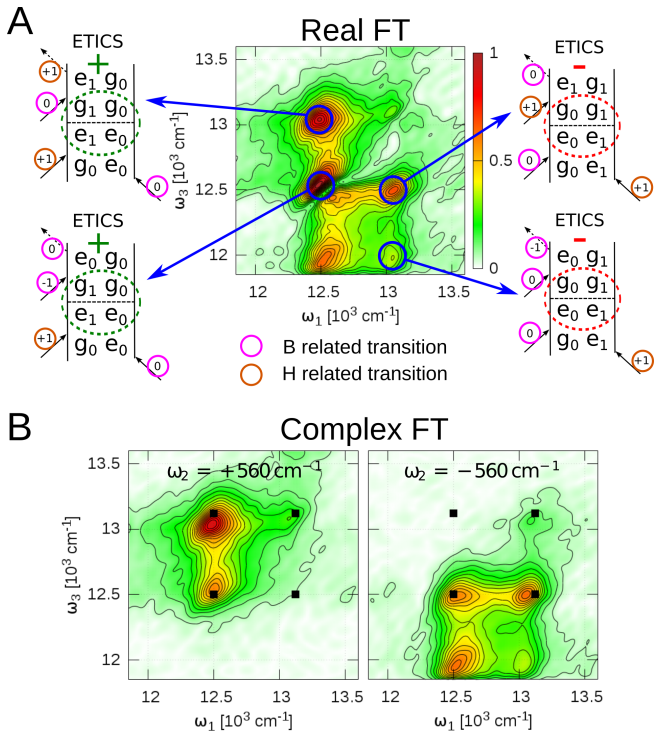

Figure 3: *Cancellation of signals at the diagonal peak at 12.5 cm-1 demonstrates ETICS. (A) Coherent amplitude map are shown for* $\omega_2 = 560\,\mathrm{cm}^{-1}$ *computed from real-valued rephasing spectra measured between* $\mathrm{t}_2 = 216 - 1740\,\mathrm{fs}$. *The Feynman diagrams show all the rephasing ETICS pathways, which are complementary to their SE analogues (see SI Fig. 3). g and e denote the ground and electronically excited states, the superscript indicates the vibrational quantum number. The number on the transition arrows indicates the change of vibrational quantum number. (B) Computing the Fourier transform from complex-valued data separates* $\pm\omega_2$ *frequencies.*

To resolve this mismatch, we inspect coherence amplitude maps at $\omega_2 = 560\,\mathrm{cm}^{-1}$ measured with an all-parallel pulse sequence. The pattern for the map computed from complex-valued data is consistent with a combination of coherences in the excited state (stimulated emission pathways) and ground state (ground state bleach pathways) (Fig. 3B, see SI for details). However, when computing the map from real-valued data, a line with zero signal crossing through the diagonal B peak appears (Fig. 3A). Apparently, the contributing pathways cancel out. This is inconsistent with assuming stimulated emission and ground state bleach pathways to be active, as these pathways should interfere constructively. Additionally, the coherence in the excited state should have been decayed if energy transfer to P^+ has occurred. Since $t_2 < 216\,\mathrm{fs}$ were omitted in the computation of ω_2 slices, EET to P^+ is completed and the stimulated emission signal should be absent altogether.

We therefore propose that all co-

herences observed in the maps (Fig 3A and B) are in the ground state. The first two laser pulses create a coherence which is fully or partially vibrational in the excited state of the exciton B (Fig. 3A). Then, the coherence is shifted to the ground state. Here, it turns purely vibrational, it is located on the associated bacteriochlorophylls, and it can live for several picoseconds independent of the excited state lifetime. We consider that the coherence shift is induced by energy transfer to P^+ [22] and we therefore term this process Energy Transfer Induced Coherence Shift (ETICS) (Fig. 4C).

The ETICS pathways (Fig. 3) produce signals with an opposite sign (π-phase shift) compared to the corresponding signals from stimulated emission pathways (Fig. SI3), because the third pulse interacts with the other side of the density matrix. The zero signal node in the B diagonal (Fig. 3A) is then readily explained, because the ground state bleach pathways and ETICS pathways overlap and cancel out. The sign flip of the ETICS signals is also consistent with the observed amplitude pattern of the peaks in the oscillatory maps in Fig. 3 (see SI for details). Moreover, we find that all coherences have amplitude maps that are consistent with ETICS pathways (Fig. SI1 and SI2).

ETICS should be observable directly as a π-phase shift within the first $t_2 \sim 170$ fs. We search for this behaviour in the t_2-dependence of the upper cross-peak in a cross-polarization measurement (Fig. 4AB), because this spectral position is expected to be clear of any monotonous leakage signals due to incomplete polarization of the laser pulses.

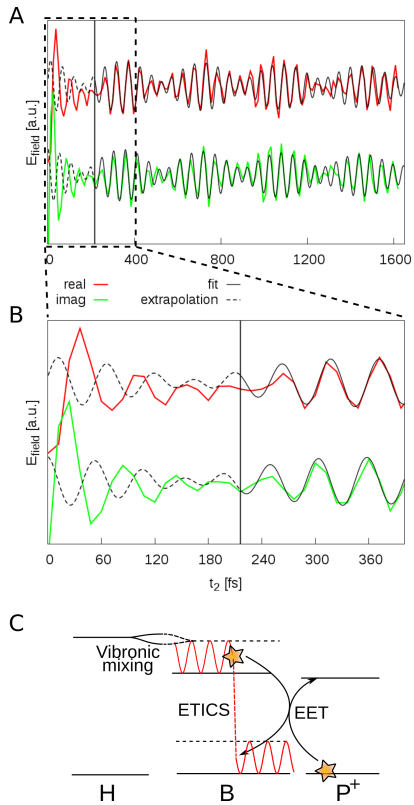

Figure 4: *ETICS is demonstrated in the time-domain. (A) Time domain residuals for the real (red) and imaginary (green) part of the upper cross-peak in the CP measurement. A fit to the sum of two complex exponentials (black) for* $t_2 > 216$ fs *is also shown. Extrapolation of the fit to* $t_2 = 0$ fs *(dashed) demonstrates a* π*-phase change compared to early population times. (B) Zoom in to the first* 400 fs *of the population time. (C) Scheme of the ETICS process demonstrating how initially created excited state coherence is shifted to the ground state during the energy transfer to the* P^+*. Vibronic mixing of B with H states leads to the observable beating signals in the CP measurement for the frequencies close to the B–H electronic gap.*

The real and imaginary traces are fitted simultaneously to a sum of two

complex exponentials, which account for the two frequencies at $560\,\mathrm{cm}^{-1}$ and $650\,\mathrm{cm}^{-1}$ in the time window $t_2 = 216 - 1620\,\mathrm{fs}$. The fits are then extrapolated to $t_2 = 0$. A π-phase shift is observed in the absorptive (real) and refractive (imaginary) part of the signal (see Fig. 4). We also determined the lifetime of the initial excited state coherence, by including it as a π-shifted component and by extending the time window to $t_2 = 0\,\mathrm{fs}$ (see SI for details). The best fit yielded $\sim 70\,\mathrm{fs}$, which is within the time scale of energy transfer from B to P^+.

We consider that ETICS is general. The requirements are that energy transfer occurs while the vibrations cool. Also, vibrational states have to be available, which are approximately degenerate with energy differences between excitons. Both requirements are typically fulfilled in photosynthetic proteins. Importantly, ETICS retains exactly the same beating patterns as the corresponding stimulated emission pathways. Therefore, its spectral signatures can easily be misinterpreted as long-lived electronic coherences [13]. Our interpretation refutes the conclusions in Ref. [18] and the new pathway is likely directly applicable to other reaction centre proteins, such as from plant photosystems [23], where the lifetime of the excited states is typically much shorter than the picosecond coherence dephasing time. We note that, this discrepancy is not as strong for antenna proteins [7, 8]. However, the conclusion that energy transport in photosynthetic proteins is wave-like rests on the assignment of coherences to superposition of excitonic states. ETICS is an alternative assignment and therefore the wave-like energy transfer should be reconsidered.

Finally, we clarify how the excited state vibrations on the associated bacteriochlorophylls are prepared. This is revealed by the signals in the coherent amplitude maps for $\omega_2 = \pm 560\,\mathrm{cm}^{-1}$ when measured with the cross-polarised pulse sequence (Fig. 2B, for , see Fig. SI2). The beam sequence excludes all conventional ground state bleach pathways [11, 13]. We find that observed oscillation patterns (Fig. 2B) match well with the two ETICS pathways at the cross-peaks (H–B and B–H) (see SI for detailed pathway analysis). These pathways can only contribute to the signal, if the two transitions $g_0 \rightarrow e_0$ and $g_0 \rightarrow e_1$ (Fig. 3A) have non-parallel transition dipole moments. This can occur if the excited states in the spectroscopic aggregate of the RC_{sph} are vibronically coupled, i.e. that the state e_1 consists of a nonadiabatic mixture of the vibrationally and electronically excited states of the associated bacteriochlorophylls and the electronic state of bacteripheophytins. This implies that vibrations on the associated bacteriochlorophylls are directly excited by absorption of a photon into H.

Vibronic coupling has recently been detected in synthetic [14] and natural [25–28] light-harvesting complexes. It has been proposed to facilitate energy transfer [27, 29], and it has also been used to explain long-lived quantum coherences [23, 24, 27, 28, 30]. In particular, Christenson et al. predicted that mixing of atomic and electronic coordinates leads to an extension of the lifetime of coherences between excitonic excited state [28]. However, we do not consider that this is a viable explanation for RC_{sph}, because the excited state lifetime is shorter than 300

fs and the coherences must be in the ground state. Tiwari et al. proposed that vibronic coupling opens up new pathways by which direct excitation of ground state coherences is facilitated [27]. Importantly, we are not able to identify the predicted strong spectral asymmetry in our 2D spectra (see Fig. 2B and SI for details). Moreover, the pathways suggested in Ref. [27] are also not inconsistent with the phase shift during energy transfer (Fig. 4). Thus, we conclude that the mechanism is not dominant in RC_{sph}. A recent photon echo experiment of RC_{sph} was interpreted as supportive of the model [30]. However, the characteristic spectral asymmetries were not presented.

Although we identify ETICS as a shift of *coherence*, equivalent shifts of *population* are equally possible. The ground state vibrational modes that we identify act as energy sinks for energy transfer steps between non-resonant electronic levels. Such low-energy modes are an integral part of downhill energy transfer and the efficiency of energy transfer directly depends on the transition probability into the sink modes. Energy transfer can occur independent of vibronic mixing in the aggregate. However, direct excitation of the vibronic states increases the probability of transition into a ground state vibrations and as such increases the transfer rates. Seen from a molecular perspective, the atoms of the chromophore are already set to oscillate with an appropriate frequency in the excited state, priming the molecules for energy transfer. The Huang-Rhys factors are typically small for photosynthetic chromophores, and therefore this increase can be manifold.

The availability of sink modes on the chromophores may explain the extraordinarily fast energy transfer rates in reaction centre proteins. Also, the possibility that the protein uses the sink modes to control the directionality of the flow of energy should not be disregarded.

Materials and Methods

RC_{sph} were isolated from *Rhodobacter sphaeroides* R-26 following standard procedures described elsewhere [31] with modifications described in Supporting Information. To oxidise RC_{sph}, potassium ferricyanide ($K_3Fe(CN)_6$) was added to a final concentration of 150 mM. Samples were mixed with glycerol at 35:65 (v/v) and cooled down to 77 K in a 0.5 mm cell made of fused silica. The samples typically had an optical density of 0.2 to 0.3 at 800 nm.

Our spectroscopy setup, the data acquisition protocol and the analysis were described previously [6, 32, 33]. Briefly, a noncolinear optical amplifier was pumped by the 1030 nm fundamental of a Pharos laser system (Light Conversion Ltd). The resulting $\sim$ 17 fs laser pulses were split into four beams using a beamsplitter and a transmissive diffraction grating. Spherical optics were used to focus all beams to $\sim$ 100 µm on the sample spot. The forth beam was attenuated by an OD=2 filter. The first two beams were simultaneously chopped by mechanical choppers and a double frequency lock-in detection scheme was used. Interferograms were continuously detected by the CCD camera (PIXIS, Princeton Instruments).

A repetition rate of 20 kHz with excitation energies of 2 nJ and 4 nJ per pulse were used for all-paralell

(AP) and cross-polarized (CP) measurements, respectively. This translates to excitation density of 10^{14} photons per pulse per cm^2 for the 2 nJ pulse energy. The population time step was 12 fs, which defines the high frequency cut-off of frequency to $\omega_2 = 1380\,cm^{-1}$. The coherence time t_1 was scanned between -199.5–294 fs (-171.5–273 fs) with the 1.75 fs step for AP (CP) measurements, respectively. In both axis, the resolution was typically $50\,cm^{-1}$ ($58\,cm^{-1}$) for AP (CP) experiments (see SI for details).

The sequences of 2D spectra in t_2 were FT to generate three-dimensional FT spectra. To reduce the complexity of the third order response signals of the molecules, as well as multiple resonant and nonresonant contributions during the pulse overlap, we analysed the oscillating signals in the following way. We extracted the oscillatory components in t_2, by subtracting multi-exponential fits with complex amplitude prefactors from each (ω_1, ω_3) data point. The Fourier transforms of the remaining oscillating residuals in t_2 yields the three-dimensional FT spectra. By slicing these spectra in ω_2 we extracted the (ω_1, ω_3) coherence amplitude and/or phase maps of oscillations with ω_2 frequency. The resolution along ω_2 is determined by the length of the t_2 scan, $0 - 1740$ fs and $0 - 1620$ fs for AP and CP, respectively and was $22\,cm^{-1}$ and $24\,cm^{-1}$ for AP and CP, respectively.

Acknowledgements

We would like to thank Darius Abramavicius, Vytautas Butkus, Leonas Valkunas, Tõnu Pullerits and Tomáš Mančal for helpful discussions. The work in Lund was supported by the Swedish Research Council and Knut and Alice Wallenberg foundations. S.W. and P. E. acknowledge funding from the Foundation of Swedish Research Sweden, the Olle Engkvist Byggmästare Foundation and the Swedish Research Council.

Author contributions

D.P., S. W. and D.Z. conceived and designed the experiments. D.P. performed the experiments. D.P. analysed the data. P.E. grew and purified the sample. D.P., D.Z., SW and E.P. wrote the paper. All authors discussed the results and commented on the manuscript.

Additional information

The authors declare no competing financial interests.

References

[1] MH Vos, MR Jones, CN Hunter, J Breton, JC Lambry, and JL Martin. Coherent dynamics during the primary electron-transfer reaction in membrane-bound reaction centers of Rhodobacter sphaeroides. *Biochemistry*, 33(22):6750–6757, 1994.

[2] Sergei Savikhin, Yinwen Zhu, Su Lin, Robert E. Blankenship, and Walter S. Struve. Femtosecond spectroscopy of chlorosome antennas from the

green photosynthetic bacterium chloroflexus aurantiacus. *J. Phys. Chem.*, 98(40):10322–10334, 1994.

[3] David C Arnett, C C Moser, P L Dutton, and N F Scherer. The First Events in Photosynthesis: Electronic Coupling and Energy Transfer Dynamics in the Photosynthetic Reaction Center from Rhodobacter sphaeroides. *J. Phys. Chem. B*, 103:2014–2032, 1999.

[4] Sergei Savikhin, Daniel R. Buck, and Walter S. Struve. Oscillating anisotropies in a bacteriochlorophyll protein: Evidence for quantum beating between exciton levels. *Chem. Phys.*, 223(2-3):303–312, 1997.

[5] David M Jonas. Two-dimensional femtosecond spectroscopy. *Annu. Rev. Phys. Chem.*, 54(1):425–463, January 2003.

[6] Tobias Brixner, Tomáš Mančal, Igor V Stiopkin, and Graham R Fleming. Phase-stabilized two-dimensional electronic spectroscopy. *J. Chem. Phys.*, 121(9):4221–4236, September 2004.

[7] Gregory S Engel, Tessa R Calhoun, Elizabeth L Read, Tae-Kyu Ahn, Tomáš Mančal, Yuan-Chung Cheng, Robert E Blankenship, and Graham R Fleming. Evidence for wavelike energy transfer through quantum coherence in photosynthetic systems. *Nature*, 446(7137):782–786, April 2007.

[8] Elisabetta Collini, Cathy Y Wong, Krystyna E Wilk, Paul M G Curmi, Paul Brumer, and Gregory D Scholes. Coherently wired light-harvesting in photosynthetic marine algae at ambient temperature. *Nature*, 463(7281):644–647, February 2010.

[9] Tobias Brixner, Jens Stenger, Harsha M Vaswani, Minhaeng Cho, Robert E Blankenship, and Graham R Fleming. Two-dimensional spectroscopy of electronic couplings in photosynthesis. *Nature*, 434(7033):625–8, mar 2005.

[10] Vytautas Butkus, Donatas Zigmantas, Leonas Valkunas, and Darius Abramavicius. Vibrational vs. electronic coherences in 2D spectrum of molecular systems. *Chem. Phys. Lett.*, 545:40–43, August 2012.

[11] Gabriela S Schlau-Cohen, Akihito Ishizaki, Tessa R Calhoun, Naomi S Ginsberg, Matteo Ballottari, Roberto Bassi, and Graham R Fleming. Elucidation of the timescales and origins of quantum electronic coherence in LHCII. *Nat. Chem.*, 4(5):389–395, 2012.

[12] RM Hochstrasser. Two-dimensional IR-spectroscopy: polarization anisotropy effects. *Chem. Phys.*, 266:273–284, 2001.

[13] Sebastian Westenhoff, David Paleček, Petra Edlund, Philip Smith, and Donatas Zigmantas. Coherent picosecond exciton dynamics in a photosynthetic reaction center. *Journal of the American Chemical Society*, 134(40):16484–7, October 2012.

[14] James Lim, David Paleček, Felipe Caycedo-Soler, Craig N. Lincoln, Javier Prior, Hans von Berlepsch, Susana F. Huelga, Martin B. Plenio, Donatas Zigmantas, and Jürgen Hauer. Vibronic origin of long-lived coherence in an artificial molecular light harvester. *Nat. Commun.*, 6(7755), 2015.

[15] Hebin Li, Alan D Bristow, Mark E Siemens, Galan Moody, and Steven T Cundiff. Unraveling quantum pathways using optical 3D Fourier-transform spectroscopy. *Nat Commun.*, 4(1390), January 2013.

[16] Joachim Seibt, Thorsten Hansen, and Tõnu Pullerits. 3D Spectroscopy of Vibrational Coherences in Quantum Dots: Theory. *J. Phys. Chem. B*, 117(38):11124–11133, September 2013.

[17] Vytautas Butkus, Donatas Zigmantas, Darius Abramavicius, and Leonas Valkunas. Distinctive character of electronic and vibrational coherences in disordered molecular aggregates. *Chem. Phys. Lett.*, 587:93–98, 2013.

[18] H Lee, YC Cheng, and GR Fleming. Coherence dynamics in photosynthesis: protein protection of excitonic coherence. *Science*, 1462, 2007.

[19] DM Jonas, MJ Lang, Yutaka Nagasawa, Taiha Joo, and Graham R. Fleming. Pump-probe polarization anisotropy study of femtosecond energy transfer within the photosynthetic reaction center of Rhodobacter sphaeroides R26. *J. Phys. Chem.*, 3654(100):12660–12673, 1996.

[20] NJ Cherepy, AP Shreve, LJ Moore, SG Boxer, and A R Mathies. Temperature dependence of the Qy resonance Raman spectra of bacteriochlorophylls, the primary electron donor, and bacteriopheophytins in the bacterial photosynthetic reaction center. *Biochemistry*, 2960(97):8559–8566, 1997.

[21] Kazimierz Czarnecki, James R. Diers, Veeradej Chynwat, Joy P. Erickson, Harry A. Frank, and David F. Bocian. Characterization of the strongly coupled, low-frequency vibrational modes of the special pair of photosynthetic reaction centers via isotopic labeling of the cofactors. *J. Am. Chem. Soc.*, 119(2):415–426, 1997.

[22] Tomáš Mančal, Jakub Dostál, Jakub Pšenčík, and Donatas Zigmantas. Transfer of vibrational coherence through incoherent energy transfer process in Förster limit. *Can. J. Chem.*, 92(2):135–143, 2014.

[23] Franklin D. Fuller, Jie Pan, Andrius Gelzinis, Vytautas Butkus, S. Seckin Senlik, Daniel E. Wilcox, Charles F. Yocum, Leonas Valkunas, Darius Abramavicius, and Jennifer P. Ogilvie. Vibronic coherence in oxygenic photosynthesis. *Nat. Chem.*, 6(July):706–711, 2014.

[24] Elisabet Romero, Ramunas Augulis, Vladimir I Novoderezhkin, Marco Ferretti, Jos Thieme, Donatas Zigmantas, and Rienk van Grondelle. Quantum coherence in photosynthesis for efficient solar-energy conversion. *Nature Phys.*, 10, 2014.

[25] Jordan M Womick and Andrew M Moran. Vibronic enhancement of exciton sizes and energy transport in photosynthetic complexes. *J. Phys. CHem. B*, 115(6):1347–1356, 2011.

[26] A. W. Chin, J. Prior, R. Rosenbach, F. Caycedo-Soler, S. F. Huelga, and M. B. Plenio. The role of non-equilibrium vibrational structures in electronic coherence and recoherence in pigment-protein complexes. *Nat. Phys.*, 9(2):113–118, 2013.

[27] Vivek Tiwari, William K Peters, and David M Jonas. Electronic resonance with anticorrelated pigment vibrations drives photosynthetic energy transfer outside the adiabatic framework. *Proc. Natl. Acad. Sci.*, 110(4):1203–1208, January 2013.

[28] Niklas Christensson, Harald F Kauffmann, Tõnu Pullerits, and Tomáš Mančal. Origin of Long-Lived Coherences in Light-Harvesting Complexes. *J. Phys. Chem. B*, 116(25):7449–7454, June 2012.

[29] Václav Perlík, Joachim Seibt, Laura J. Cranston, Richard J. Cogdell, Craig N. Lincoln, Janne Savolainen, František Šanda, Tomáš Mančal, and Jürgen Hauer. Vibronic coupling explains the ultrafast carotenoid-to-bacteriochlorophyll energy transfer in natural and artificial light harvesters. *J. Chem. Phys.*, 142(21):212434, 2015.

[30] Ian Seungwan Ryu, Hui Dong, and Graham R Fleming. Role of electronic-vibrational mixing in enhancing vibrational coherences in the ground electronic states of photosynthetic bacterial reaction center. *The journal of physical chemistry. B*, 118(5):1381–8, February 2014.

[31] Roya Farhoosh, Veeradej Chynwat, Ronald Gebhard, Johan Lugtenburg, and Harry A. Frank. Triplet energy transfer between the primary donor and carotenoids in rhodobacter sphaeroides r-26.1 reaction centers incorporated with spheroidene analogs having different extents of π-electron conjugation. *Photochemistry and Photobiology*, 66(1):97–104, 1997.

[32] Ramũnas Augulis and Donatas Zigmantas. Two-dimensional electronic spectroscopy with double modulation lock-in detection: enhancement of sensitivity and noise resistance. *Optics express*, 19(14):13126–33, July 2011.

[33] Ramūnas Augulis and Donatas Zigmantas. Detector and dispersive delay calibration issues in broadband 2D electronic spectroscopy. *JOSA B*, 30(6):1770, May 2013.

Supporting Information: Quantum Coherence as a Witness of Vibronically Hot Energy Transfer in Bacterial Reaction Centre.

[1,2]David Paleček, [3]Petra Edlund, [3]Sebastian Westenhoff and [1]Donatas Zigmantas and

[1] *Department of Chemical Physics, Lund University, P.O. Box 124, SE-22100 Lund, Sweden*

[2] *Department of Chemical Physics, Charles University in Prague, Ke Karlovu 3, 121 16 Praha 2, Czech Republic*

[3] *Department of Chemistry and Molecular Biology, University of Gothenburg, Box 462, SE-40530 Gothenburg, Sweden*

donatas.zigmantas@chemphys.lu.se

1. Oscillation maps

1.1. Noise and stability

High quality data is necessary to obtain unambiguous oscillation amplitude maps. The oscillation amplitudes are typically weak in the reaction centre protein from RC_{sph} due to weak coupling of vibrations and electronic transitions (low Huang-Rhys factors). We used a high repetition rate of 20 kHz. Besides, a double lock-in detection scheme was employed to filter out unwanted scattering of the sample [1]. Quantitatively, the strongest coherent oscillation mode $\omega_2 = 195\,\mathrm{cm}^{-1}$ has a amplitude of $\sim 7 \cdot 10^{-3}$ relative to maximum static signal in a measurement, with all pulses polarised in parallel (AP). The coherence at $650\,\mathrm{cm}^{-1}$ had an amplitude of $\sim 3 \cdot 10^{-3}$ (relative to the maximum static AP signal), with the noise level of the coherence amplitude map estimated to be $\sim 1 \cdot 10^{-4}$. The cross-polarised pulse sequence (laser pulses 1 to 4 are polarised $\pi/4, -\pi/4, \pi/2, 0$, 'CP') further reduces cross-talk between the excitation pulses and non-resonant signals. The noise level dropped to typically $\sim 6 \cdot 10^{-5}$ relative to the static AP signal. The strongest CP oscillation at $650\,\mathrm{cm}^{-1}$ has an amplitude of $\sim 9 \cdot 10^{-4}$.

Our setup is also optimised for excellent long-term stability. It took $\sim$ 20 hours to measure full 2D data set with t_1 scanned between -199.5–294 fs (-171.5–273 fs) with the 1.75 fs step for AP (CP) measurements, respectively. Population time t_2 is scanned with a time step of 12 fs and up to typically $\sim$ 1.5 ps. The small time step of t_2 enabled us to resolve the coherence at $1350\,\mathrm{cm}^{-1}$.

1.2. ETICS is observed for all coherences

We assign the coherences at $\omega_2 = 195$, 325, 890, 1150 cm^{-1} as vibrational, because they are suppressed in the measurements with the crossed-polarisation pulse sequence (see Fig. 2a in the main text). From the same figure it becomes apparent that the peak at 720 cm^{-1} is not completely suppressed, but very close to the noise level. We therefore consider it to be vibrational as well.

Fig. SI1 shows coherence amplitude maps for Fourier transforms from real ('real FT') and complex ('complex FT') data for these oscillations. The real FT maps indicate a cancellation of the amplitude on the diagonal of the B peak. This indicates ETICS, as discussed in the main text. We note that significant coherence amplitudes are observed in rephasing spectra above the diagonal peak B, which is in contradiction to Jonas' model of direct excitation of ground state coherences [2], but in agreement with the ETICS pathways (Fig. SI3A and discussion below). Thus, we conclude that ETICS occurs for all observed vibrations, which are located on the associated bacteriochlorophylls (see Fig. SI1). Whereas ETICS can occur from coherences with vibronic character, as observed for 560 cm^{-1} (main paper) and 650 cm^{-1} (see below), it can also occur for coherences with purely vibrational character. This illustrates the generality of coherence shifts upon energy transfer.

1.3. ETICS and coherence assignment for $\omega_2 = \mathbf{650}\,\mathrm{cm}^{-1}$

The coherence at 650 cm^{-1} has the strongest relative enhancement in the CP measurement. This is reasonable, since it is almost in resonance with the B–H band splitting. Fig. SI2 shows a compilation of coherence amplitude maps for 650 cm^{-1}. The spectra features are very similar to those of the oscillation amplitude maps of the 560 cm^{-1} mode (Fig. 2b and Fig. 3).

As discussed in the main paper for 560 cm^{-1}, we observe that the non-rephasing and rephasing maps show oscillations on the diagonals and off-diagonals, respectively. The fact that the coherence is observed in the CP measurement means that vibrational coherence, which would require excitation and detection through the same excitonic state manifold, can be excluded as an explanation. The beating pattern would be consistent with electronic coherence between two excited states, but the picosecond dephasing time (Fig. SI3) and the cancellation of the coherence amplitude on the diagonal of the B peak (Fig. SI1) strongly suggests that a ground state coherence, generated through ETICS, causes the oscillation.

Inspecting the amplitude coherence maps for $+650\,\mathrm{cm}^{-1}$ and $-650\,\mathrm{cm}^{-1}$ reveals that the amplitudes in the rephasing spectra are much higher than in the non-rephasing spectra (Fig SI2B). This is, because the phase of an oscillation sweeps across the peak (data not shown). The sweep is along the anti-diagonal and diagonal for rephasing peaks and non-rephasing peaks, respectively [3].

Because inhomogeneous broadening acts exclusively along the diagonal, it interferes destructively with the homogeneous line-widths of the non-rephasing oscillation peaks, which results in the reduced observed intensity of the coherence

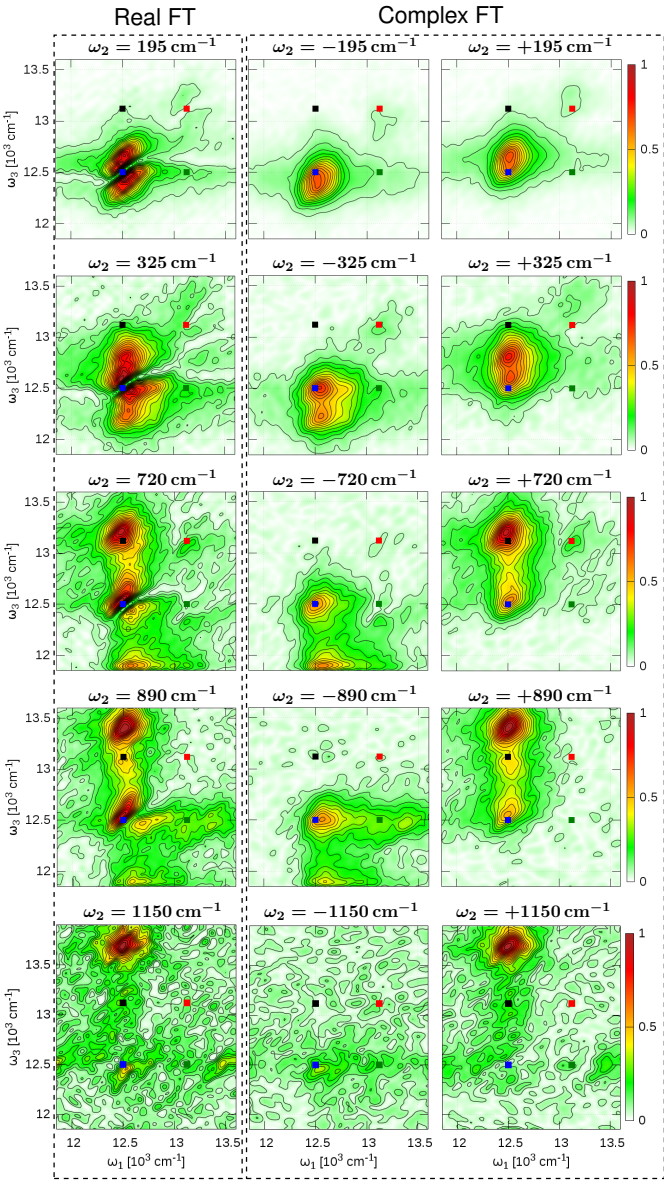

Figure 1: *Coherence amplitude maps of vibrational modes with the frequencies as stated in the figure. All data is from rephasing 2D electronic spectra from* $\mathrm{RC}_{\mathrm{sph}}$ *and with all pulse polarised in parallel. Real and complex FT stands for Fourier transform from real and complex data, respectively. The coloured rectangles depict the positions of the main diagonal peaks (B: blue and H: red) and the off-diagonal peaks as guide to the eye. The Real amplitude maps are normalised and associated complex coherence amplitude maps are plotted in proportion to them. The decreasing FT amplitude on the B diagonal and below with increasing oscillation frequency is due to steeply decreasing intensity of the laser spectrum at the red side of the spectral window.*

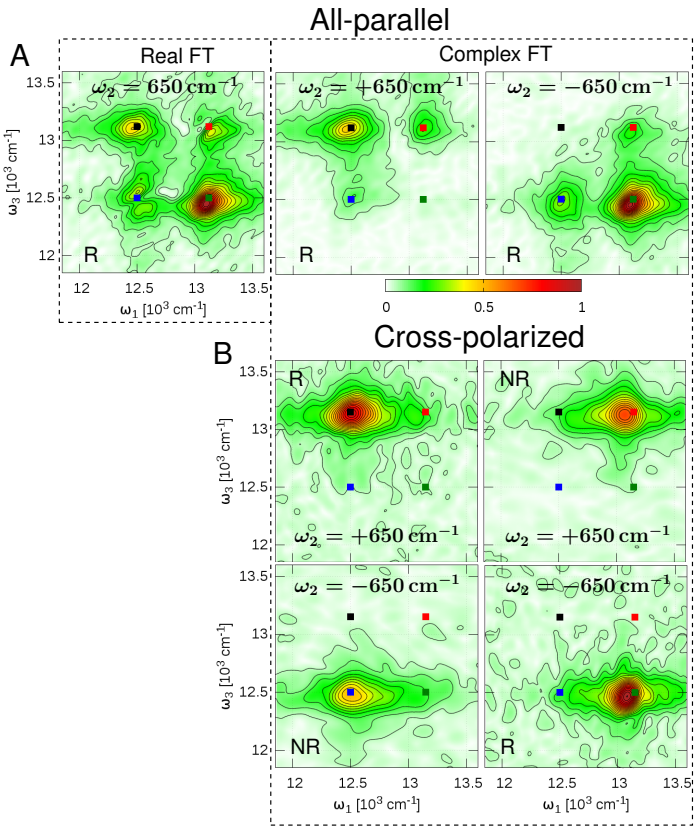

Figure 2: *(A) Coherence amplitude maps of* $\omega_2 = 650\,\mathrm{cm}^{-1}$ *in AP (All-parallel) and (B) CP (Cross-polarised) measurement, starting from populations time* $t_2 = 216\,\mathrm{fs}$. *Non-rephasing and rephasing spectra, and Fourier transforms from real and complex-valued data were used as indicated in the figure. The colour rectangles depict positions of the main peaks in the 2D spectra.*

in non-rephasing spectra [4].

2. Analysis of interaction pathways

2.1. Model and assumptions

In order to rationalise the observed coherences, we consider pathway diagrams which include a ground (g_0) and an electronically excited (e_0) state. Both states are dressed with a single vibrational level (g_1, e_1). Limiting the number of vibrational sublevels to one is justified, because the coupling between vibrational and electronic states is weak in bacteriochlorophylls (Huang-Rhys factor ≤ 0.02) [5]. At the temperature of the experiment, 77 K, the only populated resting state is the vibrational ground state. Additionally, the limited band-

width of the laser pulses precludes direct excitation of higher harmonics of the $560, \mathrm{cm}^{-1}$ or $650\,\mathrm{cm}^{-1}$ modes. For the resonant modes (560, and $650\,\mathrm{cm}^{-1}$), e_1 is an excitonic state with contributions from an electronic and vibrational excited state on an associated bacteriochlorophyll and the electron ground state of the bacteriopheophytin.

2.2. ETICS, stimulated emission (SE) and ground state bleach (GSB) pathways

We demonstrate our interaction pathways analysis on the $\omega_2 = 560\,\mathrm{cm}^{-1}$ mode. Fig. SI3A compares the real FT coherence amplitude map of $\omega_2 = 560\,\mathrm{cm}^{-1}$, recorded with rephasing pulse order, with all relevant SE pathways and their ETICS analogues. The blue circles mark the spectral positions of the contributions. The pathways on the right (left) of the map evolve as $-\omega_2$ ($+\omega_2$) and appear below (above) the diagonal. This reflects the order of the coherence evolving during the population time t_2.

Essentially, the ETICS pathways produce exactly the same coherence pattern as their SE analogues, with exception for the phase of the signal, which is shifted by π. This is, because the third interaction is with the opposite side of the Feynman diagram. The shift in phase occurs when the coherence shifts to the ground state during the population time, e.g. when energy transfer occurs. There are also four GSB pathways contributing to the coherence maps (see Fig. SI3B). They form a square pattern, which is typical for the GSB coherences [3].

2.3. Rationalizing the observed peak shapes

In the following we will rationalise three observations using the pathways. Recapitulating the argument from the main text, the GSB pathways overlap with the SE and/or ETICS pathways on the B diagonal (compare Fig. SI3A and B). The ground state bleach pathways are expected to interfere constructively with the SE pathways, but they will interfere destructively with the ETICS pathways. The latter is observed in the data as a nodal line of zero signal through the B peak. Secondly, contributions from ETICS and GSB interfere on the H-B cross peak and below it (compare Fig. SI3A and Fig. SI3B). Comparing these oscillation amplitudes to the amplitude detected below the B diagonal reveals that the latter is stronger or equal to the former. The opposite would be expected considering that the H-B cross peak receives higher excitation intensities from the laser pulses (see Fig. 1A) and those two (one ETICS or SE and one GSB pathway) contribute to the signal at the cross peak, but only one below the diagonal of B. Again, the shift in phase for ETICS pathways explains the relatively reduces amplitude of the H-B cross peak. Finally, we observe coherences above the diagonal in Fig. SI3 and we omitted $t_2 < 216\,\mathrm{fs}$ in the analysis. This implies that the coherences must be placed on the ground state, since the excited states (B and H) are only populated for $\sim 300\,\mathrm{fs}$. Thus, we conclude that coherences in the ground state, and not the excited state, give rise to the

observed coherences in Figs. 2, 3, SI1, SI2, and SI3. Shift of the coherence upon energy transfer provides a reasonable explanation for how the coherences reach the ground state.

3. Vibronic coupling

We consider energy transfer induced coherence shifts (ETICS) as a general photophysical process, which should occur independently of whether chromophores couple to form excitonic states. However, in all photosynthetic proteins excitonic states occur. Our amplitude maps computed from CP spectra of RC_{sph} show that some coherences are still observed, even though the first and second, and third and fourth pulse are orthogonally polarised. This was also observed for LHC2 [6]. This can be rationalised if excitonic states with vibronic coupling are present, because then the (+1) transitions (see Fig. SI3A) have transition dipole moments, which are tilted with respect to the (-1) and (0) transitions. Brown and pink circles in Fig. SI3A highlight this difference. In rephasing coherence amplitude maps (Figs. 3 and SI3), the ETICS pathways on the cross peaks H–B and B–H are expected to be observed in the CP measurements (but not the pathways on the diagonal), which is confirmed by Fig. 2B. For RC_{sph} vibronic coupling implies that the electronically excited state of the bacteriopherophytins couple to the electronically and vibrationally excited state of the associated bacteriochlorophylls and form exciton H (e_1 in Fig. SI3).

4. Comparison to the pathways suggested by Tiwari *et al.* (Ref. [2])

Assuming vibronic coupling, the GSB pathway on the HB crosspeak (Fig. SI3B, red dashed rectangle) can survive the cross-polarisation measurement as well. This pathway was identified by [2], where it was suggested to be responsible for the observed long-lived oscillations in the Fenna-Matthews-Olson antenna complex (FMO) [7, 8]. Ref. [2] proposes that ground state coherences are responsible for the observed oscillations, which is consistent with our model. However, the pathways presented in Ref. [2] are not consistent with our data. Firstly, we observe a symmetric oscillation pattern in the CP coherence amplitude maps (see Fig. SI2B and Fig. 2). Specifically, the intensity on the upper cross peak is similar to the lower cross peak. In contrast, the pathways in [2] would predict high intensity on the lower cross peak, intermediate intensity on the diagonals and vanishing intensity on the upper cross peak. Secondly, for the pathways in [2], the ground state coherences are populated directly, and are therefore inconsistent with the π-phase shift observed in our experiments. Thus, we conclude that the delocalised vibrations as suggested by Tiwari *et al.* are at most a minor effect in the 2D spectra of the reaction centre protein.

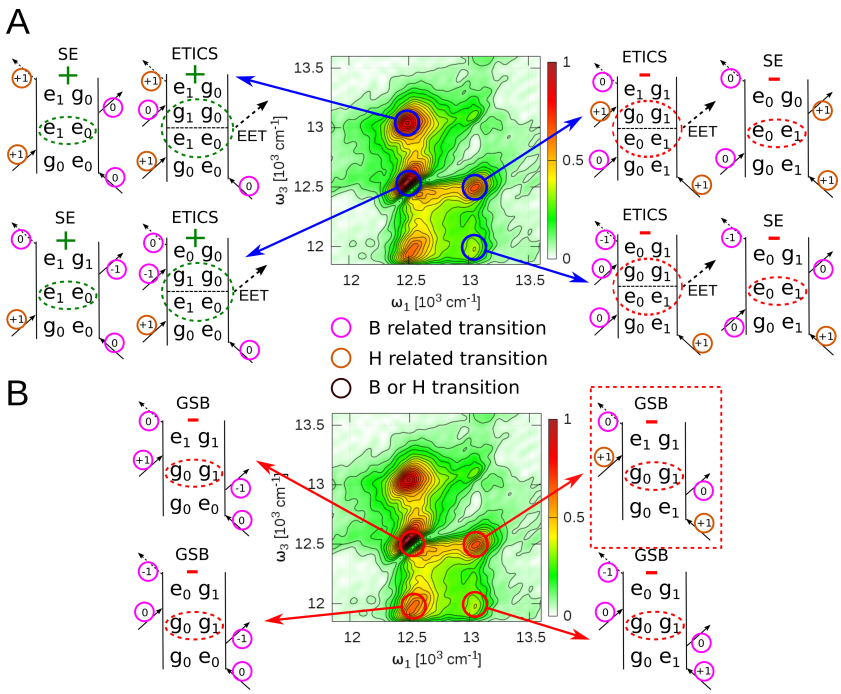

Figure 3: *(A) The SE pathways and their ETICS analogues are shown together with the coherence amplitude map for* $\omega_2 = 560\,\mathrm{cm}^{-1}$ *, extracted from all-parallel rephasing 2D electronic spectra. The red and green dotted circles denote evolution with negative and positive frequency, respectively, during the population time. The numbers -1, 0, +1 denote the change in vibrational quantum number during the transition. Within the framework of the model described in the text, only +1 transitions (marked pink) can contain contributions from the bacteriopheophytin molecules. The dipole moments of these transitions are not parallel to the transition dipole moments of -1 and 0, which predominantly contain contributions from the associated bacteriochlorophylls. See text for more details. Red dashed rectangle highlight the pathway proposed by Tiwari et al. [2] to be responsible for long-lived coherences in light-harvesting proteins.*

5. Direct observation of the phase shift in the time-domain

The upper crosspeak was chosen as the most reliable region to analyse the time-domain trace of the CP beating pattern. Fig. 3AB shows the real (red) and imaginary (green) kinetic trace residuals for the rephasing CP measurement. Since only modes at $\omega_2 = 560\,\mathrm{cm}^{-1}$ and $\omega_2 = 650\,\mathrm{cm}^{-1}$ modes survive the CP scheme, regular beats between the two closed frequencies are observed. Two decaying complex exponentials are therefore sufficient to approximate the trace for time region $216 - 1620\,\mathrm{fs}$:

$$f_{long}(t) = a_1 \mathrm{e}^{-t/\tau_1 + i(\omega_1 t + \varphi_1)} + a_2 \mathrm{e}^{-t/\tau_2 + i(\omega_2 t + \varphi_2)} + c \tag{1}$$

where a_1, a_2 are the oscillation amplitudes, τ_1, τ_2 are the oscillation lifetimes, ω_1, ω_2 are the angular frequencies, φ_1, φ_2 are the constant phase factors and c is the complex constant. Note that φ_1, φ_2 not only depend on the molecular system, but also on the spectral position were it is detected [3]. Therefore, the phases of the peaks for $\omega_2 = 560\,\mathrm{cm}^{-1}$, $650\,\mathrm{cm}^{-1}$ are shifted relative to each other. The resulting fit is displayed in Fig. 3 of the main paper and demonstrates the phase shift at early times.

To also include the dynamics at $t_2 < 200\,\mathrm{fs}$ into the model, we simply add strictly off-phase components for both modes with independent lifetimes and amplitudes:

$$\begin{aligned} f_{full}(t) =& (a_1 \mathrm{e}^{-t/\tau_{a1}} - b_1 \mathrm{e}^{-t/\tau_{b1}}) \cdot \mathrm{e}_1^{+i(\omega_1 t + \varphi_1)} + \\ & (a_2 \mathrm{e}^{-t/\tau_{a2}} - b_2 \mathrm{e}^{-t/\tau_{b2}}) \cdot \mathrm{e}^{+i(\omega_2 t + \varphi_2)} + const, \end{aligned} \tag{2}$$

The resulting fit is illustrated for both real (red) and imaginary (green) parts of the complex data in Fig. SI4. Despite the simplicity of the the model, it proves that the frequencies match between the short and long components. We obtain a lifetime of 70 fs for the the short component with the highest amplitude. This is faster than the time scale for energy transfer away from B and H (170 fs), but is close to the lifetime of H. The fit parameters for both fits are summarised in Table 1.

6. Experimental Methods

Sample Preparation

Rhodobactersphaeroides R-26 cells were incubated for ~ 12 hours in darkness to consume oxygen and were then grown anaerobically, illuminated with light at $30\,^\circ\,^\circ\mathrm{C}$, for ~ 24 hours to induce reaction centre expression. The cells were harvested and washed with 20 mM MES pH 6.8, 100 mM KCl. Cells were disrupted

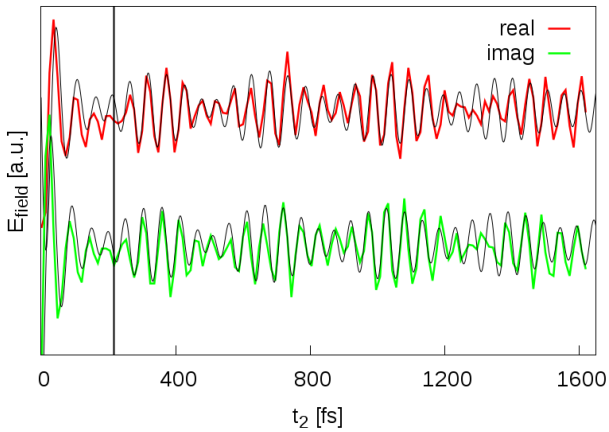

Figure 4: *Real (red) and imaginary (green) residual traces of the rephasing part of the B–H cross-peak, together with fits from $t_2 = 0$ using eq. 3.*

	$f_{long}(t)$	$f_{full}(t)$
a_1 [a.u]	0.87	1.06
τ_{a1} [fs]	10^6	$8 \cdot 10^3$
b_1 [a.u]	—	1.05
τ_{b1} [fs]	—	222
a_2[a.u]	0.74	0.88
τ_{a2}[fs]	$2 \cdot 10^3$	$1.4 \cdot 10^3$
b_2 [a.u]	—	7.54
τ_{b2} [fs]	—	70
ω_1 [cm^{-1}]	647	647
ω_2[cm^{-1}]	557	552
φ_1 [rad]	-1.16	-1.06
φ_2 [rad]	-1.54	-0.77
const	$0.14 + i6 \cdot 10^{-12}$	$0.11 + i1.5 \cdot 10^{-11}$

Table 1: *Fitting parameters of the rephasing time-domain traces for the B–H cross-peak. The first column shows the optimal parameters obtained for $t_2 = 216 - 1620$ fs fitted by eq. 1. Extending the fit to $t_2 = 0$ fs using eq. 3 results in parameters given in second column. The 70 fs component is for $\omega_2 = 552\,cm^{-1}$ and, which as a significantly higher amplitude than $\omega_2 = 647\,cm^{-1}$ at early times.*

in French press at 20000 psi and the membranes were collected by ultracentrifugation. The membrane solubilisation was performed for 10 min at room temperature, in darkness using 0.8 % N,N-dimethyldodecylamine N-Oxide (LDAO) and followed by ultracentrifugation. The obtained supernatant containing reaction centers was precipitated with 50 % ammonium sulfate in 15 mM tris/HCl, 0.1 % LDAO, 1 mM EDTA, pH 8,(TLE) and centrifuged. The floating pellet was dissolved in 15 mM tris/HCl, 1 mM EDTA to a concentration corresponding to absorbance $\mathrm{A}(802\,\mathrm{nm}) = 5\,\mathrm{cm}^{-1}$, ultracentrifuged to remove solid particles, mixed with cellite 545, again precipitated with 50 % ammonium sulfate in TLE and poured into a gravity column. The light–harvesting complexes were washed away with 25 % ammonium sulfate in TLE buffer and the reaction centres were eluted with 10 % ammonium sulfate in TLE. Collected blue fractions were loaded into a DEAE anion exchange column and the protein was eluted with a continuous NaCl gradient. The fractions with purity $\mathrm{A}(280\,\mathrm{nm})/\mathrm{A}(802\,\mathrm{nm}) < 1.25$ were pooled and concentrated to 20 mg/ml in a concentration tube (VIVASPIN) and stored in 15 mM Tris/HCl, 1 mM EDTA, 0.025 % LDAO at $-80\,^{\circ}\,^{\circ}\mathrm{C}$.

Cross-polarized 2DES

Each Liouville pathway probed in the 2DES experiment is associated with the prefactor consisting of the term proportional to the scalar product of the transition dipole strengths involved in the pathway and orientational prefactor associated with the relative orientations between individual laser pulses and transitions interacting with them. For isotropically distributed samples, the orientational prefactor reads:

$$\begin{aligned}\langle i_\alpha j_\beta k_\gamma l_\delta\rangle = \frac{1}{30}[&\langle\cos\Theta_{\alpha\beta}\cos\Theta_{\gamma\delta}\rangle(4\cos\Theta_{ij}\cos\Theta_{kl} - \cos\Theta_{ik}\cos\Theta_{jl} - \cos\Theta_{il}\cos\Theta_{jk}) + \\ &\langle\cos\Theta_{\alpha\gamma}\cos\Theta_{\beta\delta}\rangle(-\cos\Theta_{ij}\cos\Theta_{kl} + 4\cos\Theta_{ik}\cos\Theta_{jl} - \cos\Theta_{il}\cos\Theta_{jk}) + \\ &\langle\cos\Theta_{\alpha\delta}\cos\Theta_{\beta\gamma}\rangle(-\cos\Theta_{ij}\cos\Theta_{kl} - \cos\Theta_{ik}\cos\Theta_{jl} + 4\cos\Theta_{il}\cos\Theta_{jk})]\end{aligned} \tag{3}$$

where i, j, k, l denote laser pulse orientations in the laboratory frame and $\alpha, \beta, \gamma, \delta$ are the dipole moments orientations in the molecular frame. The total prefactor determines the signal strength of the pathway in the resulted spectra. For isotropic samples, configuration $(i, j, k, l) = (\frac{\pi}{4}, -\frac{\pi}{4}, \pi, 0)$ of the laser pulses is particularly useful for distinguishing the nature of the coherent beatings, because all the pathways undergoing first and/or second pair of interactions with dipoles oriented parallel to each other are completely suppressed. This includes population dynamics and purely vibrational coherences. On the other hand, electronic coherence together with mixed vibronic beatings survive the orientational averaging to the extend depending on the angle between the involved transitions, where 90° relative orientation give maximal signal in the cross-polarised measurement.

Before CP measurement, 2DES signal was optimised for all parallel configuration and then the individual pulse polarizations were set to $(\frac{\pi}{4}, -\frac{\pi}{4}, \pi, 0)$ using wire grid polarizers (contrast ratio > 800). Due to imperfections of the exper-

imental setup, such as not ideally set polarizers, typical suppression factor of signals related to population dynamics and vibrational coherences is not absolute, but ~ 80 for CP sequence. This roughly corresponds to inaccuracy of $\sim \pm 1°$ in setting the polarizers. 2DES data (for both AP and CP) were phased to all parallel pump-probe spectra by fitting the real projections of 2DES on ω_3 (according to the FT slice theorem [9]) for several population times simultaneously. For the CP measurement, this approach is justified since the "leakage" of the population–related and vibrational coherence signals through the polarizers still dominate the overall signal so that the phasing to AP pump-probe spectra can be used. Note that the proper phasing of cross-polarised measurement requires sophisticated techniques [10]. The hypothetical phasing error for the CP scheme can only result in a small phase shifts within the 2D spectra. Since only the FT amplitude maps are analysed, this phasing error does not effect any conclusions about coherent beatings discussed in this paper. 1

Data Analysis

Lock-in detected interferograms of the signal mixed with local oscillator were filtered in the time domain (t_3) determining the spectral resolution along ω_3 detection axis. Resolution along ω_1 emission axis is determined by the length of the scan of time delay between the first two pulses (t_1). The length of the scan is dictated by the detection sensitivity and the time for which the system sustains coherence between electronic ground and excited states. In both axis, resolution was typically $50\,\mathrm{cm}^{-1}$ ($58\,\mathrm{cm}^{-1}$) for AP (CP) experiment, respectively, thus measured 2D spectra consist of $37\,\mathrm{x}\,37$ and $40\,\mathrm{x}\,42$ ($\omega_1\,\mathrm{x}\,\omega_3$) pixels for AP and CP, respectively. For the 2D spectra and 3D slices presentation, the spectra were interpolated with Fourier zero padding to produce $200\,\mathrm{x}\,200$ pixel plots.

References

[1] Ramũnas Augulis and Donatas Zigmantas. Two-dimensional electronic spectroscopy with double modulation lock-in detection: enhancement of sensitivity and noise resistance. *Optics express*, 19(14):13126–33, July 2011.

[2] Vivek Tiwari, William K Peters, and David M Jonas. Electronic resonance with anticorrelated pigment vibrations drives photosynthetic energy transfer outside the adiabatic framework. *Proc. Natl. Acad. Sci.*, 110(4):1203–1208, January 2013.

[3] Vytautas Butkus, Donatas Zigmantas, Leonas Valkunas, and Darius Abramavicius. Vibrational vs. electronic coherences in 2D spectrum of molecular systems. *Chem. Phys. Lett.*, 545:40–43, August 2012.

[4] Joachim Seibt, Thorsten Hansen, and Tõnu Pullerits. 3D Spectroscopy of Vibrational Coherences in Quantum Dots: Theory. *J. Phys. Chem. B*, 117(38):11124–11133, September 2013.

[5] Margus Rätsep, Zheng Li Cai, Jeffrey R. Reimers, and Arvi Freiberg. Demonstration and interpretation of significant asymmetry in the low-resolution and high-resolution Qy fluorescence and absorption spectra of bacteriochlorophyll a. *J. Chem. Phys.*, 134(2), 2011.

[6] Gabriela S Schlau-Cohen, Akihito Ishizaki, Tessa R Calhoun, Naomi S Ginsberg, Matteo Ballottari, Roberto Bassi, and Graham R Fleming. Elucidation of the timescales and origins of quantum electronic coherence in LHCII. *Nat. Chem.*, 4(5):389–395, 2012.

[7] Gregory S Engel, Tessa R Calhoun, Elizabeth L Read, Tae-Kyu Ahn, Tomáš Mančal, Yuan-Chung Cheng, Robert E Blankenship, and Graham R Fleming. Evidence for wavelike energy transfer through quantum coherence in photosynthetic systems. *Nature*, 446(7137):782–786, April 2007.

[8] Elisabetta Collini, Cathy Y Wong, Krystyna E Wilk, Paul M G Curmi, Paul Brumer, and Gregory D Scholes. Coherently wired light-harvesting in photosynthetic marine algae at ambient temperature. *Nature*, 463(7281):644–647, February 2010.

[9] David M Jonas. Two-dimensional femtosecond spectroscopy. *Annu. Rev. Phys. Chem.*, 54(1):425–463, January 2003.

[10] Franz Milota, Valentyn I Prokhorenko, Tomáš Mančal, Hans von Berlepsch, Oliver Bixner, Harald F Kauffmann, and Jürgen Hauer. Vibronic and vibrational coherences in two-dimensional electronic spectra of supramolecular J-aggregates. *J. Phys. Chem. A*, 117(29):6007–14, July 2013.

Paper V

Cross-polarized Transient Grating to Identify Electronic and/or Mixed Vibronic Coherent Beatings

[1,2]David Paleček and [1]Donatas Zigmantas

[1]*Department of Chemical Physics, Lund University, P.O. Box 124, SE-22100 Lund, Sweden*

[2]*Department of Chemical Physics, Charles University in Prague, Ke Karlovu 3, 121 16 Praha 2, Czech Republic*

donatas.zigmantas@chemphys.lu.se

Abstract

Coherent phenomena have been suggested to play a role in efficient photosynthetic light-harvesting. Separating purely vibrational coherences from mixed vibronic/electronic ones is crucial for validating such ideas. Cross-polarized two-dimensional coherent electronic spectroscopy is selective for mixed vibronic/electronic coherences. We demonstrate that analogous selectivity can be achieved in transient grating experiments. Moreover the possibility of longer population time scans yields improved frequency resolution and allows for accurate extraction of dephasing times. The coherence lifetime is a crucial parameter which allows to estimate the relevance of the measured coherence to the energy or electron transfer phenomena.

1. Introduction

Coherent effects in biology are extensively discussed in relation to the efficient energy transfer in photosynthetic light-harvesting [1]. The hypothesis states that the absorption of the photon creates a superposition between energy eigenstates of the system setting the electronic clouds in a coherent motion. In time, the dynamically evolving coherence efficiently explores the energy landscape for a potential energy trap, for instance photosynthetic reaction center. The coherences are experimentally observable as the signal amplitude oscillations in time-resolved optical experiments. The long-lived oscillatory features have been observed in pump probe (PP) experiments and recently developed coherent two-dimensional electronic spectroscopy (2DES) of basically all photosynthetic pigment-protein complexes [2–8].

The origin of these oscillations can be quite different in nature. Apart from the collective motion of electrons (electronic coherence), the structural change due to the excitation makes the nuclei coherently oscillate at the same time, which gives rise to vibrational coherence in a form of the vibrational wave-packets. Since electrons are three orders of magnitude lighter and excited states are often short-lived, elec-

tronic coherence is expected to dephase quickly, whereas vibrational coherence can last for picoseconds [9, chap. 3]. Photosynthetic pigments posses a rich vibrational structure that is accessible through the resonance Raman (RR) or fluorescence line-narrowing experiments [10, 11].

Early 2DES experiments interpreted the oscillatory features as superpositions of purely electronic states and ignored the vibrational motions altogether [5, 6]. However, the vibrational coherence is expected to be present and interfere with the electronic coherence [12]. Recently, vibronic mixing between electronic and vibrational degrees of freedom were proposed to play a crucial role, and mixed origin beatings were identified in the 2D spectra [13–16].

With this in perspective, it is extremely important to distinguish between vibrational and electronic character of the coherence to be able to draw the conclusions about the mechanism of the energy transfer. Theoretical [12, 17] and analytical [18] tools were developed to this end. In experiments, polarization control of the individual laser pulses in 2DES experiment leads in principle to a complete suppression of the purely vibrational coherences if the pulse sequence reads (45°, −45°, 90°, 0°) for the case of isotropically oriented samples [19, 20]. In the standard 2DES experiment three excitation pulses overlap and excite the sample. First two pulses are delayed by the coherence time t_1 in respect to each other, where the second interaction defines the beginning of the population time $t_2 = 0$, when the system evolves freely. The third pulse terminates the evolution of the system during the t_2 and generates a third order nonlinear response, which is emitted at the time t_3 and is heterodyned in phase-matching direction with the attenuated fourth pulse, denoted as local oscillator (LO) [21]. Fourier transform (FT) over (t_1, t_3) yields a 2D map which correlates excitation and emission energies (ω_1, ω_3) for a given t_2. Note that the FT along t_3 is "performed" by the grating in the spectrometer, providing the frequency resolution in ω_3. In such a way, combined high temporal ($\sim 15\,\mathrm{fs}$) and spectral resolution within the $\sim 100\,\mathrm{nm}$ broad excitation pulse is obtained.

Polarization resolved pulse sequences (see above) has been applied to a number of light-harvesting systems [7, 13, 20]. By considering other experiments present in the literature, it can be seen, that oscillatory features usually show longer lifetimes than the available experimental window, which is usually given by the sample and laser stability [6, 7, 16, 22]. For example, in our previous bacterial reaction center experiments at 77 K [7], data set of 100 2D maps typically required 13 hours of data acquisition. The coherence time t_1 delay to be scanned over full optical coherence dephasing time and also the long population time to properly capture long-lived coherences. Overall, insufficiently long scanning of the coherent oscillations in 2DES leads to a sub-optimal frequency resolution and inaccurate lifetime extraction.

PP spectroscopy allows for much faster scans with two pulses available for polarization manipulation. Thus PP anisotropy measurements have proved to be valuable for coherent oscillation analysis in the past [2, 3, 23]. However PP does not provide a complete suppression of the undesirable signals and frequency resolution along

the excitation frequency axis as the polarization-resolved 2DES.

To combine the fast scanning available in PP-type of experiments and the freedom in polarization control of the 2DES, we implemented cross-polarized heterodyne-detected transient grating (CP-TG) In this experiment we obtained high frequency resolution of the beatings, complimented with the accurate dephasing time extraction.

2. Results

Heterodyned transient grating uses the same experimental scheme as 2DES with the only difference that the t_1 delay is not scanned and is set to zero during the measurement. It has been shown, that such scheme corresponds to a projection (integration) of the 2DES signal along ω_1 in the complex plain [24]. In contrast, PP corresponds to the projection of the real part of the response only [21].

We demonstrate CP-TG experiment on the photosynthetic reaction center from purple bacteria *Rhodobacter sphaeroides* (RC_{sph}). Coherent oscillation patterns in this system have been studied extensively [2, 3, 7, 16, 25, 26]. RC_{sph} embeds two strongly coupled bacteriochlorophylls *a*, two accessory bacteriochlorophylls *a* and two bacteriopheophytins *a*, all arranged in two nearly symmetric branches [27]. Together they form excitonic bands P, B, H, respectively. We use chemically oxidized P at 77 K temperature. When polarization of all pulses is oriented parallel to each other, just like in the PP or 2DES measurements, TG does not provide any selection of the contributing oscillations along t_2. After subtracting the populations-related monotonously-changing signal, purely oscillating residuals can be Fourier transformed to obtain beating frequencies, which can be compared to the selective RR spectra [10]. Fig. 1 shows the comparison between TG-, RR- and 2DES-extracted frequencies associated with the B band. We observe a good match between the frequencies obtained from the RR and time-domain measurements. 2DES with its limited range along t_2 shows substantial broadening of the line-widths associated with the individual modes.

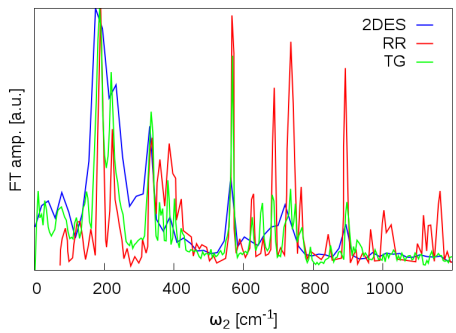

Figure 1: *Comparison of the coherent modes associated with the B band (integrated over the whole line-width) of* RC_{sph}. *RR spectrum was digitized from Ref. [10] and shows close-to-homogeneous line-widths of the modes (red). Similar information can be extracted from 2DES, however with lower frequency resolution (blue). TG improves the frequency resolution down to the RR limit (green). The lower amplitude of the higher-frequency modes in 2DES and TG experiments is caused by the spectrally limited pulses.*

Note that TG does not provide the resolution along ω_1, and thus the modes associated with different bands might contribute to the particular emission frequency of the TG signal. However, this is only true for the modes which energies match the exci-

tonic gap, in our case $\omega_2 \sim 620\,\mathrm{cm}^{-1}$. In that case, the ground state bleach oscillation of the higher lying H state below diagonal would coincide with the emission energy of the B band and the contributions can not be separated.

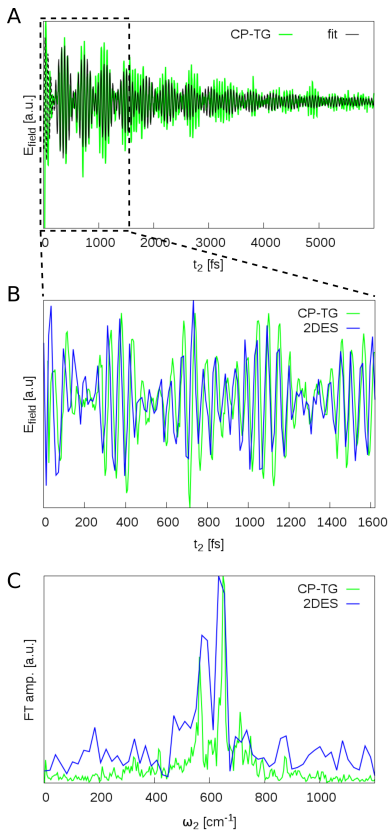

Figure 2: *Demonstration of the CP-TG by comparison to the relevant CP-2DES signal (A) CP-TG kinetic scan at* $\omega_3 = 13100\mathrm{cm}^{-1}$ *matching the H excitonic transition. The fit of the two main modes with two exponentially decaying oscillations allow for the accurate lifetime extraction. (B) Comparison of the CP-TG with the CP-2DES kinetic trace from the upper H–B cross-peak demonstrating the correspondence between the two. (C) FT of the traces (A, B) identify the coherences with mixed vibronic/electronic character.*

Comparing the three sets of data, TG with fs resolution exhibits the frequency resolution down to the linewidth obtained from RR [10]. When compared to 2DES experiments, we sacrificed the selective resolution in ω_1, but each time point was measured ~ 40 times faster including 5 averages per data point in TG experiment.

The question arises, whether we can also apply the polarization control with the same selectivity as we observed previously in $\mathrm{RC}_{\mathrm{sph}}$ [7, 16]. Fig. 2A,B shows the CP-TG, where polarization of the four beams were set to $(45°, -45°, 90°, 0°)$, kinetic traces at the ω_3 frequency corresponding to the H exciton as compared to the CP-2DES kinetic trace for the upper H–B cross-peak. This region has been identified as the most unambiguous to track mixed-vibronic/electronic coherence [28]. Even though the two signals do not have the one to one correspondence, because of the missing ω_1 resolution, there is almost a perfect match, which demonstrate the power of the CP-TG technique. The oscillation amplitudes in Fig. 2C shows good agreement and CP-TG provides frequencies and the improved resolution. The more accurately determined frequencies are $568\,\mathrm{cm}^{-1}$ and $653\,\mathrm{cm}^{-1}$, whereas they were estimated to be $570\,\mathrm{cm}^{-1}$ and $650\,\mathrm{cm}^{-1}$ from 2DES experiment, respectively. Moreover, from the complex bi-exponential fit of the full t_2 range of the CP-TG data we were able to extract the lifetimes of the two strongest modes 568, $653\,\mathrm{cm}^{-1}$ to be 1.5, 2.5 ps, respectively.

3. Conclusions

We have demonstrated that polarization-resolved CP-TG improves the frequency resolution of the oscillatory features observed in 2DES and allow for accurate extraction of their lifetimes. CP-TG is specifically sensitive to the mixed vibronic/electronic coherence oscillations, which point to the importance of the vibronic coupling for the efficient light-harvesting [13, 16, 29].

Acknowledgments

We thank Petra Edlund and Sebastian Westenhoff, Gothenburg University, for kindly providing us with the reactions centers of *Rba. sphaeroides*. The research was supported by the Swedish Research Council and Knut and Alice Wallenberg foundations.

Additional information

The authors declare no competing financial interests.

References

[1] Neill Lambert, Yueh-Nan Chen, Yuan-Chung Cheng, Che-ming Li, Guang-Yin Chen, and Franco Nori. Quantum biology. *Nat. Phys.*, 9(1):10–18, December 2012.

[2] DM Jonas, MJ Lang, Yutaka Nagasawa, Taiha Joo, and Graham R. Fleming. Pump-probe polarization anisotropy study of femtosecond energy transfer within the photosynthetic reaction center of Rhodobacter sphaeroides R26. *J. Phys. Chem.*, 3654(100):12660–12673, 1996.

[3] David C Arnett, C C Moser, P L Dutton, and N F Scherer. The First Events in Photosynthesis: Electronic Coupling and Energy Transfer Dynamics in the Photosynthetic Reaction Center from Rhodobacter sphaeroides. *J. Phys. Chem. B*, 103:2014–2032, 1999.

[4] MH Vos, MR Jones, CN Hunter, J Breton, JC Lambry, and JL Martin. Coherent dynamics during the primary electron-transfer reaction in membrane-bound reaction centers of Rhodobacter sphaeroides. *Biochemistry*, 33(22):6750–6757, 1994.

[5] Gregory S Engel, Tessa R Calhoun, Elizabeth L Read, Tae-Kyu Ahn, Tomáš Mančal, Yuan-Chung Cheng, Robert E Blankenship, and Graham R Fleming. Evidence for wavelike energy transfer through quantum coherence in photosynthetic systems. *Nature*, 446(7137):782–786, April 2007.

[6] Elisabetta Collini, Cathy Y Wong, Krystyna E Wilk, Paul M G Curmi, Paul Brumer, and Gregory D Scholes. Coherently wired light-harvesting in photosynthetic marine algae at ambient temperature. *Nature*, 463(7281):644–647, February 2010.

[7] Sebastian Westenhoff, David Paleček, Petra Edlund, Philip Smith, and Donatas Zigmantas. Coherent picosecond exciton dynamics in a photosynthetic

reaction center. *Journal of the American Chemical Society*, 134(40):16484–7, October 2012.

[8] Franklin D. Fuller, Jie Pan, Andrius Gelzinis, Vytautas Butkus, S. Seckin Senlik, Daniel E. Wilcox, Charles F. Yocum, Leonas Valkunas, Darius Abramavicius, and Jennifer P. Ogilvie. Vibronic coherence in oxygenic photosynthesis. *Nat. Chem.*, 6(July):706–711, 2014.

[9] Volkhard May and Oliver Kühn. *Dynamics of Isolated and Open Quantum Systems*. Wiley-VCH Verlag GmbH & Co. KGaA, 2011.

[10] Nerine J. Cherepy, Andrew P. Shreve, Laura J. Moore, Steven G. Boxer, and Richard A. Mathies. Electronic and nuclear dynamics of the accessory bacteriochlorophylls in bacterial photosynthetic reaction centers from resonance Raman intensities. *J. Phys. Chem. B*, 101(16):3250–3260, 1997.

[11] Margus Rätsep, Zheng Li Cai, Jeffrey R. Reimers, and Arvi Freiberg. Demonstration and interpretation of significant asymmetry in the low-resolution and high-resolution Qy fluorescence and absorption spectra of bacteriochlorophyll a. *J. Chem. Phys.*, 134(2), 2011.

[12] Vytautas Butkus, Donatas Zigmantas, Leonas Valkunas, and Darius Abramavicius. Vibrational vs. electronic coherences in 2D spectrum of molecular systems. *Chem. Phys. Lett.*, 545:40–43, August 2012.

[13] James Lim, David Paleček, Felipe Caycedo-Soler, Craig N. Lincoln, Javier Prior, Hans von Berlepsch, Susana F. Huelga, Martin B. Plenio, Donatas Zigmantas, and Jürgen Hauer. Vibronic origin of long-lived coherence in an artificial molecular light harvester. *Nat. Commun.*, 6(7755), 2015.

[14] Niklas Christensson, Harald F Kauffmann, Tõnu Pullerits, and Tomáš Mančal. Origin of Long-Lived Coherences in Light-Harvesting Complexes. *J. Phys. Chem. B*, 116(25):7449–7454, June 2012.

[15] Vivek Tiwari, William K Peters, and David M Jonas. Electronic resonance with anticorrelated pigment vibrations drives photosynthetic energy transfer outside the adiabatic framework. *Proc. Natl. Acad. Sci.*, 110(4):1203–1208, January 2013.

[16] David Paleček, Petra Edlund, Sebastian Westenhoff, and Donatas Zigmantas. are preparing manuscript to be called "Quantum Coherence as a Witness of Vibronically Hot Energy Transfer in Bacterial Reaction Centre".

[17] Joachim Seibt, Thorsten Hansen, and Tõnu Pullerits. 3D Spectroscopy of Vibrational Coherences in Quantum Dots: Theory. *J. Phys. Chem. B*, 117(38):11124–11133, September 2013.

[18] Hebin Li, Alan D Bristow, Mark E Siemens, Galan Moody, and Steven T Cundiff. Unraveling quantum pathways using optical 3D Fourier-transform spectroscopy. *Nat Commun.*, 4(1390), January 2013.

[19] RM Hochstrasser. Two-dimensional IR-spectroscopy: polarization anisotropy effects. *Chem. Phys.*, 266:273–284, 2001.

[20] Gabriela S Schlau-Cohen, Akihito Ishizaki, Tessa R Calhoun, Naomi S Ginsberg, Matteo Ballottari, Roberto Bassi, and Graham R Fleming. Elucidation of the timescales and origins of quantum electronic coherence in LHCII. *Nat. Chem.*, 4(5):389–395, 2012.

[21] Tobias Brixner, Tomáš Mančal, Igor V Stiopkin, and Graham R Fleming. Phase-stabilized two-dimensional electronic spectroscopy. *J. Chem. Phys.*, 121(9):4221–4236, September 2004.

[22] Gitt Panitchayangkoon, Dmitri V Voronine, Darius Abramavicius, Justin R Caram, Nicholas H C Lewis, Shaul Mukamel, and Gregory S Engel. Direct evidence of quantum transport in photosynthetic light-harvesting complexes. *Proc. Natl. Acad. Sci. USA*, 108(52):20908–12, dec 2011.

[23] Sergei Savikhin, Daniel R. Buck, and Walter S. Struve. Oscillating anisotropies in a bacteriochlorophyll protein: Evidence for quantum beating between exciton levels. *Chem. Phys.*, 223(2-3):303–312, 1997.

[24] David M Jonas. Two-dimensional femtosecond spectroscopy. *Annu. Rev. Phys. Chem.*, 54(1):425–463, January 2003.

[25] H Lee, YC Cheng, and GR Fleming. Coherence dynamics in photosynthesis: protein protection of excitonic coherence. *Science*, 1462, 2007.

[26] Ian Seungwan Ryu, Hui Dong, and Graham R Fleming. Role of electronic-vibrational mixing in enhancing vibrational coherences in the ground electronic states of photosynthetic bacterial reaction center. *The journal of physical chemistry. B*, 118(5):1381–8, February 2014.

[27] Christine Kirmaier, Dewey Holten, and William W. Parson. Temperature and detection-wavelength dependence of the picosecond electron- transfer kinetics measured in Rhodopseudomonas sphaeroides reaction centers. Resolution of new spectral and kinetic components in the primary charge-separation process. *Biochim. Biophys. Acta*, 810:33–48, 1985.

[28] David Paleček, Petra Edlund, Sebastian Westenhoff, and Donatas Zigmantas. are preparing manuscript to be called "Pitfalls of the Early Dynamics in the Cross-polarized Two-dimensional Electronic Spectroscopy".

[29] Jordan M Womick and Andrew M Moran. Vibronic enhancement of exciton sizes and energy transport in photosynthetic complexes. *J. Phys. CHem. B*, 115(6):1347–1356, 2011.

Paper VI

Pitfalls of the Early Dynamics in the Cross-polarized Two-dimensional Electronic Spectroscopy

[1,2]David Paleček, [3]Petra Edlund, [3]Emil Gustavsson, [3]Sebastian Westenhoff, and [1]Donatas Zigmantas

[1] *Department of Chemical Physics, Lund University, P.O. Box 124, SE-22100 Lund, Sweden*

[2] *Department of Chemical Physics, Charles University in Prague, Ke Karlovu 3, 121 16 Praha 2, Czech Republic*

[3] *Department of Chemistry and Molecular Biology, University of Gothenburg, Box 462, SE-40530 Gothenburg, Sweden*

donatas.zigmantas@chemphys.lu.se

Abstract

Experimental tools to track electronic coherences and distinguish them from purely vibrational or mixed vibronic beatings are highly desirable. Polarization resolved two-dimensional electronic spectroscopy is currently state of the art technique to disentangle coherent beatings in light-harvesting systems. There is a growing evidence that the observed long-lived coherences stem from the mixing between electronic and vibronic states. In order to track much faster decaying purely electronic coherences, the early population times have to be included in the analysis, where the signal is typically distorted by several effects, the most seriously during the pulse overlap. We show that for the case of special polarization experiment suppressing all signals except from electronic or mixed coherences for the isotropically oriented samples, the desired signals are usually so weak that early dynamics is dominated by the wrong pulse ordering effects, which can influence the kinetics up to 80 fs, well beyond the pulse overlap. Moreover, the artifact signal is oscillatory and contributes the strongest on the lower cross-peak related to energy transfer, therefore it can be easily mistaken for the fast-decaying coherent beatings.

1. Introduction

Controlling the motion of electrons in complex materials on a microscopic scale in a coherent fashion is one of the great scientific challenges today [1]. The first step, however, is to develop the experimental and theoretical approaches to understand the collective behavior of the electrons in molecular as well as solid state systems. Coherent two-dimensional electronic spectroscopy in visible range (2DES) has enabled to pursue the coherent motions of both nuclei and electrons with superior spectral and time resolution. For almost a decade, pure electronic beatings manifesting the dynamic superpo-

sition of the electronic excited states and lasting for several hundred of fs have been dominantly reported for the light-harvesting protein complexes, ignoring the nuclear motions for the time being [2–4]. Only recently, new theoretical approaches and experimental results start to unravel fundamental and complex interaction between nuclear and electronic motions after coherent excitation [5–7]. The complexity is manifested in three dimensional Fourier transform (3DFT) oscillation maps as well as in the time domain traces in particular regions of the 2DES spectra [8].

The time-domain behavior is then no longer simple coherent electronic response but rather complex evidence of the interaction dynamics between nuclei and electrons. Therefore, the attention is once again turned to very early dynamics up to 100 fs to track the coherences with strong electronic character. To this end, polarization control of individual laser pulses in 2DES experiment proved to be advantageous since it has the ability to disentangle mixed vibronic/excitonic coherences from the purely vibrational ones [3, 9]. Although there are already studies reporting on timescales down to 47 fs with the use of 22 fs pulses (autocorrelation ~ 31 fs) in the polarization resolved 2DES [3], we demonstrate in the present paper how we stumbled on the wrong pulse ordering effects even outside the pulse overlap. These are relatively enhanced due to non-selectivity of such an ordering and simultaneous great suppression ability of the normal ordering in polarization resolved experiment. Moreover the wrong pulse ordering signals appear on the crosspeaks below diagonal and can be therefore easily misinterpreted for rapidly decaying beatings. We demonstrate the phenomenon on the real pigment-protein complex of photosynthetic reaction center, and emphasize the universality of the effect which has to be taken into account whenever selective 2DES experimental schemes are used to suppress commonly dominating signals. Technical development and growth of 2DES community worldwide promises regular use of polarization control in the near future, therefore we provide general ideas how to experimentally minimize the effects of the wrong pulse ordering.

2. Materials and Methods

We employed passively stabilized 2DES setup as previously described [10–12]. Briefly, an output from noncolinear optical amplifier pumped by 1030 nm Pharos laser system (Light Conversion Ltd), ~ 17 fs laser pulses were split into four beams using beamsplitter and diffraction grating. Spherical optics were used to focus the three excitation beams and fourth attenuated beam (2 OD) to $\sim 100\,\mu$m sample spot. First two beams were simultaneously chopped by mechanical choppers and double frequency lock-in detection scheme was used. Interferograms were continuously detected by the CCD camera (PIXIS, Princeton Instruments). Polarizations of all excitation pulses are independently set by using $\lambda/4$ waveplate and four wire-grid polarizers (contrast ratio > 800).

For the 2DES experiment, coherence time is scanned between -300 to 300 fs with the 1.5 fs step. For the negative times, population time was scanned from -300fs to 60fs with 12fs

step. This measurement was compared with the fully positive population scan from 0fs to 2000 fs with 12fs step.

Mutated BRC W(L100)F where tryptophan (W) protein residue on position L100 was exchanged with phenylalanine(F) were isolated from Rhodobacter sphaeroides grown semi-anaerobically in darkness and purified following standard procedures described elsewhere [13] with following modifications. The time of solubilisation was increased to 4 hours and the LDAO concentration was 4 %. To oxidize BRC, potassium ferricyanide ($K_3Fe(CN)_6$) in resulting concentration of 150 mM was used. Samples were mixed with glycerol at 35:65 (v/v) and cooled down to 77 K in the 0.5 mm fused silica cell with optical density 0.2–0.3 at 800 nm.

3. Results

From previous investigations, bacterial reaction centers (BRC) manifest various oscillatory patterns and polarization resolved experiments provided valuable insight into the coherent dynamics phenomena. Long-lived vibrational, vibronic and mixed vibronic/excitonic coherences have been reported [9, 14]. The most relevant cross-polarization (CP) scheme in terms of the focus on the mixed vibronic/excitonic coherences is when relative polarization directions read $(\pi/4, -\pi/4, \pi/2, 0)$ for the beams $(\vec{k}_1 - \vec{k}_4)$, respectively, in the case of isotropically oriented samples [3, 9, 15]. Within this scheme, it is possible to suppress the static population-related and vibrational coherence signals up to $\sim 80 - 100$ times, which improves sensitivity to detect generally very weak coherences with excitonic character [9]. To present the effect of the wrong pulse ordering we extend our CP experiment into negative population times.

Fig. 1A illustrates how the pulses are scanned during the standard 2DES data acquisition procedure. Population time $t_2 = 0$ fs is fixed, coherence time delay t_{12} between the first two pulses is adjusted by scanning $\vec{k}_1$ ($t_{12} > 0$, rephasing part) or $\vec{k}_2$ ($t_{12} < 0$, non-rephasing part) into negative t_2, respectively. Time delay t_{34} between $\vec{k}_3$ and $\vec{k}_4$ is kept constant ($t_{34} \sim 2.5$ ps) and the pulse pair delay is scanned in respect to $t_2 = 0$ fs, setting the population time [10].

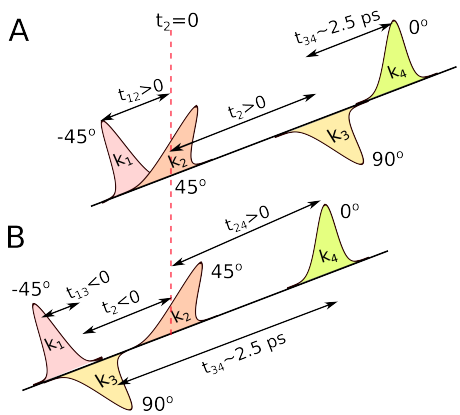

Figure 1: *Two pulse sequences considered in the text. A) Cross-polarized sequence $(\pi/4, -\pi/4, \pi/2, 0)$ specifically enhancing coherent beating pathways with mixed vibronic/excitonic character. During the measurement for a given population time t_2, $\vec{k}_1$ ($\vec{k}_2$) pulses are scanned to $t_2 < 0$ to obtain rephasing (non-rephasing) part of the 2DES spectra, respectively, as the delay t_{34} between $\vec{k}_3$ and $\vec{k}_4$ is kept constant. B) Wrong pulse ordering sequence $(\pi/4, \pi/2, -\pi/4, 0)$ where pulses $\vec{k}_2$ and $\vec{k}_3$ switch order was identified as the source of the signal in the negative t_2, during pulse overlap and even beyond.*

Since the signal is detected in the phase-matching direction $-\vec{k}_1+\vec{k}_2+\vec{k}_3$ [16], the only alternative pulse ordering contributing to our signal is $-\vec{k}_1+\vec{k}_3+\vec{k}_2$ and $\vec{k}_3-\vec{k}_1+\vec{k}_2$, where the $\vec{k}_2$, $\vec{k}_3$ interaction order is reversed. The former corresponds to rephasing and latter to non-rephasing like signals. This situation occurs only for negative t_2 and during the pulse overlap around $t_2 = 0$ and we denote it as "Wrong Pulse Ordering Sequence" (WPOS) throughout the text. Note that the other alternative pulse ordering ($\vec{k}_2 + \vec{k}_3 - \vec{k}_1$, $\vec{k}_3 + \vec{k}_2 - \vec{k}_1$) correspond to double quantum coherence pathways and contribute negligibly to presented data.

3.1. Wrong pulse ordering sequence (WPOS)

For a given population time t_2, 2DES spectrum correlates excitation and emission energies which are conjugated Fourier transform pairs of the time delays t_{12} and t_{34}, respectively. In the case of WPOS when $\vec{k}_2$ and $\vec{k}_3$ interact in reversed order, the role and notation of the time delays change accordingly: $t_{12} \rightarrow t_{13}$; $t_{34} \rightarrow t_{24}$. The $\vec{k}_1$ pulse effectively scans coherence time around $\vec{k}_3$ as the $\vec{k}_2$ acts as the signal generating pulse (see Fig. 1B). In standard 2DES experiment, the uncertainty in the t_{12}, t_{34} makes them a matter of phasing procedure in order to determine $t_{12}, t_{34} = 0$, hence separate real (absorptive) and imaginary (refractive) part of the complex-valued 2DES spectra by matching their projection to an independently measured pump-probe spectra for $t_2 > 0$. For WPOS however, their function is adapted by t_{13} and t_{24} instead and since these two delays change with every negative population time $t_2 < 0$, the interference pattern of the 2DES signal for the WPOS shifts along the diagonal in the time domain 2DES representation plot of (t_{12}, t_{34}) as the t_2 gets more negative (see Fig. 2). This implies that the WPOS signals appear predominantly in the rephasing part of the 2DES spectrum for the negative times. Note that the signal is $\sim$ 10x stronger for $t_2 = -240$ fs than for $t_2 = 60$ fs.

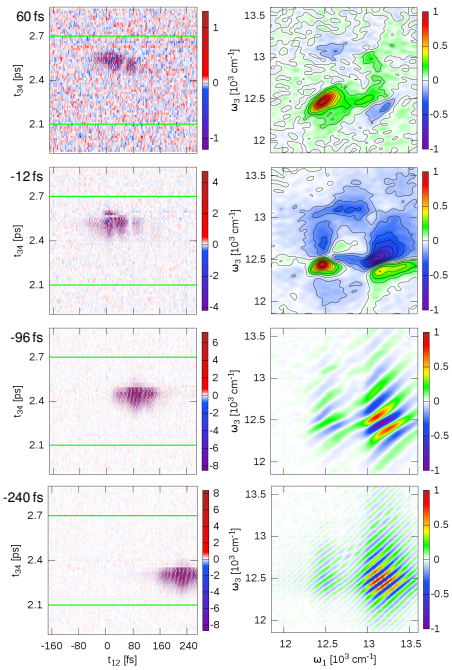

Figure 2: *Raw 2DES interferograms (left) for several population times, together with total real 2DES spectra (right) when phased for $t_2 > 0$. Green lines mark the full width half maximum of the Fourier filter in t_{34}. For the negative times, interference fringes shift linearly in both t_{12} and t_{34} axes, therefore the fringes in the resulting 2DES spectra appear in both horizontal (ω_1) and vertical (ω_3) direction.*

3.2. WPOS phasing

First, whole data set spanning $t_2 = -300 \rightarrow 60$ fs with 12 fs step was phased with parameters obtained from phasing the positive delay times $t_2 > 0$ only. Different values of t_{13}, t_{24} for WPOS compared to t_{12}, t_{34} (normal ordering for $t_2 > 0$) is expected to cause spectral fringes along the corresponding frequency axes for WPOS signal according to Fourier shift theorem[17]. As the time differences increase, the spectral fringes get denser as illustrated in Fig. 2. To prove this hypothesis and demonstrate the spectral position and shape of the WPOS signal, each 2DES frame's phasing parameters for $t_2 < 0$ can be approximately adjusted to compensate for the reverse order of the $\vec{k}_2$ and $\vec{k}_3$ pulses and corresponding time delays. The parameters change linearly with t_2 as expected and the result for $t_2 = -240$ fs frame is illustrated in Fig. 3. In two separate steps, we get rid of the vertical (horizontal) spectral fringes by adjusting t_{34} to equal t_{24} (compare left panel Fig. 3 with Fig. 2) and then t_{12} to equal t_{13}, respectively. The resulted re-phased signal is non-oscillatory and located on the HB energy transfer cross-peak below diagonal (see middle and right panels in Fig. 3) in accordance with the polarization effects discussed below. The spectral location in the 2DES spectrum is significant, since the lower cross-peak is very often analyzed in relation to coherent beatings and energy transfer dynamics [2, 4].

The necessity of taking these signals into account in quantum coherence studies arises from the fact they are oscillatory in nature if no adjustments to the phasing parameters are applied. The spectral fringes are t_2–dependent since they get denser with increasingly negative t_2 which effectively leads to oscillation kinetics in the population time t_2 of the arbitrary (ω_1, ω_3) 2DES data point (see Fig. 5).

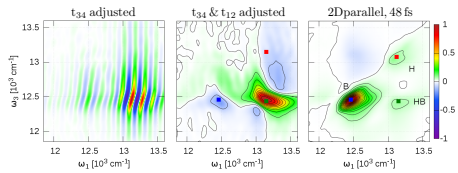

Figure 3: *Correction of the wrong phasing parameters in the negative population times for the WPOS. (Left) 2DES frame at $t_2 = -240$ fs from Fig. 2 where t_{34} is adjusted to match t_{24} in order to get rid of the vertical fringes. (Middle) Further compensation of t_{12} to match t_{13} leads to the signal located at the position of the energy transfer cross-peak below the diagonal (Right).*

3.3. Effect of polarization

Two features about the WPOS mentioned above are still to be clarified, the location of the WPOS on the lower cross-peak and why the signal is up to 10-times stronger for $t_2 < 0$ than the real signal for $t_2 > 0$. Both issues can be resolved if we assume polarization of the individual laser pulses. For the polarization resolved 2DES on isotropic samples, every possible interaction pathway (so called Liouville) associates with orientational prefactor which contains scalar products of the molecular transition dipole moments and unit vectors in the direction of the polarized electric fields [15].

If we assume two molecular dipole moments (A,B) with nonzero angle between them, then the four laser fields can interact only either with one of them (AAAA, we skip symmetric pathways interacting with dipole B first) or

both (AABB, ABAB, ABBA). AAAA, AABB pathways describe population and vibrational coherence dynamics, whereas the ABAB, ABBA represent the mixed vibronic/excitonic coherence pathways. In most cases, these coherence signals are weak compared to population dynamics and vibrational coherences, which are both well suppressed for all angles between the dipole moments in CP measurement (see Fig. 4, blue).

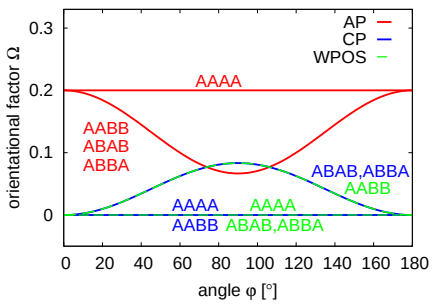

Figure 4: *Dependence of the orientational prefactor on the angle between the transition dipole moments φ for the selected polarization schemes. Two contributions stem from population dynamics and/or vibrational coherence (AAAA, AABB) and another two from coherence beatings with mixed vibronic/excitonic character (ABAB, ABBA). For pulses oriented all parallel (AP, red), all pathways contribute to the overall 2DES signal. Both cross-polarization schemes are selective as some pathways vanish for all possible angles φ. CP selects solely the mixed vibronic/excitonic coherence pathways (ABAB, ABBA, blue), whereas the energy transfer and some of the vibrational coherence pathways survive the WPOS (AABB, green).*

However, the reversed pulse order for WPOS leads in fact to the polarization sequence $(\pi/4, \pi/2, -\pi/4, 0)$ which exhibits different selection rules for Liouville pathways (see Fig. 4, green). It allows only for AABB contribution, which includes energy transfer and some of the vibrational coherence pathways. These signals can be several times stronger and can therefore significantly distort the initial part of overall weak signal of mixed vibronic/excitonic coherences in CP measurement.

3.4. Time traces analysis

Presented analysis of the WPOS for $t_2 < 0$ argues for the origin of the oscillation in 2DES spectra around zero population time being the wrong pulse ordering. However, important are the consequences this can have on the data for $t_2 \geq 0$. Since we have already identified the spectral position of the WPOS signal on the lower cross-peak, the question is how far the signal extends. Fig. 5 shows cross-peak time domain traces for the CP measurement for $t_2 = -300 \rightarrow 60$ fs and another one going from $t_2 = 0$ fs further. It is clear from the overlap of the independent measurements that the oscillating signals are reproducible. The long-lived beatings in the BRCs for CP were shown to originate from vibronic mixing, which exhibit similar amplitude at both the cross-peaks . The beatings asymmetry between upper and lower cross-peak in the early times lead us to conclusion that even with the ~ 17 fs pulses (autocorrelation of ~ 24 fs), first $70 - 80$ fs of the kinetics can be distorted due to the WPOS effect.

The reason is that even though the pulse overlap effects decay as $\sim \mathrm{e}^{-x^2}$, the WPOS signal is 10-times stronger at $t_2 = 0$ fs and the detection is sensitive enough to resolve it even beyond the pulse overlap. Note that even fast

purely excitonic component would exhibit the same beating amplitudes at the cross-peaks as well. In theory, vibronic mixing and large Huang-Rhys factors can cause amplitude asymmetry [7]. The latter is not the case for the BRC and vibronic mixing can not account for the asymmetry observed in the early population times.

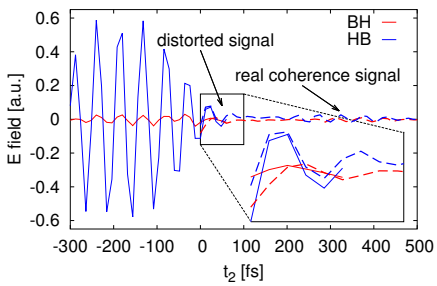

Figure 5: *t_2 kinetics for the lower (blue) and upper (red) cross-peak for the CP measurement on the W(L100)F BRC mutant. The lower cross-peak oscillates heavily in the negative times which influences the first $70-80$ fs of the positive t_2, since the coherence signals are expected to posses similar amplitude (see text for details).*

Fourier transform over t_2 for each point in the 2DES spectra enables to visualize the oscillatory amplitudes within the 2DES spectra by plotting the 2D slices of 3DFT spectra [8, 18]. Integrating the amplitude of the obtained 2D slices provide information about the dominant beating frequencies within the system as shown in Fig. 6. Without any adjustments of the phasing parameters, kinetics exhibit spectrally broad and strong oscillations with the maximum amplitude identified for $\sim 700\,\mathrm{cm}^{-1}$. Adjustment of the t_{34},t_{12} diminishes the FT amplitude and the maximum eventually shifts towards $\omega_2 = 0$, indicating non-oscillatory signal as expected from excitation energy transfer crosspeak. Importantly, the frequencies of the real coherence signals coincide with those of WPOS oscillations for $t_2 < 0$ if no adjustments to phasing are applied. Moreover, the amplitudes of the real coherence signal are ~ 50 times weaker, so that even fast-decaying artifact oscillation affects the first $70-80$ fs.

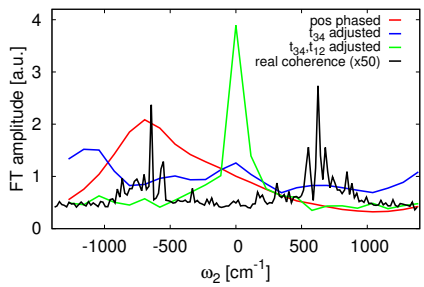

Figure 6: *Effect of the phasing on the overall oscillatory amplitudes and frequencies within the 2DES spectra. Negative time FT amplitudes obtained from CP measurement between $t_2 = -300 \rightarrow -24$ fs when: (red) data were phased to positive t_2 frames, (blue) t_{34} phasing adjusted to match t_{24}, (green) additional adjustment of t_{12} to match t_{13}. For comparison, real coherence FT amplitude extracted from the independent CP measurement for $t_2 = 0 \rightarrow 1800$ fs is shown (black). The frequencies of the real coherence signals coincide with the spectral shape of the oscillations in negative t_2 if no adjustments to phasing are applied.*

We note that the relative strength of the artifact signal will strongly depend on the phase stability of the 2DES setup since the reverse order of the $\vec{k}_2$ and $\vec{k}_3$ pulses makes the WPOS scheme prone to phase instability of the setup or the laser system in the case of passively stabilized 2DES setup [10]. Here

we see the opportunity to experimentally minimize the WPOS effects by introducing for instance piezo element on the mirror reflecting the beams $\vec{k}_3$, $\vec{k}_4$ which would keep the phase stability within the pulse pairs ($\vec{k}_1$, $\vec{k}_2$) and ($\vec{k}_3$, $\vec{k}_4$), but would disrupt the phase relation between them, which is necessary for observing WPOS signal. Another issue is the accuracy in polarization settings which strongly influence the suppression of the typically dominating signals, inherently connected to the relative enhancement of the WPOS signal.

4. Conclusions

Technical improvements in the phase stability and polarization control together with the more elaborate analysis and theoretical modeling extending into the pulse overlap region of the 2DES brings out the need for understanding the pulse overlap region, at least to be aware of the possible experimental artifacts. In the presented paper, we specifically investigated wrong pulse ordering effects for the cross-polarized pulse sequence enhancing coherent beatings with mixed vibronic/excitonic character for the isotropically oriented samples. The effect was found to easily dominate the pulse overlap region, extending up to 80 fs positive time delays for certain 2DES spectral region even if 17 fs pulses are used. Moreover, the wrong pulse ordering signals are oscillatory in nature, dominant at the lower cross-peak of the 2DES spectra with the oscillation frequency range covering the modes typically occurring and accessible in the 2DES. Because of that, such artifacts can be easily misinterpreted for rapidly decaying coherent beatings.

Acknowledgments

We would like to thank Erling Thyrhaug for helpful comments on the manuscript. The research was supported by the Swedish Research Council and Knut and Alice Wallenberg foundations.

Additional information

The authors declare no competing financial interests.

References

[1] Graham R. Fleming and Mark a. Ratner. Grand challenges in basic energy sciences. *Phys. Today*, 61(7):28–33, 2008.

[2] Elisabetta Collini, Cathy Y Wong, Krystyna E Wilk, Paul M G Curmi, Paul Brumer, and Gregory D Scholes. Coherently wired light-harvesting in photosynthetic marine algae at ambient temperature. *Nature*, 463(7281):644–647, February 2010.

[3] Gabriela S Schlau-Cohen, Akihito Ishizaki, Tessa R Calhoun, Naomi S Ginsberg, Matteo Ballottari, Roberto Bassi, and Graham R Fleming. Elucidation of the timescales and origins of quantum electronic coherence in LHCII. *Nat. Chem.*, 4(5):389–395, 2012.

[4] Gregory S Engel, Tessa R Calhoun, Elizabeth L Read, Tae-Kyu Ahn, Tomáš Mančal, Yuan-Chung Cheng, Robert E Blankenship, and Graham R Fleming. Evidence for wavelike energy transfer through quantum coherence in photosynthetic systems. *Nature*, 446(7137):782–786, April 2007.

[5] Vytautas Butkus, Donatas Zigmantas, Darius Abramavicius, and Leonas Valkunas. Distinctive character of electronic and vibrational coherences in disordered molecular aggregates. *Chem. Phys. Lett.*, 587:93–98, 2013.

[6] Niklas Christensson, Harald F Kauffmann, Tõnu Pullerits, and Tomáš Mančal. Origin of Long-Lived Coherences in Light-Harvesting Complexes. *J. Phys. Chem. B*, 116(25):7449–7454, June 2012.

[7] Vivek Tiwari, William K Peters, and David M Jonas. Electronic resonance with anticorrelated pigment vibrations drives photosynthetic energy transfer outside the adiabatic framework. *Proc. Natl. Acad. Sci.*, 110(4):1203–1208, January 2013.

[8] Hebin Li, Alan D Bristow, Mark E Siemens, Galan Moody, and Steven T Cundiff. Unraveling quantum pathways using optical 3D Fourier-transform spectroscopy. *Nat Commun.*, 4(1390), January 2013.

[9] Sebastian Westenhoff, David Paleček, Petra Edlund, Philip Smith, and Donatas Zigmantas. Coherent picosecond exciton dynamics in a photosynthetic reaction center. *Journal of the American Chemical Society*, 134(40):16484–7, October 2012.

[10] Tobias Brixner, Tomáš Mančal, Igor V Stiopkin, and Graham R Fleming. Phase-stabilized two-dimensional electronic spectroscopy. *J. Chem. Phys.*, 121(9):4221–4236, September 2004.

[11] Ramũnas Augulis and Donatas Zigmantas. Two-dimensional electronic spectroscopy with double modulation lock-in detection: enhancement of sensitivity and noise resistance. *Optics express*, 19(14):13126–33, July 2011.

[12] Ramūnas Augulis and Donatas Zigmantas. Detector and dispersive delay calibration issues in broadband 2D electronic spectroscopy. *JOSA B*, 30(6):1770, May 2013.

[13] MarkL. Paddock, ScottH. Rongey, EdwardC. Abresch, George Feher, and MelvinY. Okamura. Reaction centers from three herbicide-resistant mutants of rhodobacter sphaeroides 2.4.1: sequence analysis and preliminary characterization. *Photosynth. Res.*, 17(1-2):75–96, 1988.

[14] Ian Seungwan Ryu, Hui Dong, and Graham R Fleming. Role of electronic-vibrational mixing in enhancing vibrational coherences in the ground electronic states of photosynthetic bacterial reaction center. *The journal of physical chemistry. B*, 118(5):1381–8, February 2014.

[15] RM Hochstrasser. Two-dimensional IR-spectroscopy: polarization anisotropy effects. *Chem. Phys.*, 266:273–284, 2001.

[16] David M Jonas. Two-dimensional femtosecond spectroscopy. *Annu. Rev. Phys. Chem.*, 54(1):425–463, January 2003.

[17] R.N. Bracewell. *The Fourier Transform and Its Applications*. McGraw-Hill international editions. McGraw Hill, 2000.

[18] Vytautas Butkus, Donatas Zigmantas, Leonas Valkunas, and Darius Abramavicius. Vibrational vs. electronic coherences in 2D spectrum of molecular systems. *Chem. Phys. Lett.*, 545:40–43, August 2012.

Paper VII

Quantitative Evaluation of the Vibronic Mixing in Relation to Excitation Energy Transfer in the Photosynthetic Reaction Center.

[1,2]David Paleček, [3]Emil Gustavsson,[3]Petra Edlund, [3]Sebastian Westenhoff, and [1]Donatas Zigmantas

[1]*Department of Chemical Physics, Lund University, P.O. Box 124, SE-22100 Lund, Sweden*

[2]*Department of Chemical Physics, Charles University in Prague, Ke Karlovu 3, 121 16 Praha 2, Czech Republic*

[3]*Department of Chemistry and Molecular Biology, University of Gothenburg, Box 462, SE-40530 Gothenburg, Sweden*

donatas.zigmantas@chemphys.lu.se

Abstract

Vibronic effects in light-harvesting is intensively studied research topic. Coherent two-dimensional electronic spectroscopy has the potential to quantify the vibronic mixing and follow it on a femtosecond timescale with the superior spectral resolution. Using bacterial reaction centers from *Rhodobacter sphaeroides* and its three analogues with specific point mutations along the active branch, we developed systematic experimental approach to quantify the vibronic mixing. We also attempt to relate these effects to the excitation energy transfer through the core antenna towards the special pair, where the charge separation takes place.

1. Introduction

Many natural processes are driven by the charges moving along the electrochemical gradients across the biological membranes. Photosynthetic process generates the energy-rich compounds, which are decomposed by the vast majority of living organisms in the reversed process of aerobic respiration, generating cellular energy. The efficiency of primary processes in photosynthesis encompassing the conversion of the absorbed light energy to the primary charges is close to unity [1]. The reason lies in the ultrafast nature of these processes, funneling the excitation energy towards the reaction center, where the trans-membrane charge separation takes place. The natural light-harvesting is highly optimized in terms of efficiency, unidirectionality, regulation and environmental diversity [2, 3]. Control of the energy and electron transfer, especially on the nanoscale [4] leads to the new applications [5, 6] as well as to the new materials [7]. Approaching the fundamental scales for the electron motions in time and space, i.e. fem-

toseconds and nanometers, the quantum effects are expected to progressively manifest themselves. Quantum coherence, where the superpositions of the system's energy states evolve in time is one example. Utilizing the coherence has been proposed as the next step in controlling the motions of electrons [8]. Photosynthetic light harvesting is a natural candidate to look for such phenomena.

The most abundant light-harvesting molecules are chlorin derivatives such as chlorophylls and pheophytins. Their spectroscopic properties are well utilized by the photosynthetic organisms. Tuning the energy of the states by the electronic coupling between the pigments and by their interaction with a protein scaffold are the dominant ways for the photosynthetic organisms to achieve efficient funneling of the excitation energy towards the reaction center. Moreover, the light-harvesting pigments posses the rich vibrational structure, which is relevant to the excitation energy transfer through the exciton-vibronic coupling [9–11] and was suggested to facilitate the process. Vibrationally assisted excitation energy transfer (EET) [12] and electron transfer (ET)[13] are well developed concepts. However experimental evidence and quantification how these effects contribute to the overall transfer rates is not sufficiently explored and therefore not understood. The reason lies in the complex interplay of many factors such as coupling constants, vibrational structure, resonance effects, etc.

Coherent two-dimensional electronic spectroscopy (2DES) enables to directly follow and disentangle excited state population dynamics, interactions with bath and to investigate coherent phenomena [14]. In 2DES experiment a sequence of three excitation pulses generates nonlinear polarization of the sample, emitted later in the direction of the attenuated fourth pulse (LO). Precise control of the delays between the first two pulses (t_1) provides resolution along excitation axis, which is not accessible by conventional time-resolved spectroscopies. Delay between the second and third pulse (t_2) follows the evolution of the system. Delay between the emitted polarization, following the interaction with the third pulse at (t_3), and LO determines the spectrally resolved interference pattern detected on the CCD [15]. The data in (t_1, ω_3) obtained by Fourier filtering of the measured spectrograms is Fourier transformed over the t_1 coherence time, which yields the 2D maps that correlate excitation and emission energies (ω_1, ω_3). Pulse ordering of the first two pulses allows to separate rephasing (photon echo-type signal, $t_1 < 0$ [16]) and non-rephasing (free induction decay, $t_2 < 0$ [17]) parts of the response. Heterodyne detection scheme [18] enables to access both real and imaginary parts of the signal. In the case of coherences evolving in time, it is possible to distinguish phase evolution direction of the superposition state during the population time t_2, i.e. sign of the ω_2 [19, 20]. Together with spectral resolution along the excitation axis, these features makes 2DES an excellent tool for coherent dynamics studies [21].

The coherent oscillations during the population time stem from the created superpositions of the various energy eigenstates by the ultrashort and broadband excitation pulses. In principle two distinct cases are discussed in literature. One is the superposi-

tion created between electronic excited states (electronic coherence) and other — superposition between vibrational states in the ground or excited electronic state (vibrational coherence). It was surprising, when the quantum coherences lasting for several hundreds of femtoseconds were assigned to purely electronic coherences present in the light-harvesting complexes [22, 23]. First, the expected dephasing rate of the excited state coherences is on the order of tens or hundred of femtoseconds [24]. Second, the pigments' vibrations were mostly ignored even though they have to appear in 2DES since they have been found in complementary experiments [25, 26]. More elaborate hypotheses including vibrations and their mixing with electronic states have been proposed recently [9, 10, 27]. Furthermore, we identified a new coherent process denoted "energy transfer induced coherence shift" (ETICS) by taking advantage of the polarization controlled 2DES experiments and extensive complex FT analysis [28]. On the theory side, two-particle vibronic/excitonic theoretical model is currently used to predict oscillation patterns in 2DES spectra for different system parameters and coupling regimes [10, 29, 30].

R-26 strain of BRC serves as a model system for the type II reaction centers in oxygenic photosynthesis. It contains almost C_2 symmetrical core antenna consisting of two bacteriopheophytins a (BPheo) mostly contributing to the H band and two bacteriochlorophyll *a* (BChl) molecules mostly contributing to the B band. Both absorption bands are used to funnel the excitation energy within ~ 200 fs towards the strongly coupled BChl dimer, called special pair (P). After the excitation energy reaches P, the charge separation and subsequent primary charge transfer occurs approximately in 1.5 ps. Specific point mutations within the RC_{sph} are often used to disturb the highly optimized functional protein structure, aiming to understand the underlying phenomena behind the function of the WT RC_{sph}. The mutants generally exhibit slower charge separation [31], but not so many studies investigated the preceding EET in mutants.

In this work, EET and coherent dynamics are compared for native RC_{sph} and three specifically mutated RC_{sph} where (1) tyrosine (Y) on the M subunit residue 210 is replaced by phenylalanin (F) denoted as Y(M210)F, (2) tryptophan L100 is replaced by phenylalanin referred to as W(L100)F and (3) glutamin L104 is replaced by leucin denoted E(L104)L. Y(M210)F interacts with the P which slows down the electron transfer rate from 3.5 ps to 16 ps, although it is not clear if there is a hydrogen bonding involved [32].

There is a growing consensus in the field, that in most cases the observed coherence in biological complexes is of mixed vibronic origin, due to the multitude of vibrational modes and electronic couplings present. The separation of the pathways according to $\pm\omega_2$ has proven to be extremely useful for determining the origin of the coherence oscillations [28, 33]. It allowed us to identify the coherence shift mechanism in the RC_{sph}, which explains the massive mismatch between the coherence dephasing and the lifetime of the excited states. Based on the detailed knowledge about the nature of the coherent oscillations, we take one step further to evaluate quantitatively the vibronic coupling

and Huang-Rhys (HR) factors for the photosynthetic reaction center of purple bacterium *Rhodobacter sphaeroides* (RC_{sph}). Moreover, we compare the results of the wild type (WT) strain R-26 to the three specifically mutated RC_{sph}.

2. Materials and Methods

Sample preparations

The WT R-26 RC was prepared and purified as described elsewhere(ref) The mutant proteins were produced in the native host in semi-anaerobic dark conditions at $30°C$ with selection with Kanamycin (final concentration 100 μg/ml) and Tetracyklin (final concentration 10 μg/ml) in a 30 l fermentor. The cells were harvested after $\sim$ 40 h culturing by centrifugation and resuspended in 20 mM MES pH 6.8, 100 mM KCl and flash frozen for storage until purification. The thawed cells was resuspended in 15 mM Tris/HCl, 100 mM NaCl, 1 mM EDTA, pH 8.0 and lysed in a frenchpress. Cell debris was removed by centrifugation and membranes were collected by ultracentrifugation at 43000 g 1 hour 4° C. The cell membranes were resuspended in the same buffer to OD(850) = 50 and LDAO was added to a final concentration of 4% and solubilisation was performed for 4 hours in darkness. The protein was salted out with ammonium sulfate and added to a celite column. The light harvesting complexes were washed away with 15 mM Tris/HCl, 100 mM NaCl, 1 mM EDTA, pH 8.0 containing 25% ammonium sulfate. The reaction center was eluted with 15 mM Tris/HCl, 1 mM EDTA, pH 8.0, 0.1% LDAO containing 15% ammonium sulfate. Salt was removed by loading the sample to a hiprep 26/10 desalting column followed by ion-exchange chromatography on a toyopearl DEAE-650M column eluted with a continuous 0-500 mM NaCl gradient. The protein was concentrated and flash frozen with liquid nitrogen. Prior to the 2DES experiments the protein samples were chemically oxidized with 150 mM $KFe(CN)_6$ and diluted in glycerol (80 %) in the ratio 1:3 to ensure high quality low temperature glass in 0.5 mm cuvette. The maximum absorbance was A(800) $\approx$ 0.3.

2DES

We employed passively stabilized 2DES setup as described previously[15, 34, 35]. Briefly, non-collinear optical parametric amplifier was pumped by the $\sim$ 1030 nm Pharos laser system (Light Conversion Ltd). On the output $\sim$ 17 fs laser pulses were split into four beams using beamsplitter and transmission grating. For polarization control a quarter waveplate and four wiregrid polarizers in each of the beams are used. Using spherical optics, the three excitation beams and the fourth attenuated beam (2 OD) were focused and overlapped in the $\sim$ 100 μm sample spot. First two beams were simultaneously chopped by opto-mechanical choppers in a double frequency lock-in detection scheme to reduce scatter influence [34]. The spectral interferograms are spectrally resolved on the CCD camera (PIXIS, Princeton Instruments). Fourier transform of the raw data in (t_1, ω_3) over the coherence time yields the resulting 2D maps that correlate excitation and emission frequencies (ω_1, ω_3).

The population kinetics were extracted by integrated entire lower

crosspeak centered at $(\omega_1, \omega_3) = (13100, 12500)\,\mathrm{cm}^{-1}$, total real part, in the all-parallel polarization sequence $(0°, 0°, 0°, 0°)$ for the pulses 1-4. The coherence delay was typically scanned between $-170 : +220$ fs leading to overall resolution of 55 and $50\,\mathrm{cm}^{-1}$ for ω_1 and ω_3, respectively. The coherent oscillations were extracted from the upper cross-peak in cross-polarization measurement $(45°, -45°, 90°, 0°)$ from rephasing real part. Coherence delay was typically scanned from -150 to 175 fs, which results in spectral resolution of $70\,\mathrm{cm}^{-1}$ along both ω_1 and ω_3.

3. Results

3.1. Huang-Rhys factors

In Condon approximation for harmonic potential surfaces, the Huang-Rhys factor corresponds to $D^2/2$, where D is the dimensionless displacement of the excited state potential in respect to the ground state one. As a consequence, the overlap between electronic ground and excited state vibrational wavefunctions changes, allowing other than 0–0 transitions. This electron-phonon coupling leads to the possibility of simultaneous vibrational excitation while the chromophore undergoes electronic transition. In theory, the vibrations can be treated as a part of the spectral density (bath) (cite) or they can be included in the system Hamiltonian [10, 29, 36]. The electron-phonon coupling is extremely important for understanding the photophysics of the light-harvesting processes [11, 37–39]. However proper treatment of the electron-phonon coupling is still a challenging task.The Huang-Rhys factors can be readily obtained from frequency domain experiments such as fluorescence line-narrowing (FLN) and resonance Raman (RR) [25, 26]. However they depend on delicate background subtraction, which brings about uncertainty. Where as FLN is linear technique, the RR probes the 3rd order non-linear response as do the time-domain techniques like pump-probe or 2DES [14]. Therefore there should be a clear correspondence between the frequency and time domain approaches.

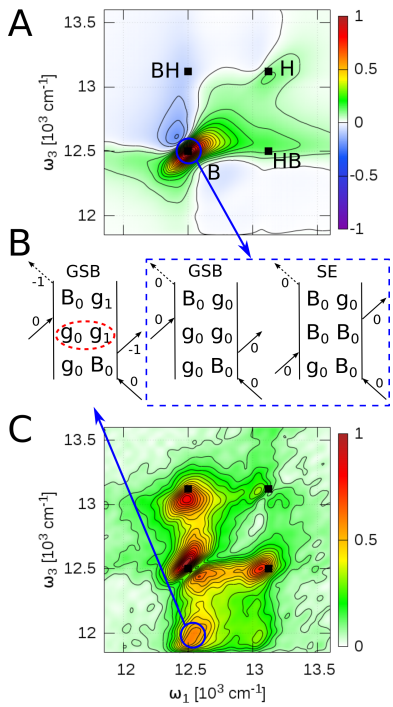

Figure 1: *Extraction of the HR factors. (A) Real rephasing 2D spectrum for WT* $\mathrm{RC}_{\mathrm{sph}}$ *at population time delay* $\mathrm{t}_2 = 24$ fs. *(B) Two population pathways, shown ans double sided Feyman diagrams, contribute to the B diagonal (dashed blue rectangle) and one pathway stems from the ground state below B. (C) Real FT oscillation map for WT* $\mathrm{RC}_{\mathrm{sph}}$ *for* $570\,\mathrm{cm}^{-1}$ *mode.*

It is known that HR factors are low for BChl *a* containing proteins [25, 26].

To extract the HR factors from 2DES, we compare amplitude of the purely vibrational coherence in the ground state to the amplitude of the population bleach near zero population time. Since we measure at 77 K, the initial state is the vibrational ground state. Together with limited laser spectrum, we can limit the analysis of beatings to only single vibrational excitation per electronic one, neglecting overtones.

With these assumptions we can analyze the interaction pathways contributing to the rephasing part of the 2D spectra. One ground state bleach (GSB) and one stimulated emission (SE) pathways are responsible for the population dynamics on B diagonal signal. On the other hand, only one purely GSB coherence pathway contributes to the peak below the B diagonal, where spacing from the diagonal is given by the frequency of the coherent oscillation (see Fig. 1). Due to the long dephasing time of the ground state coherences, we were not able to measure the whole coherence decay in 2DES experiment and achieve the frequency resolution as in RR or FLN. The precise frequencies can be extracted from heterodyne-detected transient grating experiment at the cost of the frequency resolution loss along the excitation axis ω_1 [40].

Table 1 shows the HR values for near-resonant modes extracted from the 2D spectra compared to the FLN study on BChl *a* in FMO and RC_{sph} in Fenna-Matthews-Olson (FMO) complex and RC_{sph} [26, 41]. Even though 2DES lacks the frequency resolution of the RR or FLN, the agreement is satisfactory.

Table 1: *Extracted HR factors for the near resonant modes in* RC_{sph} *compared to data obtained for WT RC measurement by resonant Raman [26] and HR factors of BChl a extracted from fluorescence line-narrowing experiments on FMO [41].*

Mode [cm^{-1}]	Mutant	HR [10^{-3}]		
		2DES	FLN (FMO)	RR (WT)
570	WT	7.6 ± 0.4	7 ± 0.5	11
	M210	6.5 ± 0.4		
	WL100	9.6 ± 0.6		
	EL104	6.1 ± 0.4		
650	WT	3.8 ± 0.2	6 ± 0.5	14
	M210	2.5 ± 0.1		
	WL100	4.6 ± 0.3		
	EL104	5.4 ± 0.3		

3.2. Quantitative evaluation of the vibronic mixing

In our previous work, we discussed the origin of the long-lived coherent oscillations with the clear signatures of the electronic excited state coherence [28, 33]. ETICS mechanism should be considered whenever the lifetime of the coherences in the excited state is longer or comparable to the energy transfer time which depopulates that excited state. This is certainly the case for the RC_{sph} since the relaxation of the B occurs in $\sim$ 170 fs in contrast to vibrational coherence dephasing of several picoseconds. Since we observe the ETICS beatings in the polarization selective 2DES, which is sensitive only to the mixed vibronic/electronic coherences, the long-lived beatings are direct witness of vibronic coupling. Vibronic mixing due to the electronic coupling between H electronic level $|H_0\rangle$, and B first vibronic level $|B_1\rangle$ results in the two excitonic levels $|(H_0B_1)\rangle$. These are the energy eigenstates of the stationary Hamiltonian and have mixed vibronic/electronic character (see Fig. 2).

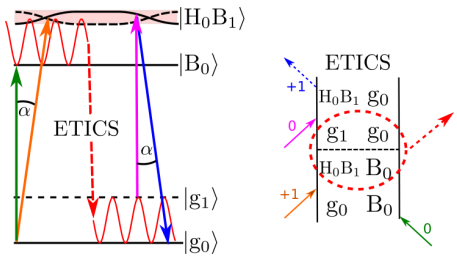

Figure 2: *Coherence interaction pathway contributing to the upper crosspeak B–H in 2D spectrum. (Left) Energy level scheme of the excitonic-vibronic B band. Vibronic mixing of the $|(H_0B_1)\rangle$ state causes the ETICS signal to survive cross-polarization measurement. (Right) ETICS pathway corresponding to the level scheme.*

Based on the all-parallel (AP) and cross-polarized (CP) measurement and knowledge of ETICS, we can pinpoint the nature of the mixed state $|(H_0B_1)\rangle$. For the analysis we chose the upper crosspeak (B–H) in rephasing part as the most unbiased region of the 2DES spectrum. The lower crosspeak (H–B) can be hindered by the wrong pulse ordering effects around the zero population time in CP [42] and directly populated GSB coherences predicted by Tiwari et al. [10]. In addition, the non-rephasing part exhibits dispersive line shapes, where the inhomogeneous broadening leads to the destructive interference since the phase of the oscillations sweeps along the diagonal [20, 43].

The relevant ETICS pathway for the B–H crosspeak coherence is shown in Fig. 2 together with the energy level scheme. The last two interactions go through the $|H_0B_1\rangle$ state. If not mixed, both transition dipole moments would be parallel to each other and no signal would be observed ([33] and references therein). Due to the low HR factors, transitions matching the electronic gaps are dominant. The third interaction 0 (without a change of vibrational quantum) is B-resonant and interacts with vibronic part of the $|H_0B_1\rangle$. In contrast, last +1 interaction is H-resonant and interacts with the electronic part of the $|H_0B_1\rangle$. During experiment we select a subset of CP interaction sequences (giving nonzero signal) out of all 3rd order nonlinear response (also a subset of all possible interactions selected via the phase matching and pulse ordering).

We define the "mixing angle" as the angle between the electronic and the vibronic part of the $|H_0B_1\rangle$ state. To extract the mixing angle we compare the B–H oscillatory cross-peak amplitudes for ETICS pathway in all-parallel and cross-polarized experiments. In the first approximation, only ETICS pathway with alternating transition dipole moment directions with difference corresponding to mixing angle contributes to the signal. Comparing the signals for different polarization sequences follows only polarization selection rules for the isotropically oriented samples [44]. However, we compare two independent measurements in two independent polarization settings, so that several issues have to be considered:

Local oscillator effect (LO_{eff}) Signal strength linearly scales with the filling of the CCD camera, which can be different for two measurements.

Waveplate effect (WP_{eff}) Quarter waveplate used for setting circular polarization does not work perfectly in the near-IR region. Intensity of the individual pulses are therefore different which changes the overall signal level.

Spectrum effect (SP_{eff}) Laser spectrum is slightly different for every measurement and shape of the spectrum is important for coherence pathways because interactions which include $0, \pm 1$ vibrational quantum use different parts of the laser spectrum.

Power effect (P_{eff}) Signal scales as the excitation intensity to the power of (3/2).

The true ratio between the amplitudes of all-parallel and cross-polarized signal is:

$$R = \frac{\mathrm{Amp_{ap}}}{\mathrm{Amp_{cp}}} \cdot \frac{1}{\mathrm{LO_{eff}} \cdot \mathrm{WP_{eff}} \cdot \mathrm{SP_{eff}} \cdot \mathrm{P_{eff}}} \quad (1)$$

where $\mathrm{Amp_{ap}}$, $\mathrm{Amp_{cp}}$ are all-parallel and cross-polarized oscillation amplitudes, respectively. From the polarization selection rules we have (see SI):

$$R = \frac{2 + 4\cos^2\alpha}{5/2(1 - \cos^2\alpha)} \quad (2)$$

where α is the mixing angle, which can be easily calculated.

3.3. Vibronic mixing in the mutated RC_{sph}

The mutations were shown to substantially alter the electron transfer dynamics [32]. It was suggested that the ultrafast charge separation in the WT RC_{sph} is driven by the low frequency vibrations of the special pair and depends on the vibrational structure of the accessory chromophores [37, 45]. For the case of the EET between H and B, high frequency modes 570, 650 cm^{-1} close to the resonance can influence the energy transfer process. Therefore we test whether the EET is changed by the mutations and whether the vibronic coupling, i.e. mixing angles for the resonant modes are altered.

Table 2: *Comparison of the mixing angles (α) and energy transfer times (τ) in WT and mutant reaction centers.*

Mutant	Mode	α	$\tau\,[fs]$
WT	570	30	370 ± 10
	650	30	
M210	570	35	410 ± 20
	650	43	
WL100	570	18	380 ± 10
	650	29	
EL104	570	25	510 ± 20
	650	28	

Table 2 summarizes the extracted mixing angles for the near resonant modes in the WT-R26 RC_{sph} and all the investigated mutant RC_{sph}. Within the estimated error ($\sim 20\,\%$) the mixing angles are very similar, as well as the mixing angles between the 570, 650 cm^{-1} modes. Since the resonance between B–H in all investigated RCs is $\sim 620\,\mathrm{cm}^{-1}$, the mixing angles are expected to be the similar.

We can compare the mixing angle results with the EET kinetics between H and B extracted from the all-parallel measurement. Fig. 3 shows the normalized integrated amplitude of the H–B cross-peak for the all-parallel measurement.

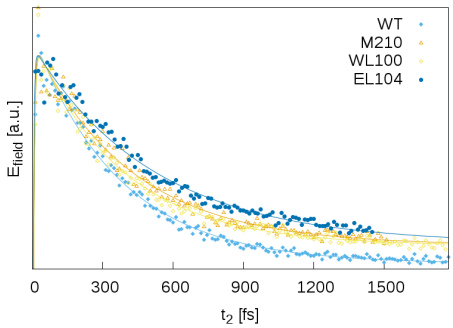

Figure 3: *All-parallel HB crosspeak kinetics for total real 2D spectra for the WT and all the mutants. The energy transfer lifetimes are summarized in Table 2 and compared to the mixing angle.*

4. Discussion

We have demonstrated previously almost perfect match of the oscillation frequencies with the RR spectra of the RC_{sph} [46]. Here we show that quantitative evaluation of the HR factors from the 2DES measurements is possible and correspond well to the FLN data [25, 41] and reasonable well with the resonance Raman. The 2DES method works particularly well for the higher frequency modes, because the corresponding peaks are better separated in the oscillation map. However, the laser spectrum is a limiting factor for the high modes. In our experiment, we have substantially lower light intensity corresponding to the -1 vibrational transition needed to access the purely GSB peak below the B diagonal. Since FLN can be measured only at helium temperatures and RR can be problematic for the fluorescent samples, 2DES can provide reliable results for wide range of systems and experimental conditions.

Here we presented procedure of extracting vibronic mixing angles that do not depend on any assumptions regarding the investigated system. Vibronic mixing in turn provides information about the vibronic coupling. With the help of theoretical modeling, it will be possible to correlate transition dipole directions of the sites with the coupled exciton-vibronic transitions probed in the experiments. One could then compare mixing angles and extract participation ratios of the purely vibrational $|B_1\rangle$ and electronic $|H_0\rangle$ states to the excitonic $|H_0B_1\rangle$.

Even though the point mutations alter significantly the charge separation and electron transfer dynamics, we show that the fast femtosecond components of the energy transfer are not affected. This corresponds well with the fact that the vibronic mixing angle is essentially the same for all the RCs.

5. Conclusions

We show conceptually how the Huang-Rhys factors can be extracted from the 2DES experiment. Relative intensities and to most extend absolute HR values of the modes agree with the complementary experiments in the frequency domain. We demonstrate how to determine the mixing angle from polarization-controlled 2DES experiments. Extracted mixing angle reports on the on the vibronic coupling resulting from the mixing between nuclear and electronic degrees of freedom in the excited state. We propose the scheme how to evaluate quantitatively evaluate the vibronic coupling, which is to our knowledge not accessible from any other experimental technique. Both HR factors and vibronic mixing are crucial ingredients for understanding the role of vibrations in the

photosynthetic light-harvesting as well as in many other functional materials.

In the case of selected mutants of the RC_{sph}, the point mutations did not alter the excitation energy transfer dynamics and did not change the vibronic mixing. From these observations we propose that the protein does not play a significant role in damping of the excessive energy on the femtosecond timescale from high-energy modes close to the excitonic resonance of $620\,cm^{-1}$.

Acknowledgments

The research was supported by the Swedish Research Council and Knut and Alice Wallenberg foundations.

Additional information

The authors declare no competing financial interests.

References

[1] Robert E. Blankenship. *Molecular Mechanism of Photosynthesis*. Blackwell Science Ltd, 2002.

[2] Akiko Tomitani, Andrew H. Knoll, Colleen M. Cavanaugh, and Terufumi Ohno. The evolutionary diversification of cyanobacteria: Molecular–phylogenetic and paleontological perspectives. *Proc. Natl. Acad. Sci.*, 103(14):5442–5447, 2006.

[3] Martin F. Hohmann-Marriott and Robert E. Blankenship. Evolution of photosynthesis. *Annu. Rev. Plant Biol.*, 62(1):515–548, 2011. PMID: 21438681.

[4] David M Adams, Louis Brus, Christopher E D Chidsey, Stephen Creager, Carol Creutz, Cherie R Kagan, Prashant V Kamat, Marya Lieberman, Stuart Lindsay, Rudolph A Marcus, Robert M Metzger, John R Miller, Marshall D Newton, Debra R Rolison, Otto Sankey, Kirk S Schanze, James Yardley, and Xiaoyang Zhu. Charge Transfer on the Nanoscale: Current Status. *J. Phys. Chem. B*, 107:6668–6697, 2003.

[5] T D Ladd, F Jelezko, R Laflamme, Y Nakamura, C Monroe, and J L O'Brien. Quantum computers. *Nature*, 464(7285):45–53, 2010.

[6] Henry J Snaith. Perovskites: The emergence of a new era for low-cost , high-efficiency solar cells. *J. Phys. Chem. Lett*, 4:3623–3630, 2013.

[7] K. S. Novoselov, V. I. Falko, L. Colombo, P. R. Gellert, M. G. Schwab, and K. Kim. A roadmap for graphene. *Nature*, 490(7419):192–200, 2012.

[8] Graham R. Fleming and Mark a. Ratner. Grand challenges in basic energy sciences. *Phys. Today*, 61(7):28–33, 2008.

[9] Niklas Christensson, Harald F Kauffmann, Tõnu Pullerits, and Tomáš Mančal. Origin of Long-Lived Coherences in Light-Harvesting Complexes. *J. Phys. Chem. B*, 116(25):7449–7454, June 2012.

[10] Vivek Tiwari, William K Peters, and David M Jonas. Electronic resonance with anticorrelated pigment vibrations drives photosynthetic energy transfer outside the adiabatic framework. *Proc. Natl. Acad. Sci.*, 110(4):1203–1208, January 2013.

[11] Jordan M Womick and Andrew M Moran. Vibronic enhancement of exciton sizes and energy transport in photosynthetic complexes. *J. Phys. CHem. B*, 115(6):1347–1356, 2011.

[12] E. K. Irish, R. Gómez-Bombarelli, and B. W. Lovett. Vibration-assisted resonance in photosynthetic excitation-energy transfer. *Phys. Rev. A*, 90:012510, Jul 2014.

[13] Ilia a Solov'yov, Po-Yao Chang, and Klaus Schulten. Vibrationally assisted electron transfer mechanism of olfaction: myth or reality? *Physical chemistry chemical physics : PCCP*, 14(40):13861–71, October 2012.

[14] David M Jonas. Two-dimensional femtosecond spectroscopy. *Annu. Rev. Phys. Chem.*, 54(1):425–463, January 2003.

[15] Tobias Brixner, Tomáš Mančal, Igor V Stiopkin, and Graham R Fleming. Phase-stabilized two-dimensional electronic spectroscopy. *J. Chem. Phys.*, 121(9):4221–4236, September 2004.

[16] N. A. Kurnit, I. D. Abella, and S. R. Hartmann. Observation of a photon echo. *Phys. Rev. Lett.*, 13(19):567–568, 1964.

[17] Richard G. Brewer and R.L. Shoemaker. Optical free induction decay. *Phys. Rev. A*, 6(6):2001–07, 1972.

[18] L Lepetit and M Joffre. Two-dimensional nonlinear optics using Fourier-transform spectral interferometry. *Opt. Lett.*, 21(8):564–6, apr 1996.

[19] Hebin Li, Alan D Bristow, Mark E Siemens, Galan Moody, and Steven T Cundiff. Unraveling quantum pathways using optical 3D Fourier-transform spectroscopy. *Nat Commun.*, 4(1390), January 2013.

[20] Joachim Seibt, Thorsten Hansen, and Tõnu Pullerits. 3D Spectroscopy of Vibrational Coherences in Quantum Dots: Theory. *J. Phys. Chem. B*, 117(38):11124–11133, September 2013.

[21] Gabriela S. Schlau-Cohen, Akihito Ishizaki, and Graham R. Fleming. Two-dimensional electronic spectroscopy and photosynthesis: Fundamentals and applications to photosynthetic light-harvesting. *Chem. Phys.*, 386(1-3):1–22, July 2011.

[22] Elisabetta Collini, Cathy Y Wong, Krystyna E Wilk, Paul M G Curmi, Paul Brumer, and Gregory D Scholes. Coherently wired light-harvesting in photosynthetic marine algae at ambient temperature. *Nature*, 463(7281):644–647, February 2010.

[23] Gregory S Engel, Tessa R Calhoun, Elizabeth L Read, Tae-Kyu Ahn, Tomáš Mančal, Yuan-Chung Cheng, Robert E Blankenship, and Graham R Fleming. Evidence for wavelike energy transfer through quantum coherence in photosynthetic systems. *Nature*, 446(7137):782–786, April 2007.

[24] Volkhard May and Oliver Kühn. *Dynamics of Isolated and Open Quantum Systems*. Wiley-VCH Verlag GmbH & Co. KGaA, 2011.

[25] Margus Rätsep, Zheng Li Cai, Jeffrey R. Reimers, and Arvi Freiberg. Demonstration and interpretation of significant asymmetry in the low-resolution and high-resolution Qy fluorescence and absorption spectra of bacteriochlorophyll a. *J. Chem. Phys.*, 134(2), 2011.

[26] Nerine J. Cherepy, Andrew P. Shreve, Laura J. Moore, Steven G. Boxer, and Richard A. Mathies. Electronic and nuclear dynamics of the accessory bacteriochlorophylls in bacterial photosynthetic reaction centers from resonance Raman intensities. *J. Phys. Chem. B*, 101(16):3250–3260, 1997.

[27] James Lim, David Paleček, Felipe Caycedo-Soler, Craig N. Lincoln, Javier Prior, Hans von Berlepsch, Susana F. Huelga, Martin B. Plenio, Donatas Zigmantas, and Jürgen Hauer. Vibronic origin of long-lived coherence in an artificial molecular light harvester. *Nat. Commun.*, 6(7755), 2015.

[28] David Paleček, Petra Edlund, Sebastian Westenhoff, and Donatas Zigmantas. are preparing manuscript to be called "Quantum Coherence as a Witness of Vibronically Hot Energy Transfer in Bacterial Reaction Centre".

[29] Vytautas Butkus, Donatas Zigmantas, Darius Abramavicius, and Leonas Valkunas. Distinctive character of electronic and vibrational coherences in disordered molecular aggregates. *Chem. Phys. Lett.*, 587:93–98, 2013.

[30] Vytautas Butkus, Leonas Valkunas, and Darius Abramavicius. Vibronic phenomena and exciton vibrational interference in two-dimensional spectra of molecular aggregates. *The Journal of Chemical Physics*, 140(3), 2014.

[31] L. M. P. Beekman, I. H. M. van Stokkum, R. Monshouwer, a. J. Rijnders, P. McGlynn, R. W. Visschers, M. R. Jones, and R. van Grondelle. Primary Electron Transfer in Membrane-Bound Reaction Centers with Mutations at the M210 Position. *J. Phys. Chem.*, 100(17):7256–7268, January 1996.

[32] Natalia P Pawlowicz, Ivo H M van Stokkum, Jacques Breton, Rienk van Grondelle, and Michael R Jones. An investigation of slow charge separation in a tyrosine M210 to tryptophan mutant of the Rhodobacter sphaeroides reaction center by femtosecond mid-infrared spectroscopy. *Physical chemistry chemical physics : PCCP*, 12(11):2693–705, March 2010.

[33] Sebastian Westenhoff, David Paleček, Petra Edlund, Philip Smith, and Donatas Zigmantas. Coherent picosecond exciton dynamics in a photosynthetic reaction center. *Journal of the American Chemical Society*, 134(40):16484–7, October 2012.

[34] Ramũnas Augulis and Donatas Zigmantas. Two-dimensional electronic spectroscopy with double modulation lock-in detection: enhancement of sensitivity and noise resistance. *Optics express*, 19(14):13126–33, July 2011.

[35] Ramūnas Augulis and Donatas Zigmantas. Detector and dispersive delay calibration issues in broadband 2D electronic spectroscopy. *JOSA B*, 30(6):1770, May 2013.

[36] Roel Tempelaar, Thomas L C Jansen, and Jasper Knoester. Vibrational Beatings Conceal Evidence of Electronic Coherence in the FMO Light-Harvesting Complex. *J. Phys. Chem. B*, 118(45):12865–12872, 2014.

[37] M Bixon and Joshua Jortner. Electron transfer via bridges. *J. Chem. Phys.*, 107(13):5154–5170, 1997.

[38] Eric O Potma and Douwe a Wiersma. Exciton superradiance in aggregates: The effect of disorder, higher order exciton-phonon coupling and dimensionality. *J. Chem. Phys.*, 108(12):4894, 1998.

[39] Gregory D. Scholes and Graham R. Fleming. On the Mechanism of Light Harvesting in Photosynthetic Purple Bacteria: B800 to B850 Energy Transfer. *J. Phys. Chem. B*, 104(8):1854–1868, mar 2000.

[40] David Paleček, Petra Edlund, Sebastian Westenhoff, and Donatas Zigmantas. are preparing manuscript to be called "Cross-polarized Transient Grating to Identify Electronic and/or Mixed Vibronic Coherence Beatings .".

[41] Margus Rätsep and Arvi Freiberg. Electron–phonon and vibronic couplings in the FMO bacteriochlorophyll a antenna complex studied by difference fluorescence line narrowing. *J. Lumin.*, 127(1):251–259, nov 2007.

[42] David Paleček, Petra Edlund, Sebastian Westenhoff, and Donatas Zigmantas. are preparing manuscript to be called "Pitfalls of the Early Dynamics in the Cross-polarized Two-dimensional Electronic Spectroscopy".

[43] Vytautas Butkus, Donatas Zigmantas, Leonas Valkunas, and Darius Abramavicius. Vibrational vs. electronic coherences in 2D spectrum of molecular systems. *Chem. Phys. Lett.*, 545:40–43, August 2012.

[44] RM Hochstrasser. Two-dimensional IR-spectroscopy: polarization anisotropy effects. *Chem. Phys.*, 266:273–284, 2001.

[45] MH Vos, MR Jones, CN Hunter, J Breton, JC Lambry, and JL Martin. Coherent dynamics during the primary electron-transfer reaction in membrane-bound reaction centers of Rhodobacter sphaeroides. *Biochemistry*, 33(22):6750–6757, 1994.

[46] NJ Cherepy, AP Shreve, LJ Moore, SG Boxer, and A R Mathies. Temperature dependence of the Qy resonance Raman spectra of bacteriochlorophylls, the primary electron donor, and bacteriopheophytins in the bacterial photosynthetic reaction center. *Biochemistry*, 2960(97):8559–8566, 1997.

Paper VIII

Mutational analysis reveals that long-lived quantum oscillations in a bacterial reaction center are intrinsic to the chromophore aggregate.

[1]Petra Edlund, [2,3]David Paleček, [1]Emil Gustavsson, [2]Donatas Zigmantas and [1]Sebastian Westenhoff

[1]*Department of Chemistry and Molecular Biology, University of Gothenburg, Box 462, SE-40530 Gothenburg, Sweden*

[2]*Department of Chemical Physics, Lund University, P.O. Box 124, SE-22100 Lund, Sweden*

[3]*Department of Chemical Physics, Charles University in Prague, Ke Karlovu 3, 121 16 Praha 2, Czech Republic*

westenho@chem.gu.se

Abstract

Reaction center proteins (RC) are central in photosynthetic organisms and use absorbed light energy for charge separation with extremely high quantum efficiency. The excitation energy used for electron transfer is provided by surrounding antenna light harvesting complexes and from the intrinsic chromophores. Energy transfers within 200 fs from the associated bacteropheophytin and bacterichlorophyll to a "special pair" of chlorophylls, where charge separation takes place. Long-lived quantum coherences have been detected in the chromophores using femtosecond two-dimensional electronic spectroscopy (2DES). Their origin is debated, but here we demonstrate that wild type and mutated RC from *Rba. Sphaeroides* show the same long lived coherent oscillations between the bacteropheophytin and bacterichlorophyll. The examined side chains M210, L100 and L104 are concluded to not be involved in stabilizing the coherent spectroscopic oscillations in other ways than providing the cofactors stability in their spatial position and orientation. An active role of the protein matrix in stabilizing the long-lived coherences is unlikely.

1. Introduction

The reaction center from *Rhodobacter Sphaeroides* contains 3 subunits, named M, L and H and holds in total 6 chromophores one non-heme Iron and a carotenoid [1]. The chromophores are arranged in two branches with almost perfect C_2 symmetry due to the highly similar fold of the L and M subunits [2]. (Figure 1) The branches are denoted A and B where branch A is the active in electron transfer [3]. The special Pair (P) consists of two closely coupled bacteriochlorophylls, and each branch contains one accessory bacterochlorophyll (B), one bacteriopheophytin (H)

and one quinone [1, 4]. The central task for RC is to convert the absorbed light energy into chemical energy in the form of ATP. This is done through charge separation, where the absorbed excitation energy is used for transferring one electron from the special pair over the chromophores in branch A to Quinone A. The electron is then furthered transferred via the non heme Iron to Quinone B [5]. The initial electron transfer from P to H_A proceed in less than 5 ps [6, 7] and is followed by the slower reduction of quinone A in 220 ps [5]. The efficiency of the electron transfer chain is nearly unity [8].

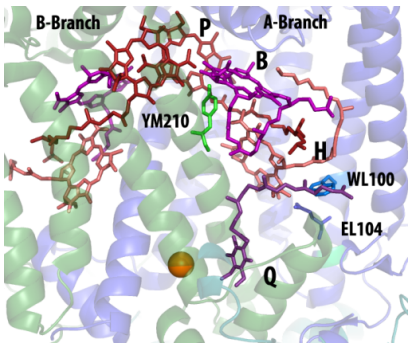

Figure 1: *The arrangement of chromophores in reaction center proteins and the mutated side chains. (pdb entry 1OGV)*

Most of the excitation energy used for electron transfer in RC is provided by the surrounding antenna light harvesting complexes, but some light is also absorbed directly by the intrinsic chromophores. The two branches in RC_{sph} serves as energy transfer pathways for the excitation energy to P where charge separation is initiated. This energy transfer is highly efficient and fast; it proceeds within 200 fs from B and H to P [9–11]. Two-dimensional visible spectroscopy and two-color photon echo spectroscopy have been used to detect coherences between H and B that live for several hundreds of femtoseconds [11–15]. The coherences bear all expected signatures expected for electronic coherences in a molecular dimer [16]. Initially, it was proposed that the protein plays and active role in stabilizing the coherence superposition of B and H. We note that the straight forward assignment of the coherence to be electronic is problematic, because the detected coherences outlive the excited state populations on the chromophores. We detail this argument in a separate paper [17].

2DES maps energy dynamics in molecular aggregates and function as a pump probe experiment with ultrashort (fs) optical pulses as excitation and probing [11, 18–22]. The laser source is split into ultrafast femtosecond pulses which are focused onto the sample. Simplified, the first two pulses interacts with the sample to create either population state or coherent state, which freely evolves during the waiting time. In combination with the third pulse, third order polarization is generated and emitted in the phase-matching direction of the fourth pulse. The resulting maps at different waiting times after excitation visualizes, with femtosecond time resolution, excited state populations, excited state couplings and energy transfer. This has previously been demonstrated for B_A and B_B energy exchange [23] and H_A to B_A energy transfer [11]. By chemically oxidizing the special pair the photocycle is shortened by blocking the electron transfer and the experiment can be performed at a higher rate without affecting the preceding energy transfer [24]. Inspired by IR-spectroscopy the use of a special combination of linearly

polarized pulses makes it possible to suppress intramolecular signals and enhance intermolecular ones [11, 25, 26].

To elucidate the role of the protein binding pocket on the function of the WT RC, specific point mutations can be used to alter the event of interest. The mutants generally exhibit slower charge separation [27] 27. In this study three constructs were expressed with mutations at potentially interesting sites. Tyrosine M210 to Phenylalanine (YM210F), Glutamic acid L104 to Leucine (EL104L), Tryptophan L100 to Phenylalanine (WL100F) (fIgure 1). The highly conserved YM210F is in close distance to P, H_A, and B_A, but not directly bonded to any of the chromophores. Mutation of YM210 drastically alters the primary electron transfer, making it aproximatelly five times slower from 3.5 ps to 16 ps [28]. At the same time, P^+B^- decay has been demonstrated to be 10 times longer in a M210 mutant compared to WT [29] and also has an effect on the charge recombination time [31]. EL100L and WL100F are positioned close to H_A and have been proposed to form hydrogen bonds to the 10a-ester and the 9-keto carbonyls on ring V of H_A , respectively [30]. EL104 is also a well conserved residue present also in *Rbs. viridis*. Although it is known that the mutations affect electron transfer, the implications for the preceding energy transfer on the femtosecond timescale remains unclear. By examining the energy transfer and coherence dynamics between H and B in wild type (WT) RC and mutated RCs using 2DES we address the question whether and possible how is the protein involved in the ultrafast energy transfer events.

2. Materials and Methods

Sample preparations

The WT R-26 RC was prepared and purified as described elsewhere[20]. The mutants were produced in the native host in semi-anaerobic dark conditions at 30°C and purified according to Paddock et al. [31] with the following modifications The solubilisation LDAO concentration was increased to 4% and the time to 3 hours. Ion-exchange chromatography was performed with a toyopearl DEAE-650M column and protein was eluted with a continuous 0-500 mM NaCl gradient. The protein was concentrated and flash frozen with liquid nitrogen. Prior to the 2DES experiments the protein samples were chemically oxidized with 150 mM $KFe(CN)_6$ and diluted in glycerol (80 %) in the ratio 1:3 to ensure high quality low temperature glass in 0.5 mm cuvette. The maximum absorbance was $A(800) \approx 0.3$.

2DES

Passively stabilized 2DES setup used in this study was described previously (cite Brixner 2004). Briefly, an amplified laser system Pharos (Light Conversion Ltd) is used to pump the home-built non-collinear optical parametric amplifier (NOPA), which generates 17 fs pulses centered around 770 nm. The laser beam is split into four replicas arranged in boxcar geometry. Population delay t_2 is set by a mechanical delay stage, whereas the coherence delay t1 is controlled by inserting 2 pairs of fused silica wedges into the first two beams. These beams are also mechanically chopped to allow for scatter free lock-in detection at sum and dif-

ference frequencies [32]. For polarization control quarter, a waveplate and four wire grid polarizers in each of the beams are used. The four beams are focused and overlapped in the 0.5 mm path cuvette cooled down to 77 K. The non-linear signal is emitted in the phase-matching direction and heterodyned with the attenuated fourth pulse. The spectral interferograms are spectrally resolved on CCD camera (PIXIS, Princeton Instruments). Fourier transform of the raw data in (t_1, ω_3) over the coherence time leads to resulting 2D maps correlating excitation and emission energies (ω_1, ω_3). The population kinetics were extracted from the lower cross-peak $(\omega_1, \omega_3) = (13000, 12500)\,\mathrm{cm}^{-1}$ in the MA polarization sequence (MA,MA,0,0) for the pulses 1-4. The coherence delay was typically scanned between $-170 : +220$ fs leading to overall resolution of 55 and $50\,\mathrm{cm}^{-1}$ for ω_1 and ω_3, respectively. The coherent oscillations were extracted from the upper cross-peak in cross-polarization measurement $(45°, -45°, 90°, 0°)$ from rephasing real part. Coherence delay was typically scanned from -150 to 175 fs, which results in spectral resolution of $70\,\mathrm{cm}^{-1}$ along both ω_1 and ω_3.

3. Results

The typical reaction center absorption spectra in Fig. 2 shows the major absorption peaks for the associated bacteriochlorphylls B at 760 nm and bacteriophephytin H at 800 nm. The special pair, P absorption which usually arises at 850 nm is absent since we chemically oxidized the special pair in the experiment to prevent electron transfer. All mutations cause a small red-shift of B. The shape of the spectra is also changed. Compared to the amplitude of the B peak, the H absorption peak is reduced for the YM210F and WL104F whereas it increased for the EL104L. This is consistent with that the change of a polar glutamic acid to the aliphatic leucine and the tryptophan to a phenylalanine raptures the possibilities of hydrogen bonding to H_A.

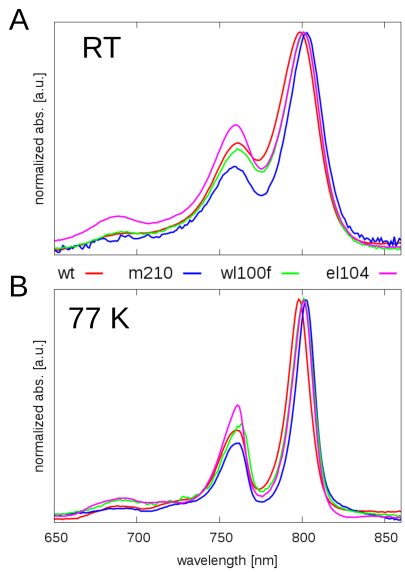

Figure 2: *Room temperature and 77 K Absorption spectra for WT Reaction center and three mutants*

Figure 3 shows 2D spectra of partially relaxed RCs at waiting time 480 fs with prominent cross-peak. The absorption on the diagonal corresponds to the ground state absorption spectrum and the absorptions of the H and B as in Figure 2. The 2D maps of WT and the mutants have similar features other than the differences spectral shape and peak position observed in the linear absorption spectra in Figure 2. The negative peak above the diagonal is due to photoinduced absorp-

tion. The positive cross-peak below the diagonal corresponds to the electronic coupling/energy transfer between the H and B chromophores. This signal appears and disappears over time in an oscillatory manner and was identified to have mixed character of initially created excited state coherence, yet evolving in the ground state. The frequency correspond to the energy difference between the excitons, therefore the oscillation can be easily mistaken for the purely electronic coherence [17].

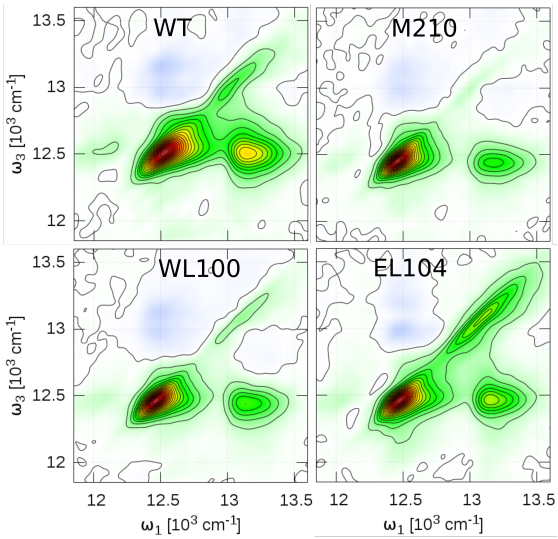

Figure 3: *2D spectra at waiting time $t_2 = 480$ fs for the wildtype RC and three mutants.*

In Figure 4 the time-dependence of the lower cross-peak over the waiting time (t_2) for magic angle are presented. The signal reflects a combination of populations of the excited states and ground state wavepackets. The WT and mutants all demonstrate the similar kinetics, with slittle differences in intensity. To separate the intermolecular contributions to the overall beating patter, cross-polarized scheme is implemented (see Section 2). First and second pulse pairs are polarized orthogonal which provides the selection, together with the orientational averaging. The beatings are shown in Figure 5 and shows the coherence, which is observable at the crosspeak. All the mutants and WT show very similar oscillating patterns.

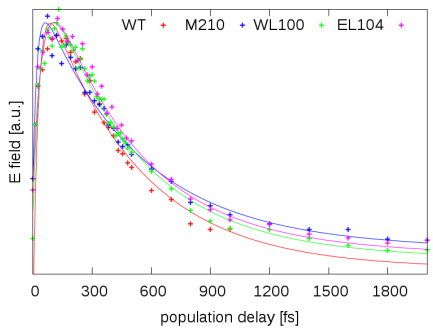

Figure 4: *H–B Energy transfer cross-peak kinetics for WT RC and mutants.*

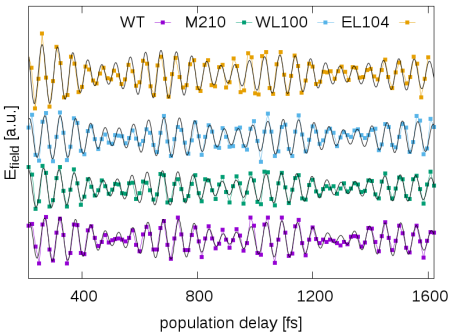

Figure 5: *Oscillations of the crosspeak for Wt and mutants in cross-polarized configuration of pulses* $(45°, -45°, 90°, 0°)$.

4. Discussion

Mutations affects the electron transfer kinetics but not affecting the chromophores position or orientation [30, 33]. However, the mutations can, by altering the hydrogen bondings or in other ways effecting the electrochemical environment can shift electronic transition energies and electronic structure [34, 35]. The exchange of the aromatic and polar tyrosine to a non polar phenylalanine in YM210F removes the possibility of forming a hydrogen bond to the special pair. The analogous is true for the EL104 in forming a hydrogen bond to H_A. The mutations do affect the electronic structure as visible in absorption spectra. However, surprisingly there is no effect on the energy transfer between the cofactors demonstrated by the in principal identical oscillating patterns of the cross peak.The studied residues do neither stabilize or destabilize the coherent energy oscillations.

5. Conclusions

Although it have been showed previously that mutations effect the electron transfer and the electronic structure of the chromophores we demonstrate here that the mutations has no effect on the ultrafast components of the energy transfer between H and B. We state that the protein matrix interaction with the chromophores energy transfer is limited.

Acknowledgments

We thank Professor James Allen from Arizona University for the kind gift of the mutants. The research was supported by the Swedish Research Council and Knut and Alice Wallenberg foundations.

Additional information

The authors declare no competing financial interests.

References

[1] J.P. Allen and J.C. Williams. Photosynthetic reaction centers. *FEBS Letters*, 438(1–2):5 – 9, 1998.

[2] Gergely Katona, Ulf Andréasson, Ehud M. Landau, Lars-Erik Andréasson, and Richard Neutze. Lipidic cubic phase crystal structure of the photosynthetic reaction centre from rhodobacter sphaeroides at 2.35 åresolution. *J. Mol. Biol.*, 331(3):681 – 692, 2003.

[3] Wolfgang Zinth and Josef Wachtveitl. The first picoseconds in bacterial

photosynthesis—ultrafast electron transfer for the efficient conversion of light energy. *Chem. Phys. Chem.*, 6(5):871–880, 2005.

[4] et al. Allen, J.P. tructure of the reaction center from rhodobacter-sphaeroides r-26 - protein cofactor (quinones and fe-2+) interactions. *Proc. Natl. Acad. Sci. USA*, 85(22):8487–8491, 1988.

[5] W Holzapfel, U Finkele, W Kaiser, D Oesterhelt, H Scheer, H U Stilz, and W Zinth. Initial electron-transfer in the reaction center from Rhodobacter sphaeroides. *Proc. Natl. Acad. Sci.*, 87(13):5168–72, July 1990.

[6] M.Y Okamura, M.L Paddock, M.S Graige, and G Feher. Proton and electron transfer in bacterial reaction centers. *Biochimica et Biophysica Acta (BBA) - Bioenergetics*, 1458(1):148 – 163, 2000.

[7] H Wang, S Lin, JP Allen, JC Williams, S Blankert, Christa Laser, and Neal W Woodbury. Protein dynamics control the kinetics of initial electron transfer in photosynthesis. *Science*, 316(5825):747–50, 2007.

[8] Robert E. Blankenship. *Molecular Mechanism of Photosynthesis*. Blackwell Science Ltd, 2002.

[9] Xanthipe J. Jordanides, Gregory D. Scholes, and Graham R. Fleming. The Mechanism of Energy Transfer in the Bacterial Photosynthetic Reaction Center. *J. Phys. Chem. B*, 105(8):1652–1669, March 2001.

[10] David C Arnett, C C Moser, P L Dutton, and N F Scherer. The First Events in Photosynthesis: Electronic Coupling and Energy Transfer Dynamics in the Photosynthetic Reaction Center from Rhodobacter sphaeroides. *J. Phys. Chem. B*, 103:2014–2032, 1999.

[11] Sebastian Westenhoff, David Paleček, Petra Edlund, Philip Smith, and Donatas Zigmantas. Coherent picosecond exciton dynamics in a photosynthetic reaction center. *Journal of the American Chemical Society*, 134(40):16484–7, October 2012.

[12] Gregory S Engel, Tessa R Calhoun, Elizabeth L Read, Tae-Kyu Ahn, Tomáš Mančal, Yuan-Chung Cheng, Robert E Blankenship, and Graham R Fleming. Evidence for wavelike energy transfer through quantum coherence in photosynthetic systems. *Nature*, 446(7137):782–786, April 2007.

[13] Gitt Panitchayangkoon, Dmitri V Voronine, Darius Abramavicius, Justin R Caram, Nicholas H C Lewis, Shaul Mukamel, and Gregory S Engel. Direct evidence of quantum transport in photosynthetic light-harvesting complexes. *Proc. Natl. Acad. Sci. USA*, 108(52):20908–12, dec 2011.

[14] Su Lin, Jon Jackson, Aileen K. W. Taguchi, , and Neal W. Woodbury. Excitation wavelength dependent spectral evolution in rhodobacter sphaeroides r-26 reaction centers at low temperatures: The qy transition region. *J. Phys. Chem. B*, 102(20):4016–4022, 1998.

[15] H Lee, YC Cheng, and GR Fleming. Coherence dynamics in photosynthesis: protein protection of excitonic coherence. *Science*, 1462, 2007.

[16] Vytautas Butkus, Donatas Zigmantas, Leonas Valkunas, and Darius Abramavicius. Vibrational vs. electronic coherences in 2D spectrum of molecular systems. *Chem. Phys. Lett.*, 545:40–43, August 2012.

[17] David Paleček, Petra Edlund, Sebastian Westenhoff, and Donatas Zigmantas. are preparing manuscript to be called "Quantum Coherence as a Witness of Vibronically Hot Energy Transfer in Bacterial Reaction Centre".

[18] Naomi S. Ginsberg, Yuan-Chung Cheng, and Graham R. Fleming. Two-dimensional electronic spectroscopy of molecular aggregates. *Accounts of Chemical Research*, 42(9):1352–1363, 2009.

[19] DM Jonas, MJ Lang, Yutaka Nagasawa, Taiha Joo, and Graham R. Fleming. Pump-probe polarization anisotropy study of femtosecond energy transfer within the photosynthetic reaction center of Rhodobacter sphaeroides R26. *J. Phys. Chem.*, 3654(100):12660–12673, 1996.

[20] David M Jonas. Two-dimensional femtosecond spectroscopy. *Annu. Rev. Phys. Chem.*, 54(1):425–463, January 2003.

[21] Gabriela S. Schlau-Cohen, Akihito Ishizaki, and Graham R. Fleming. Two-dimensional electronic spectroscopy and photosynthesis: Fundamentals and applications to photosynthetic light-harvesting. *Chem. Phys.*, 386(1-3):1–22, July 2011.

[22] G.S. Schlau-Cohen, Jahan M. Dawlaty, and G.R. Fleming. Ultrafast multidimensional spectroscopy: Principles and applications to photosynthetic systems. *Selected Topics in Quantum Electronics, IEEE Journal of*, 18(1):283–295, 2012.

[23] Gabriela S. Schlau-Cohen, Eleonora De Re, Richard J. Cogdell, and Graham R. Fleming. Determination of excited-state energies and dynamics in the b band of the bacterial reaction center with 2d electronic spectroscopy. *J. Phys. Chem. Lett.*, 3(17):2487–2492, 2012.

[24] JA Jackson, Su Lin, AKW Taguchi, JC Williams, JP Allen, NW Woodbury, and NW Woodbury. Energy transfer in Rhodobacter sphaeroides reaction centers with the initial electron donor oxidized or missing. *J. Phys. Chem. B*, 101:5747–5754, 1997.

[25] Gabriela S Schlau-Cohen, Akihito Ishizaki, Tessa R Calhoun, Naomi S Ginsberg, Matteo Ballottari, Roberto Bassi, and Graham R Fleming. Elucidation of the timescales and origins of quantum electronic coherence in LHCII. *Nat. Chem.*, 4(5):389–395, 2012.

[26] M T Zanni, N H Ge, Y S Kim, and R M Hochstrasser. Two-dimensional IR spectroscopy can be designed to eliminate the diagonal peaks and expose only the crosspeaks needed for structure determination. *Proc. Natl. Acad. Sci. USA*, 98(20):11265–70, sep 2001.

[27] L. M. P. Beekman, I. H. M. van Stokkum, R. Monshouwer, a. J. Rijnders, P. McGlynn, R. W. Visschers, M. R. Jones, and R. van Grondelle. Primary Electron Transfer in Membrane-Bound Reaction Centers with Mutations at the M210 Position. *J. Phys. Chem.*, 100(17):7256–7268, January 1996.

[28] Ulrich Finkele, Christoph Lauterwasser, and Wolfgang Zinth. Role of tyrosine M210 in the initial charge separation of reaction centers of Rhodobacter sphaeroides. *Biochemistry*, 29(1985):8517–8521, 1990.

[29] Natalia P Pawlowicz, Ivo H M van Stokkum, Jacques Breton, Rienk van Grondelle, and Michael R Jones. An investigation of slow charge separation in a tyrosine M210 to tryptophan mutant of the Rhodobacter sphaeroides reaction center by femtosecond mid-infrared spectroscopy. *Physical chemistry chemical physics : PCCP*, 12(11):2693–705, March 2010.

[30] Jacques Breton, Eliane Nabedryk, James P. Allen, and Joann C. Williams. Electrostatic influence of qa reduction on the ir vibrational mode of the 10a-ester co of ha demonstrated by mutations at residues glu l104 and trp l100 in reaction centers from rhodobacter sphaeroides. *Biochemistry*, 36(15):4515–4525, 1997.

[31] MarkL. Paddock, ScottH. Rongey, EdwardC. Abresch, George Feher, and MelvinY. Okamura. Reaction centers from three herbicide-resistant mutants of rhodobacter sphaeroides 2.4.1: sequence analysis and preliminary characterization. *Photosynth. Res.*, 17(1-2):75–96, 1988.

[32] Ramũnas Augulis and Donatas Zigmantas. Two-dimensional electronic spectroscopy with double modulation lock-in detection: enhancement of sensitivity and noise resistance. *Optics express*, 19(14):13126–33, July 2011.

[33] Arthur J. Chirino, Erik J. Lous, Martina Huber, James P. Allen, Craig C. Schenck, Mark L. Paddock, George Feher, and Douglas C. Rees. Crystallographic analyses of site-directed mutants of the photosynthetic reaction center from rhodobacter sphaeroides. *Biochemistry*, 33(15):4584–4593, 1994.

[34] J. C. Williams, R. G. Alden, H. A. Murchison, J. M. Peloquin, N. W. Woodbury, and J. P. Allen. Effects of mutations near the bacteriochlorophylls in reaction centers from rhodobacter sphaeroides. *Biochemistry*, 31(45):11029–11037, 1992.

[35] H. van Amerongen, L. Valkunas, and R. van Grondelle. *Photosynthetic Excitons*. World Scientific, 2000.